A HIERARCHICAL HISTORY MATCHING METHOD AND ITS APPLICATIONS

A Dissertation

by

JICHAO YIN

Submitted to the Office of Graduate Studies of
Texas A&M University
in partial fulfillment of the requirements for the degree of

DOCTOR OF PHILOSOPHY

December 2011

Major Subject: Petroleum Engineering

A Hierarchical History Matching Method and Its Applications

A HIERARCHICAL HISTORY MATCHING METHOD

AND ITS APPLICATIONS

A Dissertation

by

JICHAO YIN

Submitted to the Office of Graduate Studies of
Texas A&M University
in partial fulfillment of the requirements for the degree of

DOCTOR OF PHILOSOPHY

Approved by:

Chair of Committee,	Akhil Datta-Gupta
Committee Members,	Christine Ehlig-Economides
	A. Daniel Hill
	Yalchin Efendiev
Head of Department,	Stephen A. Holditch

December 2011

Major Subject: Petroleum Engineering

ABSTRACT

A Hierarchical History Matching Method and Its Applications.

(December 2011)

Jichao Yin, B.S., Tsinghua University, Beijing, China;

M.S., Tsinghua University, Beijing, China

Chair of Advisory Committee: Dr. Akhil Datta-Gupta

Modern reservoir management typically involves simulations of geological models to predict future recovery estimates, providing the economic assessment of different field development strategies. Integrating reservoir data is a vital step in developing reliable reservoir performance models. Currently, most effective strategies for traditional manual history matching commonly follow a structured approach with a sequence of adjustments from global to regional parameters, followed by local changes in model properties. In contrast, many of the recent automatic history matching methods utilize parameter sensitivities or gradients to directly update the fine-scale reservoir properties, often ignoring geological inconsistency. Therefore, there is need for combining elements of all of these scales in a seamless manner.

We present a hierarchical streamline-assisted history matching, with a framework of global-local updates. A probabilistic approach, consisting of design of experiments, response surface methodology and the genetic algorithm, is used to understand the uncertainty in the large-scale static and dynamic parameters. This global update step is

followed by a streamline-based model calibration for high resolution reservoir heterogeneity. This local update step assimilates dynamic production data.

We apply the genetic global calibration to unconventional shale gas reservoir specifically we include stimulated reservoir volume as a constraint term in the data integration to improve history matching and reduce prediction uncertainty. We introduce a novel approach for efficiently computing well drainage volumes for shale gas wells with multistage fractures and fracture clusters, and we will filter stochastic shale gas reservoir models by comparing the computed drainage volume with the measured SRV within specified confidence limits.

Finally, we demonstrate the value of integrating downhole temperature measurements as coarse-scale constraint during streamline-based history matching of dynamic production data. We first derive coarse-scale permeability trends in the reservoir from temperature data. The coarse information are then downscaled into fine scale permeability by sequential Gaussian simulation with block kriging, and updated by local-scale streamline-based history matching.

The power and utility of our approaches have been demonstrated using both synthetic and field examples.

DEDICATION

To my beloved parents, my brother and nephew for their endless love and support.

ACKNOWLEDGEMENTS

I would like to express my deepest gratitude to my academic advisor, Dr. Akhil Datta-Gupta, for his continuous enlightenment, trust, academic guidance, and financial support. His remarkable knowledge and vision made the research challenging, while his amenable personality makes life enjoyable.

I would like to thank Dr. King for his inspiring ideas through our many meetings and discussions. I would like to thank the members of my committee, Dr. Ehlig-Economides, Dr. Hill, and Dr. Efendiev, for their valuable comments and suggestions that have shaped this dissertation.

I would like to thank ExxonMobil Upstream Research Company for providing me internship opportunities. I thank Hao Huang, Li-Bong W. Lee, Jing Wan, Ted A. Long, and Bill E. Kline for their precious trust and support in my summer jobs, from which I gained lots of experience and a vision for self-development.

Special thanks to my colleagues at Texas A&M University, Han-Young Park and Jiang Xie and Zhuoyi Li, with whom I initiated the research projects, for their constructive discussions over the years. Also, to alumni of the MCERI group, Hao Cheng and Xianlin Ma, for their inspirations. To Deepak, Jong-Uk, Alvaro, Eric, Shingo, Suk-Sang, Yanbin, Satyajit, Jeong-Min, Mohan, Shusei, Zheng, thanks for your friendship and for making my graduate years memorable.

NOMENCLATURE

$\Delta\tilde{\mathbf{t}}$ = optimal generalized travel time (GTT) shift, day

$\delta\mathbf{R}$ = permeability update needed in local update, md

S = sensitivity matrix of GTT to permeability, day/md

L = second spatial-difference operator

β_1 = weight for norm penalty term in LSQR

β_2 = weight for roughness penalty term in LSQR

$\mathbf{m}_i$ = a genome of model parameters

T_n = temperature in heat-bath algorithm for generation *n*

$\alpha(\mathbf{x})$ = diffusivity coefficient at location **x**, md-psi/cp

$\tau(\mathbf{x})$ = diffusive time of flight at location **x**, $day^{1/2}$

$t(\mathbf{x})$ = arrival time of pressure 'front' at location **x**, day

Δp = bottom-hole pressure misfit, psi

ΔV = drainage volume misfit, ft^3

k = permeability, md

ϕ = porosity

μ = viscosity, cp

c_t = reservoir total compressibility, 1/psi

k_M = matrix permeability, md

k_E = enhanced area permeability, md

k_F = fracture permeability, md

C_M = matrix permeability compaction factor, 1/psi

C_E = enhanced area permeability compaction factor, 1/psi

C_F = fracture permeability compaction factor, 1/psi

X_F = half axis of elliptical fracture, ft

BHP = Bottom-hole Pressure, psi

EUR = Estimated Ultimate Recovery

EPA = Enhanced Permeability Area

DV = Drainage Volume, ft^3

FMM = Fast Marching Method

SRV = Stimulated Reservoir Volume, ft^3

GA = Genetic Algorithm

RSM = Response Surface Methodology

DOE = Design of Experiments, Experimental Design

TABLE OF CONTENTS

Page

Page

Page

LIST OF FIGURES

Page

Page

Page

LIST OF TABLES

Page

CHAPTER I

INTRODUCTION AND STUDY OBJECTIVES

Modern reservoir management typically involves simulations of geological models to predict the range of recovery estimates and providing the economic assessment of different field development strategies. These geological models are constructed by measured data: either static data such as cores, well logs, seismic data, and distributed temperature sensor data, or dynamic data that are the time dependent measurements of flow responses such as pressure, flow rate, fractional flow. Geological models derived exclusively from static data often fail to reproduce the dynamic production history observed during the life of a commercial hydrocarbon system and will possibly give poor field performance prediction. Therefore, integrating reservoir dynamic responses is a vital step to developing reliable reservoir performance models. The process is referred to as "history matching" and is usually the most tedious and time-consuming aspect of modern reservoir managements.

1.1 Overview of History Matching

In traditional manual history matching, the model calibration has commonly been conducted on a single deterministic model by sequential trial-and-error adjustment of model parameters: from global, then to flow units (regional), followed local parameters, associated with reservoir energy, flood front progression and then individual well performance (Williams et al. 2004; Williams et al. 1998). This process is tedious and for large fields it becomes close to impossible to investigate relationships between the model responses and variations of different reservoir input parameters.

This dissertation follows the style and format of the *SPE Journal*.

Assisted history matching is similar to the manual history matching, except that computers and software tools are employed to adjust the reservoir parameters rather than direct intervention of reservoir engineers. Assisted history matching can be thought of as a minimization problem, whose objective function includes the sum of squared difference between observed data and computed data. In the recent decade, geologically-based assisted history matching techniques, which commonly focus on adjustment of fine-scale reservoir properties, especially permeability in order to integrate dynamic production data, have been an active area of research and a number of methods have been reported in the literature. Approaches to such data minimization process can be broadly classified into three categories: gradient-based, sensitivity-based and, derivative-free methods. Gradient-based methods typically converge slowly (Gill et al. 1981; McCormick and Tapia 1972); The derivative-free methods are simple to implement but limited to relatively small number of parameters because of the computational burden (Oliver et al. 2001). Sensitivity-based methods are attractive because of faster convergence compared to gradient-based methods (Bissell et al. 1992). However, an important and potentially computationally expensive part of sensitivity-based history matching is the computation of the sensitivity coefficients, which are the partial derivatives of the production response with respect to the reservoir parameters of interest. The streamline-based generalized travel time inversion (GTTI) technique has proven to be an efficient means for computing the parameter sensitivities (Cheng et al. 2005; Cheng et al. 2004; Datta-Gupta et al. 2001). This technique uses an analytic approach that involves 1D integration along streamlines to efficiently compute the parameter sensitivities. The streamline trajectories are based upon a single forward simulation, which can be from either a streamline or a finite-difference simulator. The GTTI history matching approach has been utilized in a large number of field applications (Cheng et al. 2004; Hohl et al. 2006; Qassab et al. 2003; Rey et al. 2009).

Most of approaches mentioned above generally start with a single initial geological model. However, if the initial model is not representative, specifically if the large-scale structural and stratigraphic features are not captured appropriately, these methods can

result in unrealistic updates to the reservoir model, e.g., large permeability changes in order to compensate for incorrect sand-sand juxtaposition at faults or the lack of appropriate vertical barriers. Besides, this model calibration approach usually results in a single deterministic history-matched model and thus, does not readily allow for uncertainty analysis.

Compared to local search techniques, global search algorithms to the history matching process avoids the problem of convergence to local optimum nearest to the initial starting point (Cheng et al. 2008). Global search techniques such as simulated annealing (SA) (Galassi et al. 2009; Kirkpatrick et al. 1983; Ouenes et al. 1994), Markov chain Monte Carlo (MCMC) (Ma et al. 2008; Sambridge and Mosegaard 2002) and genetic algorithms (GA) (Holland 1992) have been known to be effective for history matching problems (Bittencourt and Horne 1997; Floris et al. 2001; Romero and Carter 2001; Schulze-Riegert et al. 2002; Williams et al. 2004). These stochastic search techniques are favorable to gradient search methods when the structure of the solution space is not well understood, since they do not require complicated differential equations or a smooth search space; however, these methods require large number of flow simulations, which can be computationally prohibitive, particularly when the parameter space is very large. Although the problem can be alleviated to some extent by introducing a proxy as a surrogate model to avoid simulations for less likely candidates (Cheng et al. 2008; Pan and Horne 1998; White and Royer 2003; Yeten et al. 2005; Yeten et al. 2002), global searches are still costly for problems with large sets of unknown parameters.

1.2 Objectives and Dissertation Outline

Currently most effective strategies for traditional manual history matching commonly follow a structured approach with a sequence of adjustments from global to regional parameters followed by local changes in model properties, associated with matching for

pressure (reservoir energy), flood front progression, and individual well performance. In contrast, many of the automatic history matching methods utilize parameter sensitivities or gradients to directly update the fine-scale reservoir properties, potentially combining elements at all of these scales. In this work, we mainly present a hierarchical streamline-assisted history matching framework that emulates the traditional structured procedures but in a seamless manner. A probabilistic approach is used to understand the uncertainty in the large-scale static and dynamic parameters, followed by a streamline sensitivity-based deterministic model calibration for local permeability changes in order assimilate transient dynamic production data. We'll now outline the stages of this research and the specific objectives associated to each phase.

In Chapter II, we will first develop a hierarchical history matching method with global and local updates. In the probabilistic global calibration, design of experiments and response surface methodology with the genetic algorithm are used to calibrate the global parameters including multipliers for regional pore volumes, regional vertical and areal transmissibilities, fault transmissibilities and aquifer strengths. Key global parameters are first identified via a sensitivity analysis. A proxy model using experimental design and response surface methodology. Then a proxy-assisted genetic algorithm with heat-bath selection is used to generate an updated ensemble of models conditioned to static MDT pressures and total liquid rates at the wells, corresponding to a traditional pressure history match. Next, each ensemble member is updated using water-cut, GOR and flowing BHP via sensitivity-based local permeability calibration. We utilize streamline-derived analytic sensitivities to determine the spatial distribution and magnitude of these local changes.

In Chapter III, we then apply the genetic global calibration to unconventional shale gas reservoir, at the same time we include stimulated reservoir volume as a constraint in the data integration to improve history matching and reduce prediction uncertainty. First we introduce a novel approach for efficiently computing well drainage volume for shale gas wells with multistage fractures and fracture clusters. Next, we filter stochastic shale gas reservoir models by matching this fast drainage volume with the measured SRV

within specified confidence limits. Models passing SRV check will then proceed in evolutionary history matching for calibrating well pressure responses. In this process, SRV constrains the estimation of fracture parameters and shows better performance than response surface proxy model in the uncertainty quantification.

In Chapter IV, we show the value of integrating downhole temperature measurements as coarse-scale constraint in addition to streamline-based dynamic production data. We use a thermal model and a transient, 3D, multiphase flow reservoir model to calculate the wellbore temperature distribution in horizontal wells. We first derive coarse-scale permeability trends in the reservoir inferred from temperature data via MCMC algorithm. Then the coarse information are downscaled into fine scale permeability by sequential Gaussian simulation with block Kriging, and updated by local scale streamline-based history matching. The results show that combining production history matching with the temperature distribution in the wellbore, we can get an improved geological model that can match not only dynamic production history but also locate the water entry correctly, which provide guidance in optimizing well.

1.3 Software Prototype

The primary deliverable of this work will be a software prototype implementing an improved genetic algorithm with various optimization algorithms including design of experiments, response surface methodology and different genetic operators. The developed tool works in an object-oriented architecture where multiple attributes including well-based, and reservoir objects are stored in a dynamic hierarchical framework.

Policy-based design pattern was adopted for designing evolutionary history matching software, and therefore, each element of the methodology is ready to be implemented in different algorithms or interfaced with different external packages. For instance the application is already interfaced with several different industry standard commercial simulators as well as a streamline simulator from the MCERI research group at Texas

A&M University. Also, additional algorithms, for example different methods of experimental design can be easily implemented to replace the existing Latin Hypercube sampling design. This will lead to significant savings in time and man power in further development of new applications or algorithms.

CHAPTER II

GLOBAL-LOCAL MODEL CALIBRATIONS*

In this chapter we present a hierarchical streamline-assisted history matching approach that emulates the traditional structured procedures. First, a probabilistic approach is used to understand the uncertainty in the large-scale static and dynamic parameters, and to calibrate these global parameters. In this global calibration, the intent is to develop multiple plausible models that all match the field performance. This global calibration is followed by a streamline sensitivity-based deterministic model calibration for local permeability changes in which each of the distinct models created in the global match are history matched in additional detail.

2.1 Introduction

Modern reservoir management typically involves the use of history matched simulation models to predict the range of recovery estimates or to provide the economic assessment of different field development strategies. In traditional manual history matching, model calibration has commonly been conducted on a single deterministic model by sequential trial-and-error adjustment of model parameters: from global, then to flow units (regional), followed local parameters, associated with reservoir energy, flood front progression and then individual well performance (Williams et al. 2004; Williams et al. 1998).

In the recent decade, geologically-based assisted history matching techniques, which commonly focus on adjustment of fine-scale reservoir properties, have been an active

---

* Part of this chapter is reproduced with permission of the copyright owner from "A Hierarchical Streamline-Assisted History Matching Approach with Global and Local Parameter Updates" by Jichao Yin, Han-Young Park, Akhil Datta-Gupta, Michael J. King, Manoj K. Choudhary, 2010. Paper 132642 presented at SPE Western Regional Meeting, Anaheim, California, USA, 27-29 May. Further reproduction is prohibited without permission.

area of research and a number of methods have been reported in the literature. Integration of production data typically requires the minimization of a predefined objective function, which consists of a data misfit between observed and simulated production responses and appropriate penalty terms. There are a variety of approaches to such minimization, which can be broadly classified into three categories: gradient-based, sensitivity-based and, derivative-free methods. Gradient-based methods typically converge slowly (Gill et al. 1981; McCormick and Tapia 1972); The derivative-free methods are simple to implement but limited to relatively small number of parameters because of the computational burden (Oliver et al. 2001). Sensitivity-based methods are attractive because of faster convergence compared to gradient-based methods (Bissell et al. 1992). The streamline-based generalized travel time inversion (GTTI) technique has proven to be an efficient means for computing the parameter sensitivities (Cheng et al. 2005; Cheng et al. 2004; Datta-Gupta et al. 2001). This technique uses an analytic approach that involves 1D integration along streamlines to efficiently compute the parameter sensitivities. The streamline trajectories are based upon a single forward simulation. The GTTI history matching approach has been utilized in a large number of field applications (Cheng et al. 2004; Hohl et al. 2006; Qassab et al. 2003; Rey et al. 2009).

However, most of approaches mentioned above generally start with a single initial geological model. If the initial model is not representative, these methods can result in unrealistic updates to the reservoir model. Another drawback of this model calibration approach is that it usually results in a single deterministic history-matched model and thus, lacks uncertainty analysis. On the other hand, compared to local search techniques, global search algorithms avoids the problem of convergence to local optimum nearest to the initial starting point (Cheng et al. 2008). Global search techniques such as simulated annealing (SA) (Galassi et al. 2009; Kirkpatrick et al. 1983; Ouenes et al. 1994), Markov chain Monte Carlo (MCMC) (Ma et al. 2008; Sambridge and Mosegaard 2002) and genetic algorithms (GA) (Holland 1992) have been known to be effective for history matching problems (Bittencourt and Horne 1997; Floris et al. 2001; Romero and Carter

2001; Schulze-Riegert et al. 2002; Williams et al. 2004). These stochastic search techniques are favorable to since they do not require complicated differential equations or a smooth search space but they require large number of flow simulations, which can be computationally prohibitive when the parameter space is very large or when the forward simulation is costly. Although the problem can be alleviated to some extent by introducing a proxy as a surrogate model to avoid simulations for less likely candidates (Cheng et al. 2008; Pan and Horne 1998; White and Royer 2003; Yeten et al. 2005; Yeten et al. 2002; Yin et al. 2010), global searches are still costly for problems with large sets of unknown parameters.

In this chapter, we present a hierarchical assisted history matching framework which combines elements of both the stochastic and deterministic approaches to history match different levels of reservoir responses. First, the genetic algorithm, one of the derivative-free global search techniques, is used to estimate a relatively small set of uncertainties in large-scale geological features, resulting in a suite of models calibrated to the global reservoir response in field pressures and cumulative liquid production. Next, each of these models is further updated by a sensitivity-based model calibration for fine scale permeability changes to match flood front progression and individual well responses. We demonstrate our approach using both synthetic and field examples.

2.2 Approach Outline

2.2.1 Outline of Hierarchical History Matching Method

Our proposed method follows a two-step approach: global and local. First, in the global calibration we use design of experiments and response surface methodologies with evolutionary algorithms to calibrate global parameters associated with reservoir pressure such as regional pore volume multipliers, areal and vertical transmissibility multipliers, fault transmissibilities and aquifer strength. The global calibration step follows the steps outlined by Cheng et al. (2008) and Schulze-Riegert et al.(2003). The global objective function is defined as the sum of logarithms of multiple misfits between simulated and observed data which quantify reservoir energy and flow at a global level, such as field total fluid productions (total liquids, total water, and total gas), well shut-in bottom hole pressures (SBHP) and modular dynamic tester (MDT) or sequential formation tester (SFT) pressures. The outcome of the global calibration is an ensemble of plausible geological models matched to the reservoir energy and large scale connectivity.

The global updates are followed by local calibration where local parameter sensitivities are used to match water-cut development and well by well response. Specifically, grid-scale permeabilities will be adjusted for each ensemble member of the global match in order to match the water-cut, gas-oil-ratio and flowing bottom-hole pressure. Briefly, our hierarchical history matching approach consists of the following steps:

- ***Sensitivity analysis and proxy construction.*** A small set of key global parameters are first identified via a sensitivity analysis and low-level experimental design using high-low values for each of the potential parameters. A proxy of the objective function with respect to selected key global parameters is constructed using a detailed experimental design and response surface methodology (Pan and Horne 1998; Yeten et al. 2002). This proxy model will be used to prescreen models before an actual simulation is carried out. Here kriging

is used for constructing proxy model.

- ***Global model calibration.*** A genetic algorithm with a proxy check and a stretched heat bath fitness function (Sen et al. 1995) is used to generate updated ensemble of models conditioned to well MDT pressures, total liquid production and shut-in bottom-hole pressures. From the ensemble of updated models, a set of representative models are selected via a cluster analysis.
- ***Local model calibration.*** Each selected member of the globally calibrated ensemble is further calibrated to individual production history using a streamline-based sensitivity and the generalized travel time inversion (GTTI) technique (Cheng et al. 2006). We utilize streamline-derived analytic sensitivities to determine the spatial distribution and magnitude of the local permeability changes. Each model is re-examined to ensure that the global match is preserved after the local calibration. A 'norm' constraint which minimizes the property adjustments from the global model has generally ensured that the global match is not invalidated. **Fig. 2.1** shows a complete workflow of hierarchical history matching using global and local updates.

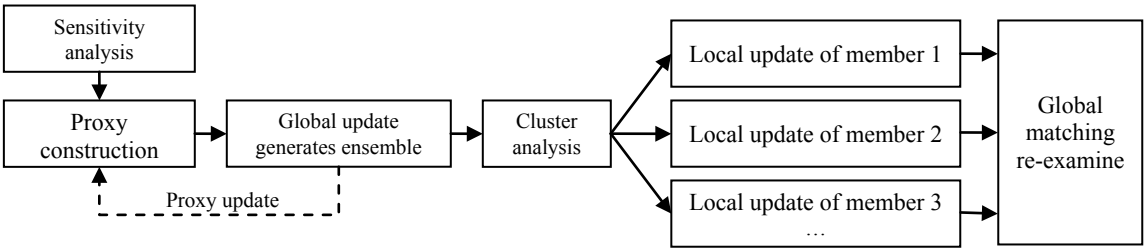

Fig. 2.1 Overview of hierarchical history matching

2.2.2 Illustration of the Procedure: A Synthetic Example

Before going into the mathematical details, we will first illustrate our procedure using a synthetic example, which is a three-dimensional three-phase reservoir consisting of 11×11×6 grid blocks, with one injector and four producers. For this synthetic example, we assumed that three global regions have been defined according to facies distribution in the geologic description: layers 1-2 is region 1, layers 3-4 is region 2 and layers 5-6 is region 3 (**Fig. 2.2**). First, a base model is defined that consists of the porosity and permeability fields in **Fig. 2.3** and **Fig. 2.4**, respectively. Then, a stochastic ensemble of initial models is generated by applying geologic structural multipliers to the base model. Through forward simulation, each initial ensemble member is then used to simulate the well production responses that are applied in the history match. For construction of the initial ensemble, the geologic structures deemed as globally uncertain include two vertical barriers located between the regions (TRANZ), regional pore volumes (PORV) and regional horizontal permeabilities (PERMX, PERMY). These 8 global unknowns, as shown in **Table 2.1** (reference multipliers shown in right column), will be calibrated to match field cumulative liquid production data. In local update, PERMX /PERMY /PERMZ are further calibrated at a higher resolution to integrate water-cut data. Results of the hierarchical history match are shown in **Fig. 2.5** and **Fig. 2.6**, which includes responses of the field and one of the producers P2, respectively. In both figures, the left-most column shows the initial model response, the center column shows the responses from the globally updated models, and the right-most column shows the result of the global-local update. Solid curves are the reference model response and are treated as the observed data. Last three columns of Table 2.1 also show three updated multiplier variables associated with results in Fig. 2.5 and Fig. 2.6.

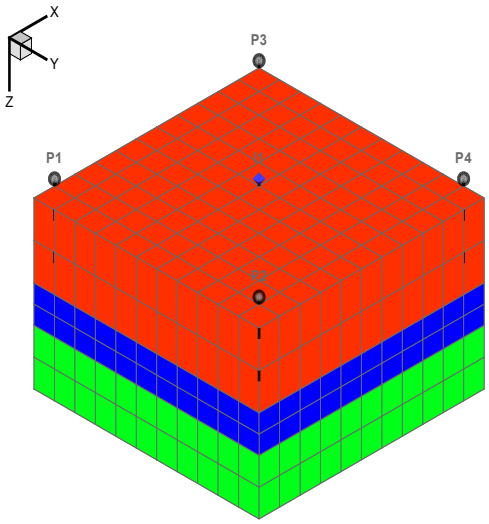

Fig. 2.2 Region definition

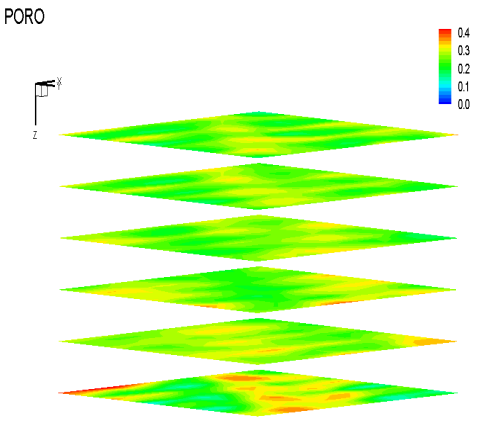

Fig. 2.3 Base porosity

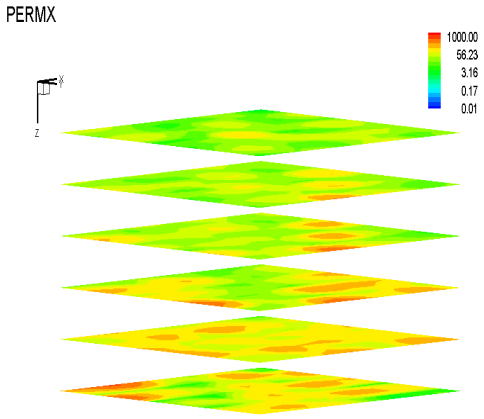

Fig. 2.4 Base horizontal permeability

Table 2.1 A full set of parameter definition and ranges

Variable Multipliers	Range	True	Model 1	Model 2	Model 3
TRANZ between zone 1 & 2	1E-7.00~1E-2.00	1E-6.00	1E-6.13	1E-2.35	1E-6.67
TRANZ between zone 2 & 3	1E-6.00~1E-1.00	1E-4.00	1E-2.98	1E-1.76	1E-5.17
Pore volume of zone 1	0.40~1.80	1.20	1.27	1.37	1.21
Pore volume of zone 2	0.30~1.00	0.80	0.64	0.85	0.65
Pore volume of zone 3	0.50~2.00	1.50	1.44	0.93	1.50
PERMX / PERMY of zone 1	0.50~4.00	1.80	1.72	2.12	1.78
PERMX / PERMY of zone 2	0.20~2.00	0.50	0.35	0.90	0.83
PERMX / PERMY of zone 3	0.80~5.00	1.60	1.52	1.33	1.69

- ***Results of global model calibrations.*** In Fig. 2.5, initially there are large discrepancies in field pressures, cumulative oil, and gas production. Also, in Fig. 2.6 the modeled MDT pressures are very different from observations, both in terms of locations and gradients. After global updates, in which SFT pressures and total fluid productions (WPT, GPT) are matched, not only total fluids and SFT but also reservoir pressures follow the observed data.

- ***Results of local model calibrations.*** The global update is followed by local model calibration using streamline-derived sensitivity in which grid block permeabilities are changed to match the production from each well. In Fig. 2.5 and Fig. 2.6 the right-most column shows responses from the final locally updated models. Note that matching of the local responses such as water-cut and GOR has not adversely impacted the global match.

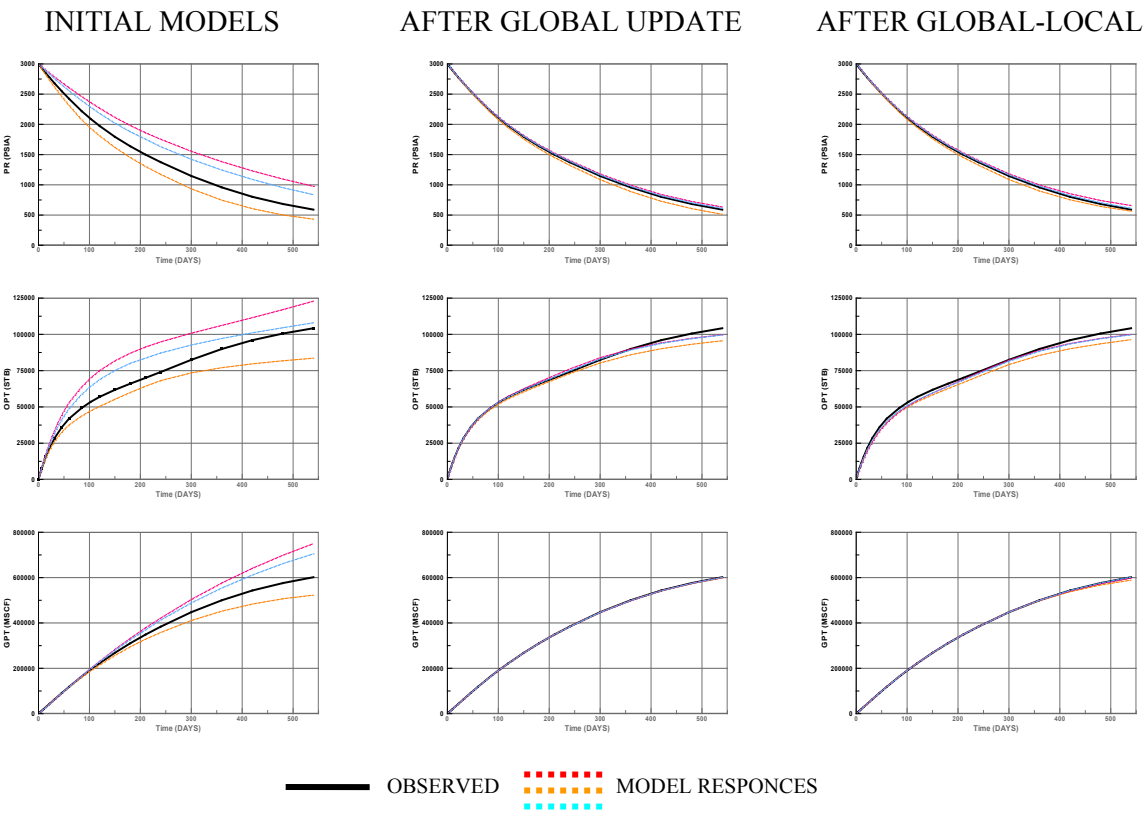

Fig. 2.5 Field pressure and total production of oil/gas

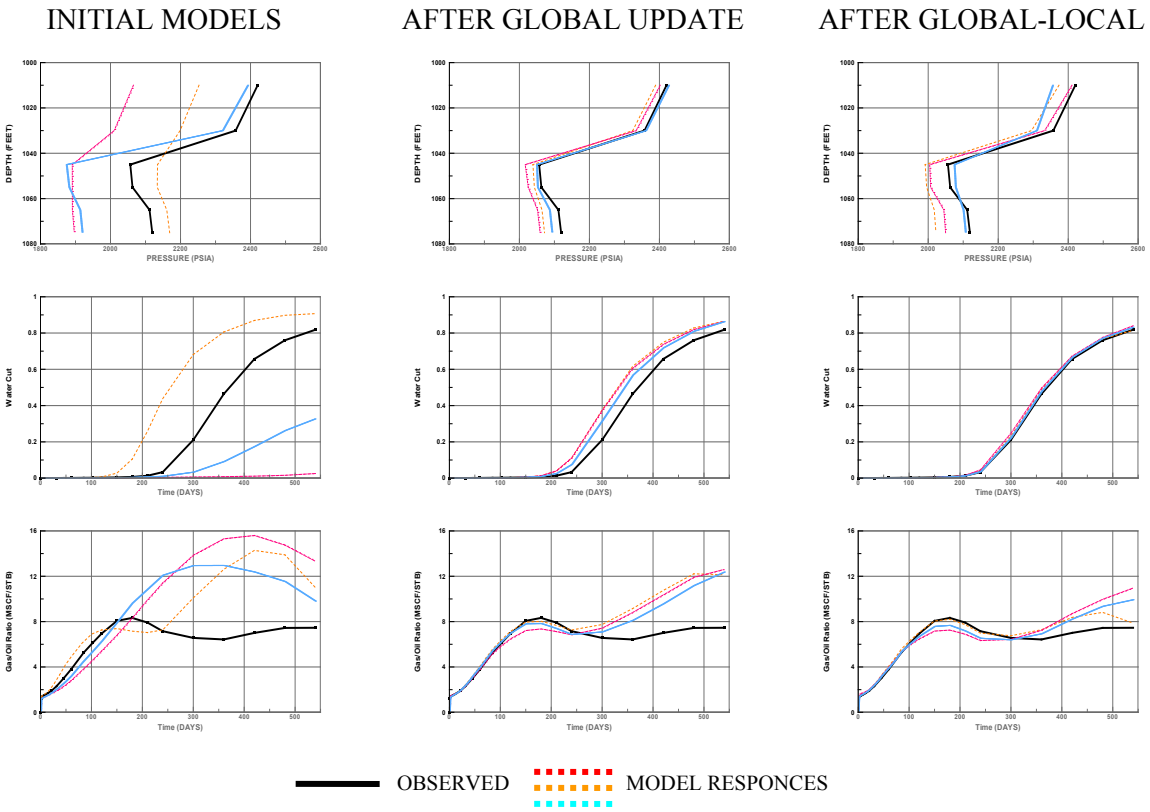

Fig. 2.6 Producer P2 MDT, water-cut and GOR

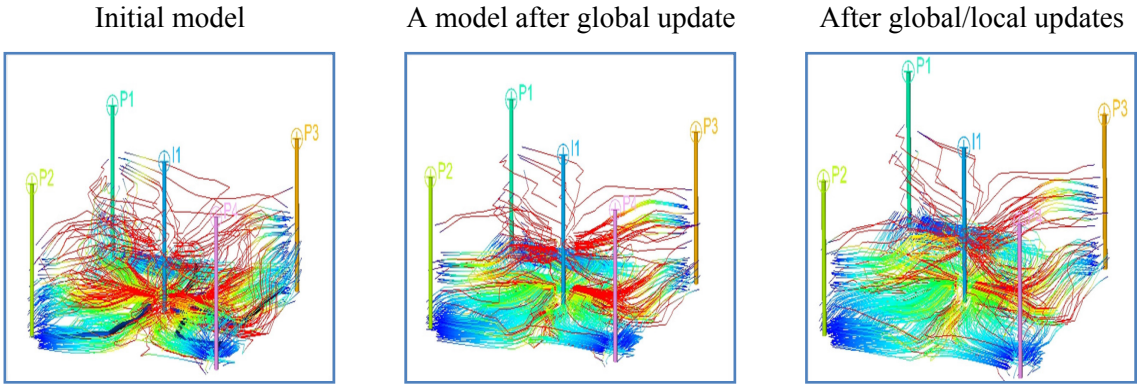

Fig. 2.7 Streamlines TOFs comparisons

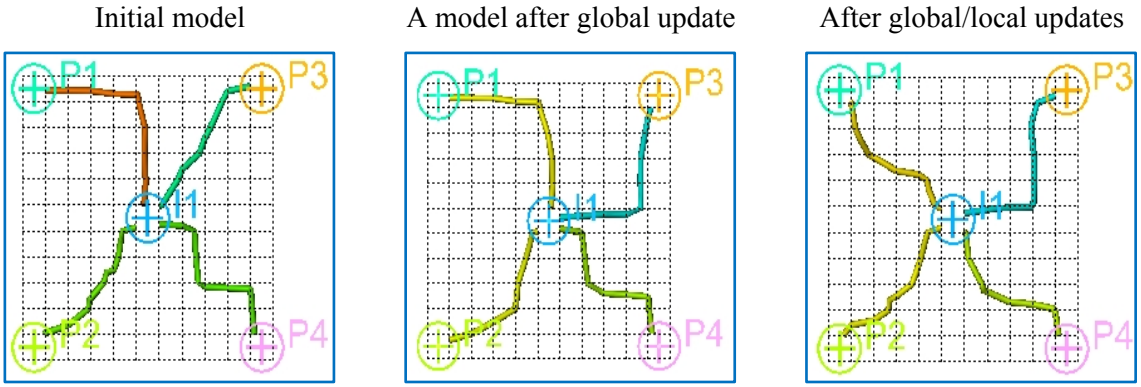

Fig. 2.8 Total liquid flux map comparisons

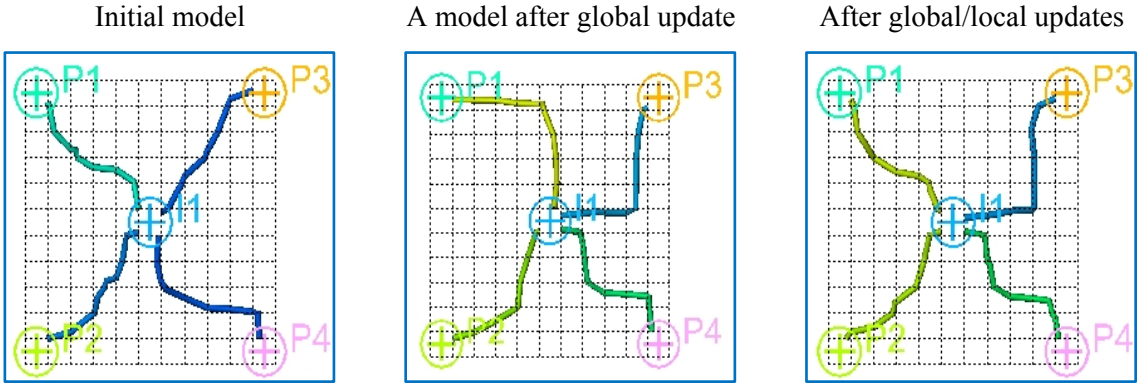

Fig. 2.9 Water flux map comparisons

- ***Flux map***. **Fig. 2.7** shows streamlines traced from finite difference simulation before and after the global-local updates. The streamlines are colored by the values of time-of-flight (TOF) from the producers. After the global update, model TOFs are generally reduced associated with an overall increase in lateral transmissibility. The detailed streamline trajectories continue to shift after the fine tuning from the local update of permeability inversion but we do not see the large changes associated with the global update. This reduction in streamline TOF's is consistent with the earlier water-cut breakthrough of the global and global-local updated models in Fig. 2.6. We can also visualize the flux between injectors and producers, and how it changes during the match, by displaying the breakthrough streamline for each well pair and coloring it by the total flux between those wells. Fig. 2.8 shows the total liquid (oil+water) flux and Fig. 2.9 shows the water flux. Both figures show the redistribution of flux among wells after the global and local updates.

2.3 Background and Mathematical Formulation

In the literature, there are previous researchers using evolutionary algorithm for reservoir characterization (Cheng et al. 2008; Schulze-Riegert et al. 2003; Yeten et al. 2002). Similarly, design of experiments (DOE), response surface methodology (RSM), and genetic algorithm (GA) have been used for calibrating reservoir geological features at the global and regional scales.

2.3.1 Define a Global Objective Function

The objective function is used to evaluate a proposed model by how well it can provide solution to our inverse problem. The smaller value of the objective function will result in higher probability of being selected by evolutionary algorithms during inversion.

Multi-objective optimization is considered when defining the global objective function since optimal decisions need to be taken in the presence of trade-offs between two or more conflicting objectives, specifically in this research, total liquid production, formation tester pressure, shut-in bottom-hole pressure. How to normalize, prioritize and weight the contributions of the various objectives in arriving at a suitable measure is non-trivial. A common approach in multi-objective optimization is to optimize a weighted average of all the objective functions:

$$f = w_1 f_1 + w_2 f_2 + \cdots w_n f_n \quad \text{.....(2.1)}$$

However, it is often difficult to choose appropriate weights for different objectives, especially when they are in different scales for example: pressure misfit in psi, total production misfit in STB et al. In the implementation of this research it is defined as sum of logarithm residual:

$$f = \ln f_1 + \ln f_2 + \cdots \ln f_n \quad \text{.....(2.2)}$$

Specifically for global model calibration, objective function in **Eq. 2.2** is defined as:

$$f(\mathbf{m}) = f(m_1, m_2, \ldots, m_N) = \ln |\Delta P_{MDT}| + \ln |\Delta Q| + \ln |\Delta P_{SBHP}| + \cdots \quad \text{.....(2.3)}$$

where **m** is the list of global variables, typically include regional pore volume multipliers, inter-regional transmissibility multipliers, shape and end-point parameters of relative permeability curves, coefficients of spatial basis functions from discrete cosine transformation (DCT) or grid connectivity based transformation (GCT) (Bhark et al. 2011a, 2011b). Right-hand-side objectives include Modular Formation Dynamics Tester (MDT) pressure misfit, cumulative liquid or oil production (LPT), shut-in bottom-hole pressure (SBHP) from well testing et al. By this definition, optimization algorithm will automatically reconcile large misfit term and gradually reduce all objective misfits.

2.3.2 Sensitivity Analysis and Proxy Construction by Experimental Design

Given a large set of potential parameters based on our concepts of geologic uncertainty, we perform a sensitivity analysis by a Plackett-Burman 2-level screening experimental design combining high and low values for each parameter (Beres and Hawkins 2001; Plackett and Burman 1946). Simulations will be performed for each of the experiments. Afterwards, the effects of each parameter on the objective function are ranked. The parameters with the strongest influence on the global objective function will be kept and other less sensitive parameters will be discarded. This is a standard procedure for parameter screening (Schulze-Riegert et al. 2003).

A proxy model is extremely helpful for large field applications since the response surface can be used to reject potential solutions where the proxy approximation to the objective function is higher than an acceptable threshold, without going through costly flow simulations (Cheng et al. 2008; White and Royer 2003; Yeten et al. 2005). Introduction of proxy models enables stochastic search algorithms such as GA, SA, MCMC to be practically feasible for field-scale applications, especially when relatively large numbers of parameters are input to the optimization problem. Proxy models are constructed assisted by efficient experimental design.

Fig. 2.10 shows a flowchart of sensitivity analysis and proxy construction, which serves as a perquisite for global update. Below are detailed steps of using experimental design to fulfill sensitivity analysis and assist initial proxy model construction.

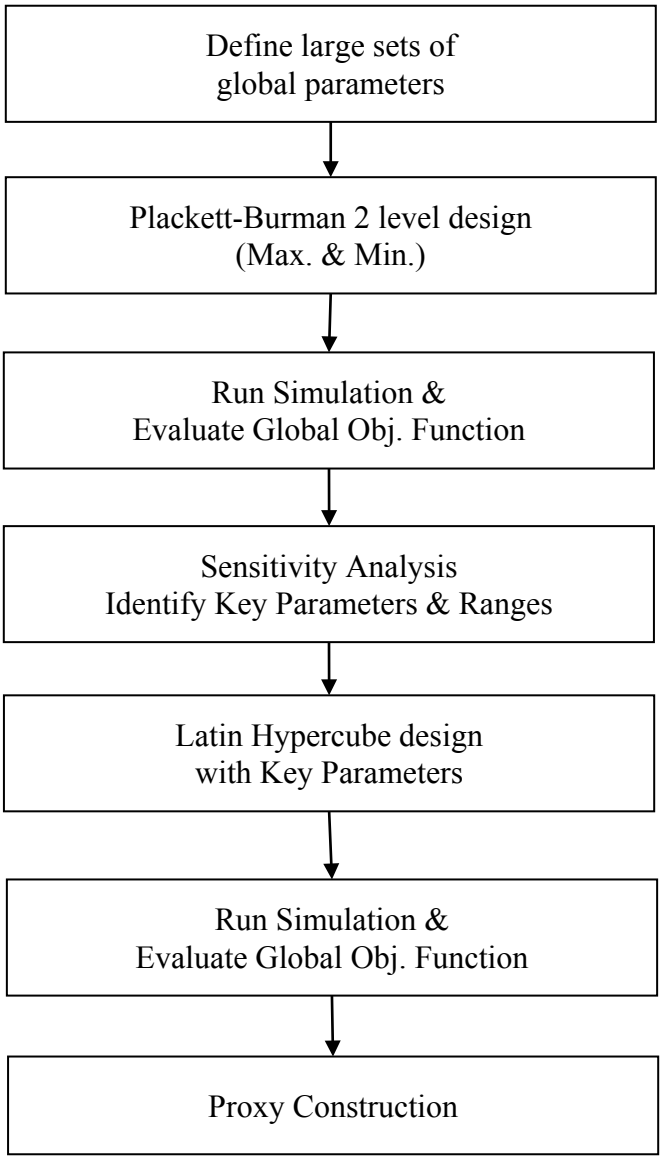

Fig. 2.10 Flowchart of proxy construction

Step 1: Plackett-Burman Design for Sensitivity Analysis

Plackett-Burman designs (PBD) are very economical two-level designs where the number of runs is only a multiple of four (rather than a power of 2) in two-level full factorial design. Often, individual factors or their interactions have no distinguishable effects on a response. This is especially true of higher order interactions. As a result, a well-designed experiment can use fewer runs for estimating model parameters. The theoretical minimum number is n+1. Commonly Plackett-Burman design, also called Hadamard designs, uses a Hadamard matrix to define this minimal number of runs (Ryser 1963). Hadamard matrices are matrices of 1's and -1's whose columns are orthogonal,

$$H^T H = HH^T = nI \quad \text{.....(2.4)}$$

An n-by-n Hadamard matrix with n > 2 exists only if mod(n, 4) = 0. Hadamard matrices can be generated by a general method called Reed–Muller code (Muller 1954; Reed 1954). A simplified special version called "Sylvester's construction" (Sylvester 1867), which gives symmetric and traceless Hadamard matrices, is demonstrated as:

$$H_1 = [1],\ H_2 = \begin{bmatrix} 1 & 1 \\ 1 & -1 \end{bmatrix},\ H_{2^k} = \begin{bmatrix} H_{2^{k-1}} & H_{2^{k-1}} \\ H_{2^{k-1}} & -H_{2^{k-1}} \end{bmatrix} = H_2 \otimes H_{2^{k-1}} \quad \text{.....(2.5)}$$

where for $2 \le k \le n$, $\otimes$ denotes the Kronecker product or tensor product of matrices. In this manner, Sylvester constructed Hadamard matrices of order 2^k for every non-negative integer *k*. In **Table 2.2**, last 7 columns of H_8 matrix give 8 runs for a 7-variable PBD; in **Table 2.3**, last 11 columns of H_{12} matrix give 12 runs for an 11-variable PBD, where 1 standards the upper-bound of a variable factor, and "-1" standards for its lower-bound. **Fig. 2.11** shows sparsity pattern of higher order Hadamard matrices and **Fig. 2.12** shows an example of Pareto chart from sensitivity analysis.

Table 2.2 PBD of 8 runs with 7 variables

Run	N/A	A	B	C	D	E	F	G
1	1	1	1	1	1	1	1	1
2	1	-1	1	-1	1	-1	1	-1
3	1	1	-1	-1	1	1	-1	-1
4	1	-1	-1	1	1	-1	-1	1
5	1	1	1	1	-1	-1	-1	-1
6	1	-1	1	-1	-1	1	-1	1
7	1	1	-1	-1	-1	-1	1	1
8	1	-1	-1	1	-1	1	1	-1

Table 2.3 PBD of 12 runs with 11 variables

Run	N/A	A	B	C	D	E	F	G	H	I	J	K
1	1	1	1	1	1	1	1	1	1	1	1	1
2	1	-1	1	-1	1	1	1	-1	-1	-1	1	-1
3	1	-1	-1	1	-1	1	1	1	-1	-1	-1	1
4	1	1	-1	-1	1	-1	1	1	1	-1	-1	-1
5	1	-1	1	-1	-1	1	-1	1	1	1	-1	-1
6	1	-1	-1	1	-1	-1	1	-1	1	1	1	-1
7	1	-1	-1	-1	1	-1	-1	1	-1	1	1	1
8	1	1	-1	-1	-1	1	-1	-1	1	-1	1	1
9	1	1	1	-1	-1	-1	1	-1	-1	1	-1	1
10	1	1	1	1	-1	-1	-1	1	-1	-1	1	-1
11	1	-1	1	1	1	-1	-1	-1	1	-1	-1	1
12	1	1	-1	1	1	1	-1	-1	-1	1	-1	-1

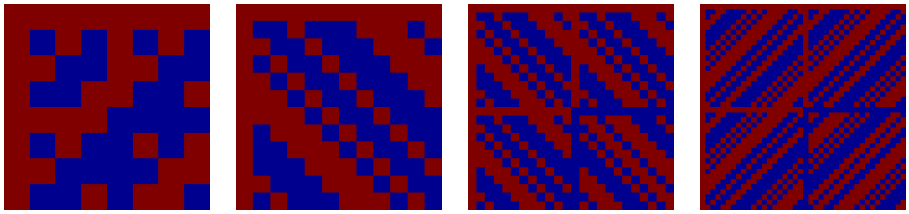

Fig. 2.11 Hadamard matrices of order 8, 12, 24, 40 for PB design

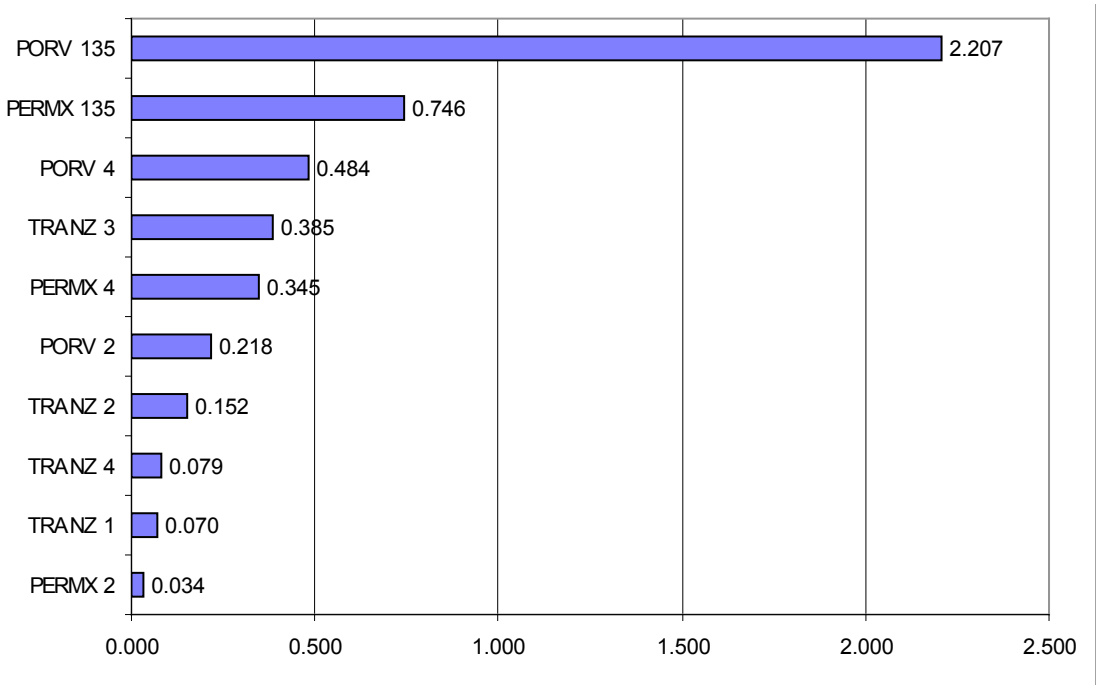

Fig. 2.12 An example of Pareto chart from sensitivity analysis

Step 2: Latin Hypercube Design for Efficient Initial Response Surface Sampling

Design of experiments is used to guide the proxy construction. Latin Hypercube Sampling (LHS) (Iman et al. 1980) with a space filling design (Yeten et al. 2005) is

implemented in this research to construct an initial proxy for the objective function with respect to the selected key global parameters. LHS is a stratified-random procedure, and provides an efficient way of sampling variables from their distributions. Unlike simple random sampling, this method ensures a full coverage of the range of each variable by maximally stratifying each marginal distribution. LHS requires fewer experiments compared to a full factorial design or a D-optimal design. **Fig. 2.13** is a demonstration of two-variable LHS design, in which 5 experiments were sampled. Steps for a Latin Hypercube sampling of N experiments include:

1) Divide CDF(0~1) of each variable into N intervals;
2) Sample uniformly CDF for each interval;
3) Get quantile at each sampled CDF value;
4) Randomly pair sampled variable values;
5) Iterate until minimum distance maximized or correlation minimized.

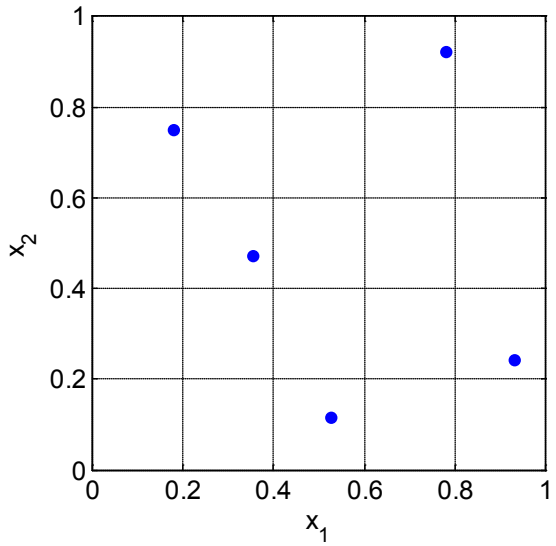

Fig. 2.13 Two-variable Latin hypercube sampling design of 5 experiments

Step 3: Dynamic Response Surface Construction by Kriging

A response surface, also called surrogate model or proxy, is an approximate representation of a real system or its simulation. It becomes useful even necessary when direct evaluation of a random sample is computationally expensive. In the literature there exist four types of proxy-models applied in reservoir simulation:

1) Polynomial regression (least square method);
2) Multivariate Kriging;
3) Thin-plate splines;
4) Artificial neural networks.

Among them Kriging (Krige 1951) and Thin-plate splines (Li and Friedmann 2005; Yeten et al. 2005) are data-exact, namely they will reproduce the observed value at a sampled location. Due to this and the relative simplicity, Kriging has been implemented in this research.

Kriging interpolates the value $Z(x_0)$ of a random field $Z(x)$ at an unobserved location x_0 from known observations $z_i = Z(x_i), i = 1,\ldots,n$ of the random field at nearby locations $(x_i, i = 1,\ldots,m \le n)$. It computes the best linear unbiased estimator $\hat{Z}(x_0)$ of $Z(x_0)$ based on a stochastic model of the spatial dependence quantified either by typically the variogram $\gamma(x, y)$ the random field. Generally, Kriging estimator is given by

$$\hat{Z}(x_0) = \sum_{i=1}^{m} w_i(x_0) Z(x_i) \quad \text{..... (2.6)}$$

Ordinary Kriging (OK) assumes a constant but unknown mean, and its weights fulfill the unbiasedness constraint $\sum_{i=1}^{m} w_i(x_0) \equiv 1$ by a Lagrange multiplier μ used in the minimization of the Kriging error in the ordinary Kriging equation

$$\begin{bmatrix} \gamma(x_1,x_1) & \cdots & \gamma(x_1,x_m) & 1 \\ \vdots & \ddots & \vdots & \vdots \\ \gamma(x_m,x_1) & \cdots & \gamma(x_m,x_m) & 1 \\ 1 & \cdots & 1 & 0 \end{bmatrix} \begin{bmatrix} w_1 \\ \vdots \\ w_m \\ \mu \end{bmatrix} = \begin{bmatrix} \gamma(x_1,x) \\ \vdots \\ \gamma(x_m,x) \\ 1 \end{bmatrix} \quad \text{..... (2.7)}$$

And ordinary Kriging error of **Eq. 2.7**

$$Var(\hat{Z}(x_0) - Z(x_0)) = \begin{bmatrix} w_1 \\ \vdots \\ w_m \\ \mu \end{bmatrix}^T \begin{bmatrix} \gamma(x_1,x_0) \\ \vdots \\ \gamma(x_m,x_0) \\ 1 \end{bmatrix} \quad \text{.....} \quad \text{(2.8)}$$

Several variogram models were developed to calculate the spatial correlation between the sampled points separated by a distance of *h*, while a power law variogram model is sufficient to give an interpolated response surface of acceptable quality.

$$\gamma(h) = ch^{\omega}, c = 1, 0 < \omega < 2 \quad \text{.....} \quad \text{(2.9)}$$

Fig. 2.14 shows steps of using Latin Hypercube design and Kriging for response surface. It shows that Kriging has data-exact feature at experiment points. In order not to have a singular covariance matrix of the Kriging system, redundant points, which are highly possible in stochastic inversion methods, are removed from experiment pool.

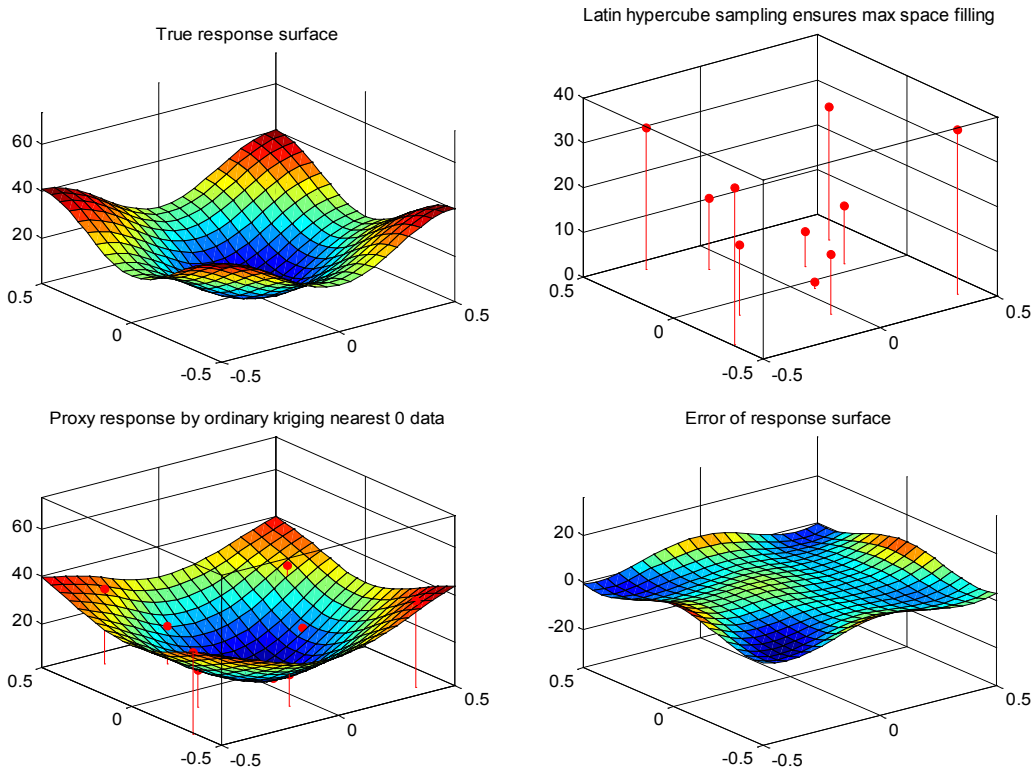

Fig. 2.14 Response surface by LHS design and Kriging is smooth and data-exact

The response surface will be improved later every time when a new experiment, here namely a new simulation occurs. So the proxy model will be better and better in approximating or surrogating the true response. However, if we use all existing experiments to construct a global response surface, the global covariance matrix in **Eq. 2.7** will be larger and large, thus closer and closer to singular when more and more data-points included, which will disable the further improvement of proxy model when more experiment points sampled. Therefore, only a small subset of experiment points will be used for Kriging the response surface. In this research, a given number, typically around twice the variable list lengths (number of degree-of-freedom), of points that are closest to every unknown point of interest are selected to construct a local response surface. **Fig. 2.15** and **Fig. 2.16** show that statistically majority (typically around 90%) of unknown

sample predictions by proxy model give less than 5% relative error compared to later true simulation runs. As more and more data, especially new ones with large error, are introduced to experiment candidate pool, future in-situ proxies become more and more accurate in estimating the performance of an unknown sample.

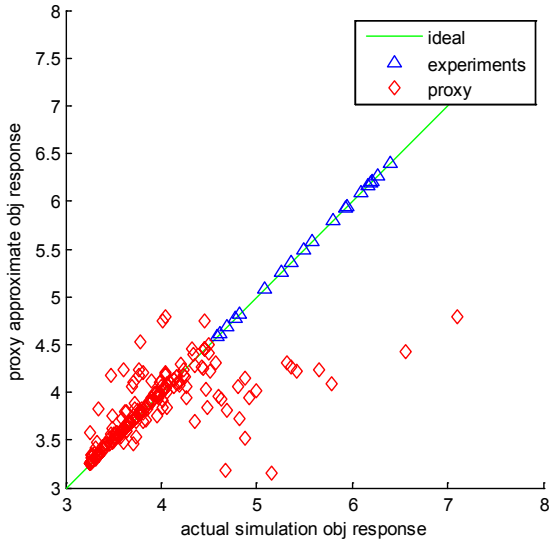

Fig. 2.15 Proxy uncertainty analysis

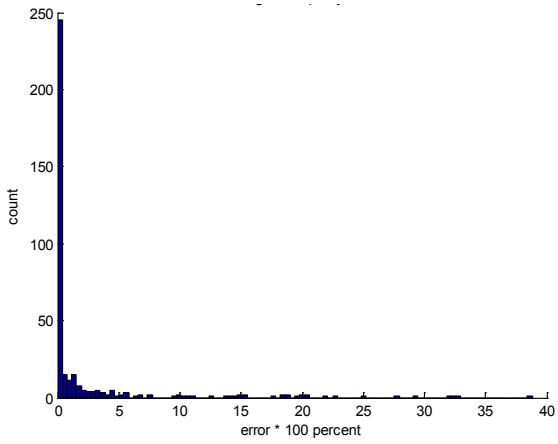

Fig. 2.16 Error histogram of response surface proxy model

2.3.3 Global Model Calibration Using Proxy-assisted Genetic Algorithm

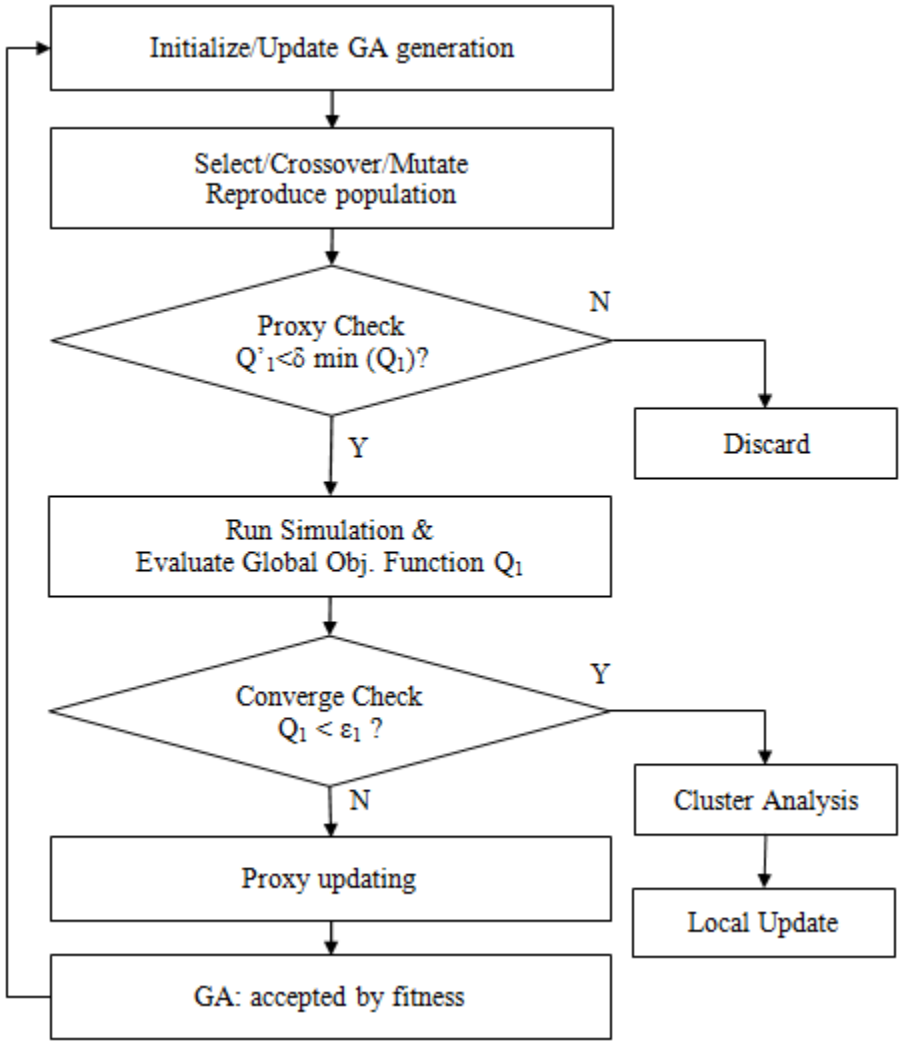

Fig. 2.17 Flowchart of GA with proxy

We have used the genetic algorithm (GA), one of the evolutionary algorithms, for calibration of global parameters. The genetic algorithm imitates biological principals of evolution – survival of the fittest. It has been extensively applied to the history matching problem (Bittencourt and Horne 1997; Floris et al. 2001; Romero and Carter 2001;

Schulze-Riegert et al. 2002; Williams et al. 2004). With outline of global model calibration shown in **Fig. 2.17**, several key things for a genetic algorithm (Wall 1996) are explained in following paragraphs.

Step 4: Representation of Variables: Encode a Genome

Usually, a list of degree-of-freedom (DoF) variables is encoded as binary strings of 0's and 1's. The full binary string containing all variables is called a genome or chromosome, and each genome represents a single solution to the problem. Genetic algorithm will evolve a population or populations of these binary strings and generate new ones, called "offspring", with the original ones called "parents". After genetic operations, the binary strings (also called genotype) will be decoded back into updated values of input DoF variables (also called phenotypes), and then tested with solving the inverse problem.

From **Table 2.4**, a continuous variable in range of [0.01, 2.56], linearly mapped into discrete domain [0, 255], that can be represented by an 8-bit binary number or string. Any further modification on the binary string will reflect on its phenotype values, which is the fundamental of using binary encoding for optimization.

Table 2.4 Binary encoding representation of one variable with 8 bits

Genotype	Binary string	Integer value	Phenotype
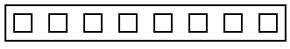	00000000	0	0.01 (min)
	11111111	255	2.56 (max)
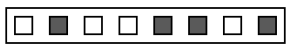	01001101	77	0.78

Generally, the evolution starts from a population of randomly generated individuals. In each generation, the fitness of every individual in the population is evaluated. Multiple individuals are stochastically selected from the current population (based on their fitness), and modified (recombined and possibly randomly mutated) to form a new population. The new population is then used in the next iteration of the algorithm. Commonly, the algorithm terminates when either a maximum number of generations has been produced, or a satisfactory fitness level has been reached for the population.

Step 5: Selection Operator for Optimal Subset to Reproduce Generation

For history matching problems, we minimize an objective function $f(\mathbf{m}_i)$ while maximizing the fitness of genomes, as in **Eq. 2.10**. This is equivalent to maximizing a fitness function g($\mathbf{m}_i$) (**Table 2.5**) Commonly selection is done by Roulette-wheel algorithm (**Fig. 2.18**), basically the probability of a sample $\mathbf{m}_i$

$$P(\mathbf{m}_i) = \frac{g(\mathbf{m}_i)}{\sum_i g(\mathbf{m}_i)} = \frac{\exp(-f(\mathbf{m}_i))}{\sum_i \exp(-f(\mathbf{m}_i))} \quad \text{..... (2.10)}$$

Table 2.5 An example of selection operator

m(i)	**1**	**2**	**3**	**4**	**5**	**6**
f(i)	0.100	0.600	0.200	0.050	0.300	0.800
g(i)	0.905	0.549	0.819	0.951	0.741	0.449
fraction	0.205	0.124	0.185	0.216	0.168	0.102

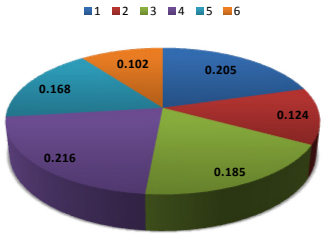

Fig. 2.18 Roulette-wheel selection

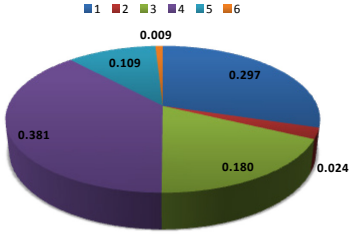

Fig. 2.19 Roulette-wheel selection with heat-bath stretching

Heat-Bath Algorithm. In our implementation of the GA, we incorporate a stretching of the fitness function to facilitate the selection process. Specifically, the 'heat bath' algorithm is a fitness scaling method that increases the probability of samples around the solution while speeding up the convergence (Sen et al. 1995). The selection probability of model $\mathbf{m}_i$ is given by:

$$P(\mathbf{m}_i) = \frac{g(\mathbf{m}_i)}{\sum_i g(\mathbf{m}_i)} = \frac{\exp[-f(\mathbf{m}_i)/T_n]}{\sum_i \exp[-f(\mathbf{m}_i)/T_n]}; \quad T_n = \alpha^n T_0; \quad 0 < \alpha < 1 \ldots\ldots\ldots\ldots \quad (2.11)$$

In **Eq. 2.11** T_n is a 'temperature' like parameter, which is gradually reduced at

regular intervals (*n* is incremented after a fixed number of generations) by a ratio of α as the population evolves, much like the simulated annealing algorithm (Kirkpatrick et al. 1983). To evaluate the objective function and thus the fitness of a newly generated genome, we first check the proxy value for that genome. If it has a value smaller than a predefined threshold then a flow simulation will be carried out. Otherwise it is assigned a large objective score with zero fitness and will be discarded in the next GA generation.

Fig. 2.19 shows that after heat-bath adjustment of fitness function when we are getting closer to global solution, fitness fraction of samples with lower objective function values are enlarged relatively to ones with higher objective functions, thus we can accelerate converging to stochastic solution compared Fig. 2.18. **Fig. 2.20** compares convergence with and without the heat-bath selection algorithm. Heat-bath accelerates convergence and thus requires fewer simulations to reduce the objective function to a same level. This completes the description of each stage of the global history matching process. A flowchart with all the steps is shown in **Fig. 2.17**.

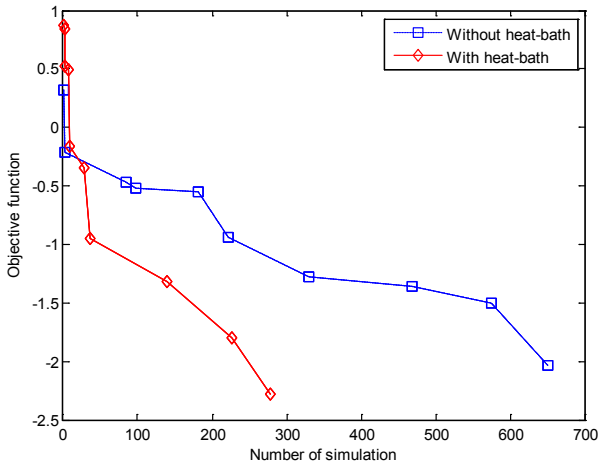

Fig. 2.20 Convergences GA with and without using heat-bath algorithm

***Elitism Algorithm*.** Elitism is not directly related to selection scheme but with similar effects in optimization (Pfeifer 2010). It addresses the problem of losing good solutions during the optimization process due to random effects. One way to deal with this problem is to combine the old population and the offspring, i.e., the mating pool after variation, and to apply a deterministic selection procedure—instead of replacing the old population completely by the modified mating pool. Alternatively, elitism always saves the best genome and carries over to the new generation.

In the implementation of this research for example, the whole population of samples are ranked and sorted by fitness scores, top 20%~30% samples (each of them took a full simulation and proxy evaluation time) preserved and rest of 70~80% samples substituted by newly reproduced samples. Practices proved that elitism is fundamentally important to speed up stochastic inversion process by save a lot of simulation runs. However, as every coin has two sides, elitism will increase the probability of trapping into local optima, therefore the GA solution are probably not the ideal search global optima. One should be very careful when choosing the parameter of replacing ratio for elitism.

Step 6: Crossover Operator Provides Local Hill-climbing

Crossover is the key process of producing new samples by recombining old samples. It is assumed that recombination of fitter parent will produce well and even better performing offspring, the major objective function reduction is accomplished by crossover operator locally. This step also differentiates GA from other evolutionary algorithms like evolutionary strategy (Cheng et al. 2008). However, under certain circumstances it is more favorable that crossover operator is not applied in every iteration, but rather with a "crossover probability", which is close to 100% (e.g. 90%) in the majority of cases.

Crossover is the major factor for new genomes and thus new samples (each sample composed of several genomes). A reasonable genetic algorithm should have crossover that allows population diversity while reducing the objective function. There are several different algorithms for crossover operator, which are all implemented in this research

from scratch.

Single-point Crossover. This is simplest scheme for binary genomes. A randomly is chosen position within a genome string from which it swap with another. As illustrated in **Fig. 2.21**.

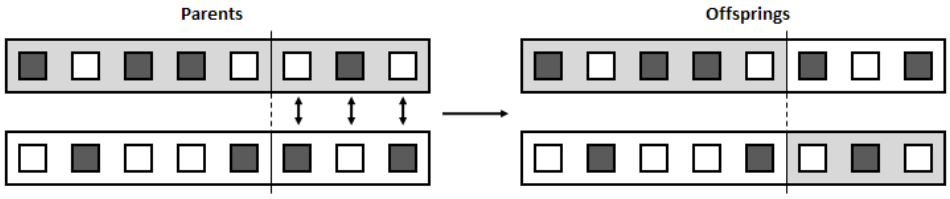

Fig. 2.21 Single-point crossover

Multi-point Crossover. Also called segmented crossover, n locations selected to partition genome into n+1 segments and each of last n segments (not the first segment) take a crossover probability to swap with same segment of the other genome, shown in **Fig. 2.22**.

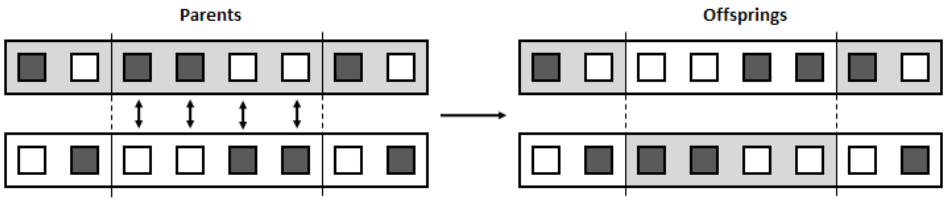

Fig. 2.22 Multi-point crossover

Uniform Crossover. At each position, the pair of bits from two parents will take a probability to swap. This probability is 0.5 always, shown in **Fig. 2.23**. Uniform crossover introduces diversity faster than n-point crossover (Pfeifer 2010) and thus is

selected by default in this chapter.

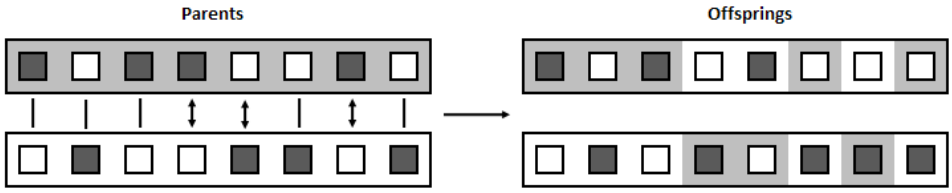

Fig. 2.23 Uniform crossover

Step 7: Mutation Operator Helps to Jump out of Local Optima

Mutation imitates "asexual" influences to a genome by for example environmental change. Though it is commonly paradoxical because most of them are harmful or at most neutral (Sawyer et al. 2007), it is still a key component to introduce new diversity to the generation. Each bit of a genome binary string flip with a very low (1/1000) probability, as shown in **Fig. 2.24**. The mutation step is typically following crossover for each recombined sample of string. For an optimization problem, most of the hill climbing is via gene reproduction by crossover while occasional mutation forces trial over all space thus provides chances to converge to global optima.

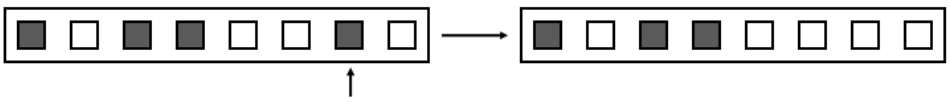

Fig. 2.24 Uniform mutation

Step 8: Cluster Analysis to Select Representative Models

At the final stage of the global model calibration, a representative ensemble of globally updated models is selected based on a similarity measure among the individual models that is quantified by a genome `distance'. The distance function, for either phenotype or genotype distance, determines how different one genome is from another. **Fig. 2.25** demonstrates an example of two-variable cluster analysis plotted in a normalized scaled. The clustering algorithm consists of an iterative partitioning that minimizes the sum of the within-cluster sums, of point-to-cluster-centroid distances, over all clusters. Following the cluster analysis, the model closest to each cluster-centroid is selected to proceed with local model calibration.

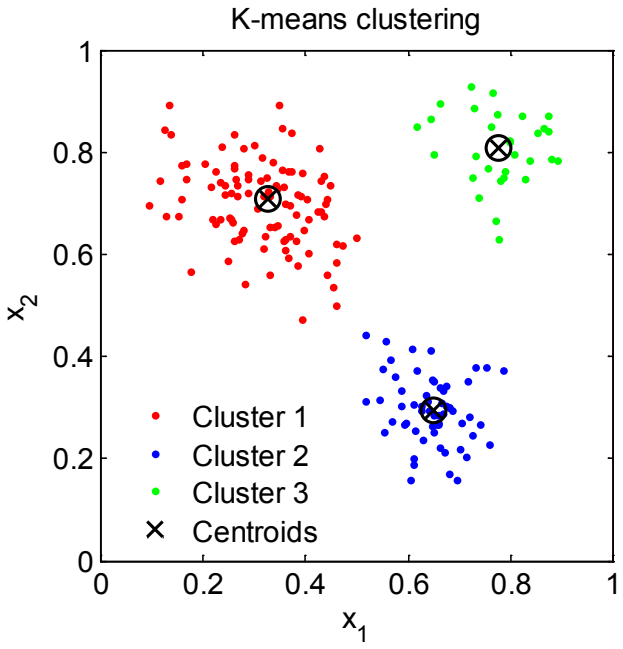

Fig. 2.25 An example of two-variable cluster analysis

2.3.4 Local Model Calibration Using Streamline Sensitivity and GTTI

The global updating results in a suite of representative models calibrated with respect to global and regional production and pressure data. Next, we use the streamline-based generalized travel time inversion to match the production response for each well. The details of the generalized travel time inversion can be found elsewhere (Cheng et al. 2005; He et al. 2002). **Fig. 2.26** illustrates a flowchart of local update.

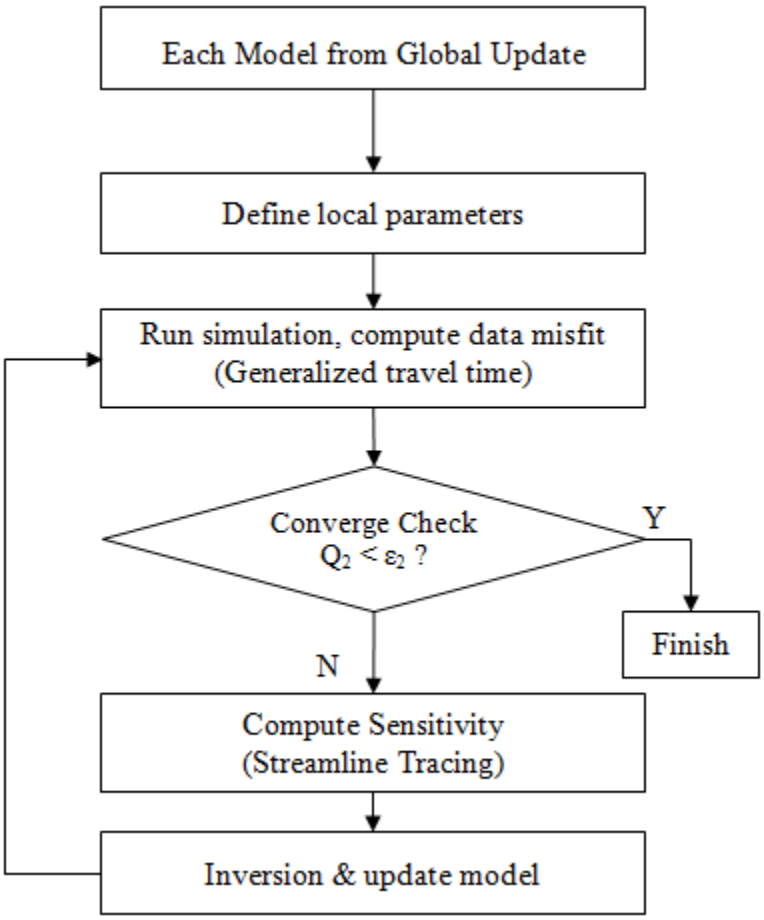

Fig. 2.26 Illustration of local model calibration

Step 8: Finite Difference Simulation and Streamline Tracing

The production response and fluid flow in the reservoir might be obtained using either a streamline simulator or a finite-difference simulator. Streamline models are not only computational efficient in run-time , but also offer some unique advantages for dynamic production data integration to field-scale geologic models. In streamline simulations, 3-D fluid flow calculations are approximated by a sum of 1-D calculations along streamlines. The streamline approach is extremely effective for modeling convection-dominated flows in the reservoir especially when heterogeneity is the predominant factor controlling oil recovery, for example in water-flooding (Datta-Gupta and King 2007). This is often the case when we have global model update that calibrates large scale reservoir fluids and movements such that the major model uncertainty lies on permeability heterogeneity.

Another important advantage of streamline formulations is that the sensitivity of travel time misfit with respect to logarithm of grid permeability exhibits quasi-linear relationship with the tight-of-flight of streamlines passing the grid block of interest (Cheng et al. 2005), which greatly facilitates inversion process. In this step, we'll utilize finite difference simulation for its versatility and robustness in modeling complex flow physics, such as three-phase, unfavorably displacing etc, and geologic features, such as faults, non-neighbor connections etc, while streamlines are constructed based on numerical velocity fields generated by the finite difference simulator, sensitivity of travel time misfit to logarithm permeability can be formulated from streamlines (Cheng et al. 2006; He et al. 2002).

Step 9: Generalized Travel Time Inversion Using Streamline Analytical Sensitivity

The production data integration via local updating involves the minimization of a penalized misfit function as given below

$$f(\delta\mathbf{R}) = \left\| \Delta\tilde{\mathbf{t}} - \mathbf{S}\delta\mathbf{R} \right\| + \beta_1 \left\| \delta\mathbf{R} \right\| + \beta_2 \left\| \mathbf{L}\delta\mathbf{R} \right\| \quad \text{.....(2.12)}$$

In the above equation, the first term includes data misfit, which is quantified by taking individual well response (either water-cut or GOR) and systematically shift observed to simulated response to get max correlation between the two, this correlation defined by

$$r^2(\Delta t_j) = 1 - \frac{\sum\left[y_j^{obs}(t_i + \Delta t_j) - y_j^{cal}(t_i)\right]^2}{\sum\left[y_j^{obs}(t_i) - \overline{y_j^{obs}}\right]^2} \quad \text{.....(2.13)}$$

We call the optimal time-shift when *r* maximized in **Eq. 2.13** generalized travel time (GTT) misfit (He et al. 2002), as denoted by $\Delta\tilde{\mathbf{t}}$ in Eq. 2.12. **Fig. 2.27** shows the optimal time-shift according to the correlation function.

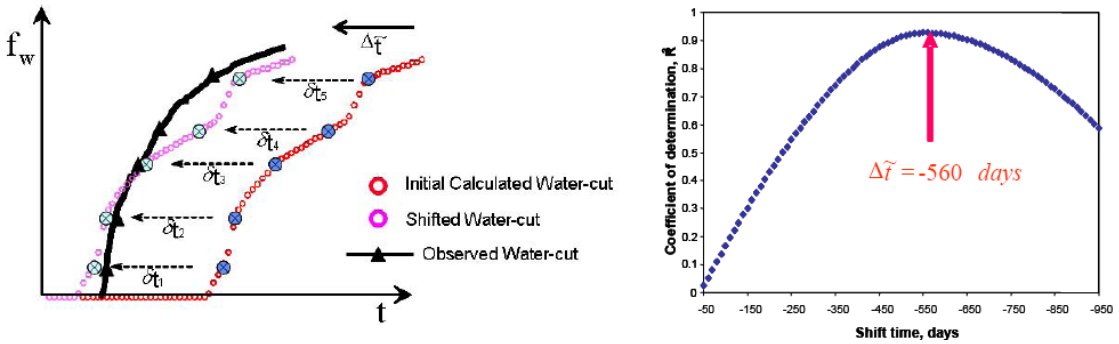

Fig. 2.27 Generalized travel time misfit and correlation function (Cheng et al., 2004)

We are try to minimize this misfit using streamline analytical sensitivities (Cheng et al. 2006), **S** denotes the sensitivity of the GTT at each well with respect to grid log permeability while **δR** corresponds to the change to make to minimized GTT misfit.

The second term is the 'norm' penalty and the third term is the roughness penalty, and **L** is a second-spatial-difference operator. The first term ensures that the difference

between the observed and model simulated production responses is minimized. The second term, 'norm' penalty minimizes the changes to the globally updated model. This ensures that the global misfit is not adversely impacted by the local updates, and is an important characteristic of our approach.

The third term is a roughness penalty that ensures that the changes to the model are smooth and consistent with the large-scale and low resolution of the production data. The weights β_1 and β_2 determine the relative strengths of the prior model and the roughness term. The selection of these weights can be somewhat subjective although there are guidelines in the literature (Parker 1994). In general, the inversion results will be sensitive to the choice of these weights. The minimization of **Eq. 2.12** leads to an augmented least-squares system of equations is given as follows.

$$\begin{pmatrix} \mathbf{S} \\ \beta_1 \mathbf{I} \\ \beta_2 \mathbf{L} \end{pmatrix} \delta\mathbf{R} = \begin{pmatrix} \Delta\tilde{\mathbf{t}} \\ \mathbf{0} \\ \mathbf{0} \end{pmatrix} \quad \text{.....(2.14)}$$

An iterative least squares solution approach via the LSQR algorithm (Paige and Saunders 1982) is used to solve **Eq. 2.14**.

For sensitivity calculation, consider two-phase incompressible flow of oil-water in a nondeformable, permeable medium, the transport equation can be written in the streamline time-of-flight (TOF) coordinates as follows (Cheng et al. 2005; Datta-Gupta and King 2007)

$$\frac{\partial S_w}{\partial t} + \frac{\partial F_w}{\partial \tau} = 0 \quad \text{.....} \quad (2.15)$$

where τ represents time of flight which is the travel time along a streamline, ψ, and s(**x**) is the "slowness" defined as the reciprocal of the total interstitial velocity

$$\tau = \int_{\psi} s(\mathbf{x}) dr \quad \text{.....(2.16)}$$

$$s(\mathbf{x}) = \frac{1}{|\mathbf{v}(\mathbf{x})|} = \frac{\phi}{k\lambda_{rt}|\nabla P|} \quad \text{.....} \quad (2.17)$$

With the assumption that streamline paths do not shift significantly because of small changes in reservoir properties we can relate the change in travel time to the change in reservoir properties and thus slowness by

$$\delta\tau = \int_{\psi} \delta s(\mathbf{x}) dr = \int_{\psi} \left(\frac{\partial s}{\partial k}\delta k + \frac{\partial s}{\partial \phi}\delta\phi \right) dr = \int_{\psi} \left(-\frac{s}{k}\delta k + \frac{s}{\phi}\delta\phi \right) dr = \int_{\psi} \left(s\delta \ln k + \frac{s}{\phi}\delta\phi \right) dr \quad (2.18)$$

....

In this research effective permeability are primary parameters to calibrate, therefore

$$\frac{d\tau}{d\ln k} = \int_{\psi} s dr \quad \text{.....} \quad (2.19)$$

Which can be further related to arrival time of a particular concentration (e.g., water front) by

$$\frac{\partial t}{\partial \ln k} = \frac{\partial t}{\partial \tau}\frac{d\tau}{d\ln k} = \frac{dS_w}{dF_w}\frac{d\tau}{d\ln k} \quad \text{.....} \quad (2.20)$$

And this generalized travel time (GTT) sensitivity can be calculated by averaged sensitivities for all time steps for the well of interest. It is:

$$\mathbf{S} = \frac{d\Delta\tilde{t}_j}{dm} = -\overline{\frac{\partial t_j}{\partial m}} \quad \text{.....} \quad (2.21)$$

where m is the reservoir parameter, j is the well number, and **S** is the sensitivity, and this sensitivity will be used for dynamic data integration.

Step 10: Model Reexamination

Before finishing inversion, models from local update need to be checked for consistency with geology, as well as global model calibration, since local model calibration starts with multiple dissimilar models, some of which might be unrealistic in terms of matching dynamic production data. This is especially true because β_1 in Eq. 2.12 serves to limit the globally-updated models from changing dramatically and may result in models that fail to provide good data matches as quantified by the local objective function terms. However, from the global updates we are provided a large population of models with diversity and, subsequently, those (typically few models according to our experience) that are potentially viable for global model calibration but unviable for local model calibration are discarded during the last workflow step, i.e. model re-examination while the majority of models give reasonable improvements in the local objectives with limited permeability updates. Therefore, looping back to global calibration is typically unnecessary because the local calibration induces small, grid-cell-scale changes to the permeability that do not deteriorate the global update. Additionally, from the initial ensemble there are typically several alternative models that are consistent with the observation data after both global and local updates.

2.4 Field Application of Global and Local Model Updates

In this section we demonstrate the application of our proposed approach with the full field history match of a turbidite reservoir.

2.4.1 E Field Descriptions

The E field was discovered in May 2001. To date, thirty-three exploration and appraisal wells have been drilled, which identified multiple hydrocarbon accumulations, principally in normally pressured Campanian-age reservoirs. Seismic mapping (**Fig. 2.28**) identifies two meandering east-west canyons that were initiated during the Albian and persisted through at least the Campanian. The north-east canyon is where the reservoir E is located. The E reservoir has an average depth of 1,000 m and dips on a monocline to the northwest as shown in **Fig. 2.29**, in approximately 65 m of water. Six down-to-basin normal faults, initiated during the Campanian, occur near and eastward of one of the up-dip appraisal wells. Faults within the reservoir do not appear to be sealing, but may be baffles to fluid communication. An oil-water contact is identified in one of the appraisal wells but no free gas or gas-oil contact has been observed.

The reservoir is subdivided vertically into zones or genetic units between erosional bounding surfaces, which generally correspond to Campanian biostratigraphic markers. Within these zones, mappable seismic events (seismic geobodies) further define individual sandstones and associated facies. The structural framework was built to represent seven zones within the E reservoir. Each zone was divided into multiple layers utilizing proportional layering resulting in a total of 424 layers. 22 faults were incorporated into the model resulting in 12 fault blocks which were also used as material balance regions in the simulation model. Most geobodies appear to be in pressure communication based on the development drilling results and are interpreted as channel sands with associated lateral and vertical facies. Four primary facies associations have been identified:

- Channel Facies: Facies 1 and Facies 5. These facies is associated with the highest reservoir quality, represented by the highest permeability and the lowest water saturations.
- Interchannel / Channel Margin / Channel Abandonment Facies: Facies 2 (2 to 20 cm thick sand beds) and Facies 3 (<2 cm sand-shale interbeds).
- Hemipelagic Mudstones / Muddy Debris Flows: Facies 6 (massive to finely laminated and highly contorted mudstones).
- Carbonate-Cemented Sandstones, Conglomerates, and Mudstones: Facies 4.

The E reservoir is currently being produced and developed from a Central Processing Facility (CPF) and three satellite platforms. Currently there are 13 active producers and six active injectors (**Fig. 2.30**) in this field. Production commenced from this field in December 2006 and water injection commenced in April 2007. Production and injection history for the E field is shown in **Fig. 2.31**. A few months after the start of water injection in April 2007, some of the mid dip producers showed water cut development. Currently the water cut is increasing at four of the producers. The E field is currently being operated under a combination of depletion and pressure maintenance strategy to maximize oil recovery. In order to maximize reserves, certain key elements of field management are being implemented (e.g. conservation of reservoir energy, application of artificial lift, reservoir surveillance etc.) and a better calibrated full field model will support these activities.

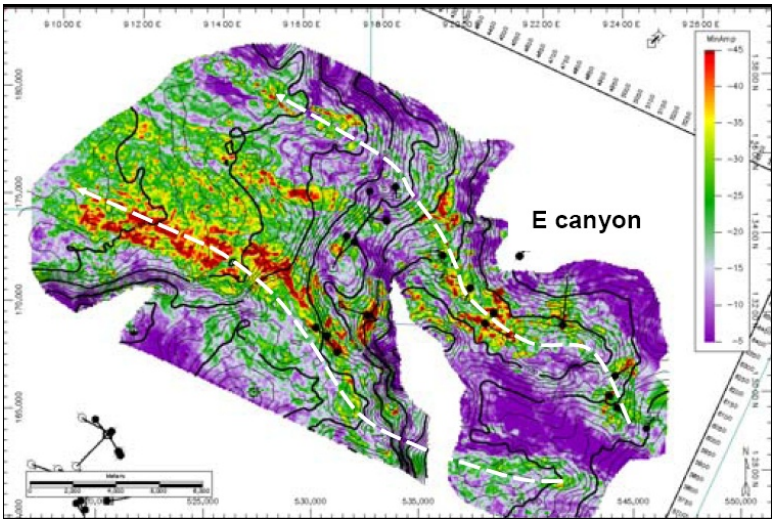

Fig. 2.28 E field seismic amplitude map

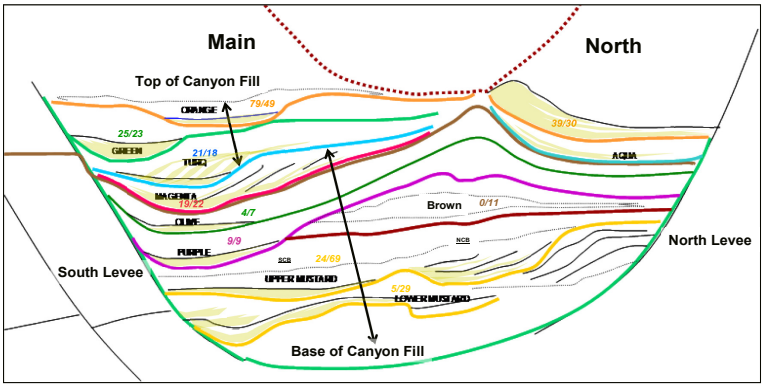

Fig. 2.29 E field reservoir stratigraphy

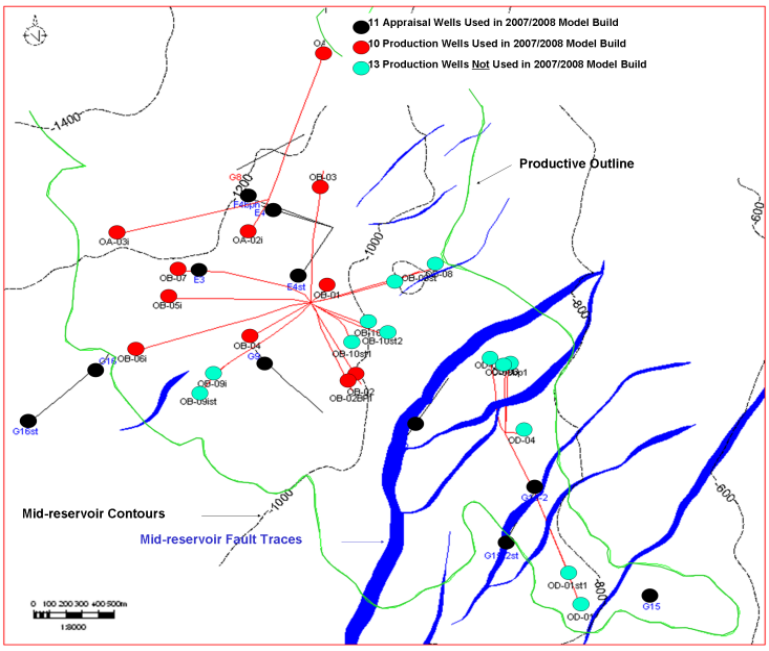

Fig. 2.30 E field configuration of wells and faults

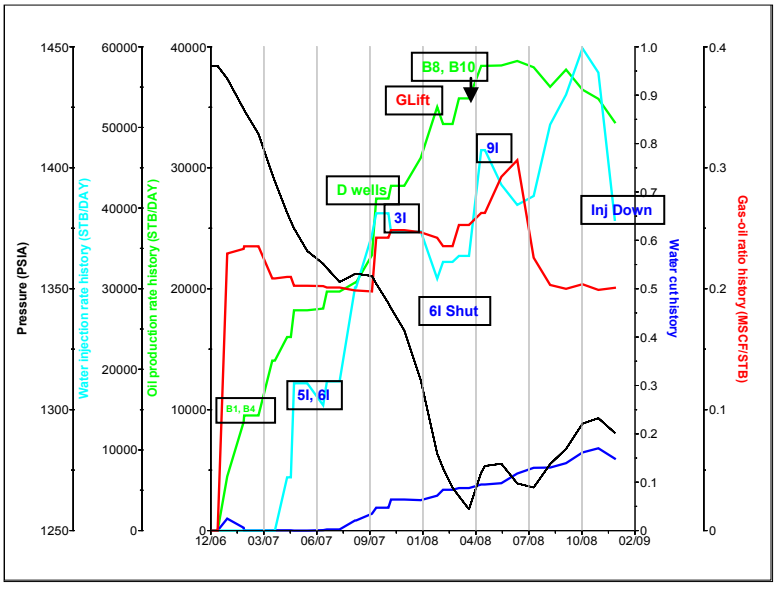

Fig. 2.31 Field historical production and injection

2.4.2 Geological Modeling

In the first stage of modeling for this field, multiple static geological realizations of the reservoir were created to evaluate the oil in place, reservoir behaviors, and to optimize the development plan. Seismic volumes are used to condition the distribution of facies as the seismic data contains an imprint of the depositional architecture. Experimental design methodology was used to perform the uncertainty analysis while minimizing the number of models required.

Table 2.6 shows a full set of uncertainty parameters during geologic modeling. These uncertainties were reduced to three static uncertainty variables (first three rows in Table 2.6) after a screening procedure using the sensitivity analysis. Afterwards, 27 geomodels were built by a full three-level (P10, P50, P90) factorial design of these three static uncertainties: facies (**Fig. 2.32**), water saturation and porosity. The factorial design provides the means to efficiently evaluate the interaction and impact of each variable over the full range of uncertainty during the model construction.

All geomodel realizations honor the fluid contact data and seismically defined stratigraphical relationships. Away from the wells, seismic attributes are used to condition the geomodels.

Table 2.6 Uncertainty parameters in geological modeling

	Uncertainty Variables	Low Value	Mid Value	High Value	Distribution
Static Uncertainties	Facies	-1	0	1	Discrete Uniform
	Water Saturation	-1	0	1	Discrete Uniform
	Porosity	-1	0	1	Discrete Uniform
Baffles/Barriers	Inter-Region Transmissibility Multipliers	1.E-06	1.E-03	1.E+00	Continuous Uniform
	Fault Transmissibility Multipliers	1.E-06	1.E-03	1.E+00	Continuous Uniform
Relative Permeability	Sorw1(Thin Bed)	0.30	0.36	0.42	Continuous Uniform
	Sorw2(Thick Bed)	0.25	0.32	0.38	Continuous Uniform
	Krwe1	0.30	0.45	0.60	Continuous Uniform
	Krwe2	0.21	0.33	0.45	Continuous Uniform
	Nw1	1.50	1.05	0.60	Continuous Uniform
	Nw2	2.50	2.00	1.50	Continuous Uniform
	Now1	3.20	11.60	20.00	Continuous Uniform
	Now2	2.40	2.80	3.20	Continuous Uniform
Rock Property	Rock Compressibility	5	20.50	36	Continuous Uniform
Pore Volume	Aquifer PV Multiplier	1	10.50	20	Continuous Uniform
Transmissibility	Horizontal Transmissibility	0.5	0.75	1	Continuous Uniform
	Vertical Transmissibility	0.1	0.55	1	Continuous Uniform

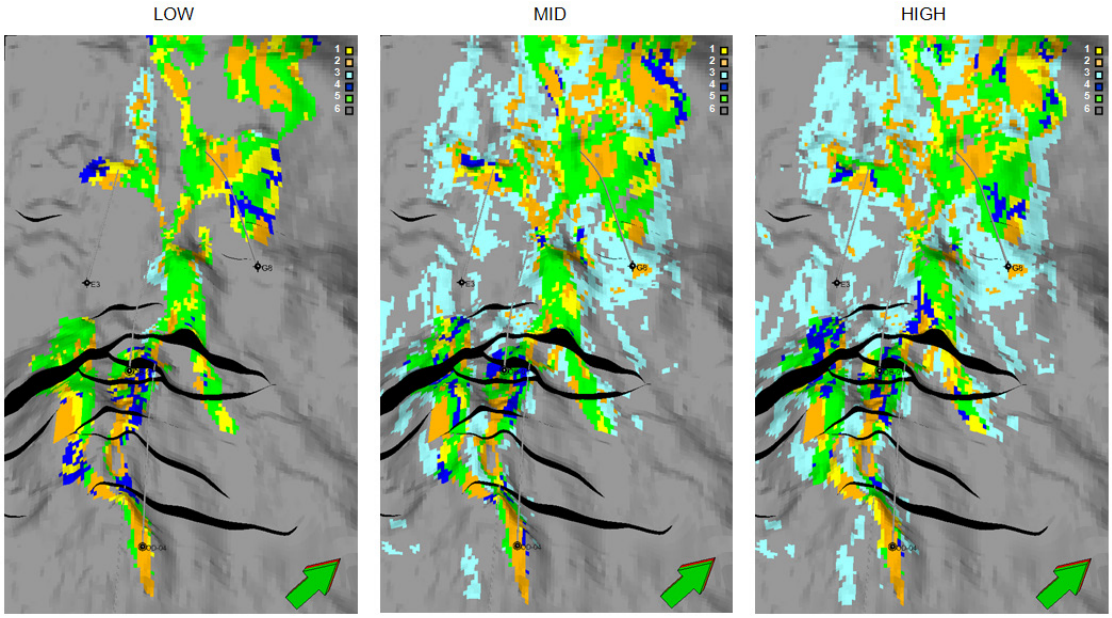

Fig. 2.32 Geological modeling example: facies- Low/Mid/High cases

Table 2.7 List of key global variables and their ranges from sensitivity analysis

Variable multipliers	Low	High	Matched
PORV of zone 2 (layer 51-75)	1.00	2.00	1.10
TRANZ of zone 2 & 3 (layer 75)	1.00E-08	1.00E-05	3.43E-07
PORV of zone 3 (layer 76-95)	0.10	1.00	0.563
PORV of zone 4 (layer 96-120)	0.10	1.00	0.537
PORV of zone 5 (layer 121-140)	0.10	1.00	0.724
PORV of zone 6 (layer 141-175)	0.10	1.00	0.522
TRANZ of zone 6 & 7 (layer 175)	1.00E-08	1.00E-05	1.36E-06
PORV of zone 7 (layer 176-210)	0.40	0.90	0.831

In the second stage, each of the 27 geomodels was calibrated using proxy GA to condition well data including shut-in bottom-hole pressures, MDT pressures and up to date cumulative liquid productions. Each updated ensemble of geomodel realization provides an estimation of STOIIP and a deterministic view of the reservoir heterogeneity. Specifically, for each geomodel, regional and inter-regional uncertainties were introduced and analyzed including pore volume multipliers and horizontal permeability multipliers for each zone, and vertical transmissibility multipliers between zones. **Table 2.7** shows the final list of key global variables for GA after sensitivity analysis of a selected geomodel, and the right column shows a realization of updated multipliers.

2.4.3 Results of Global and Local Updates

Fig. 2.33 shows the well MDT pressure match for one geomodel selected after the global update. Blue triangles represent measured MDT pressures, red solid lines are the uncalibrated model responses from the geomodel without property adjustment and the dashed lines are the updated global models.

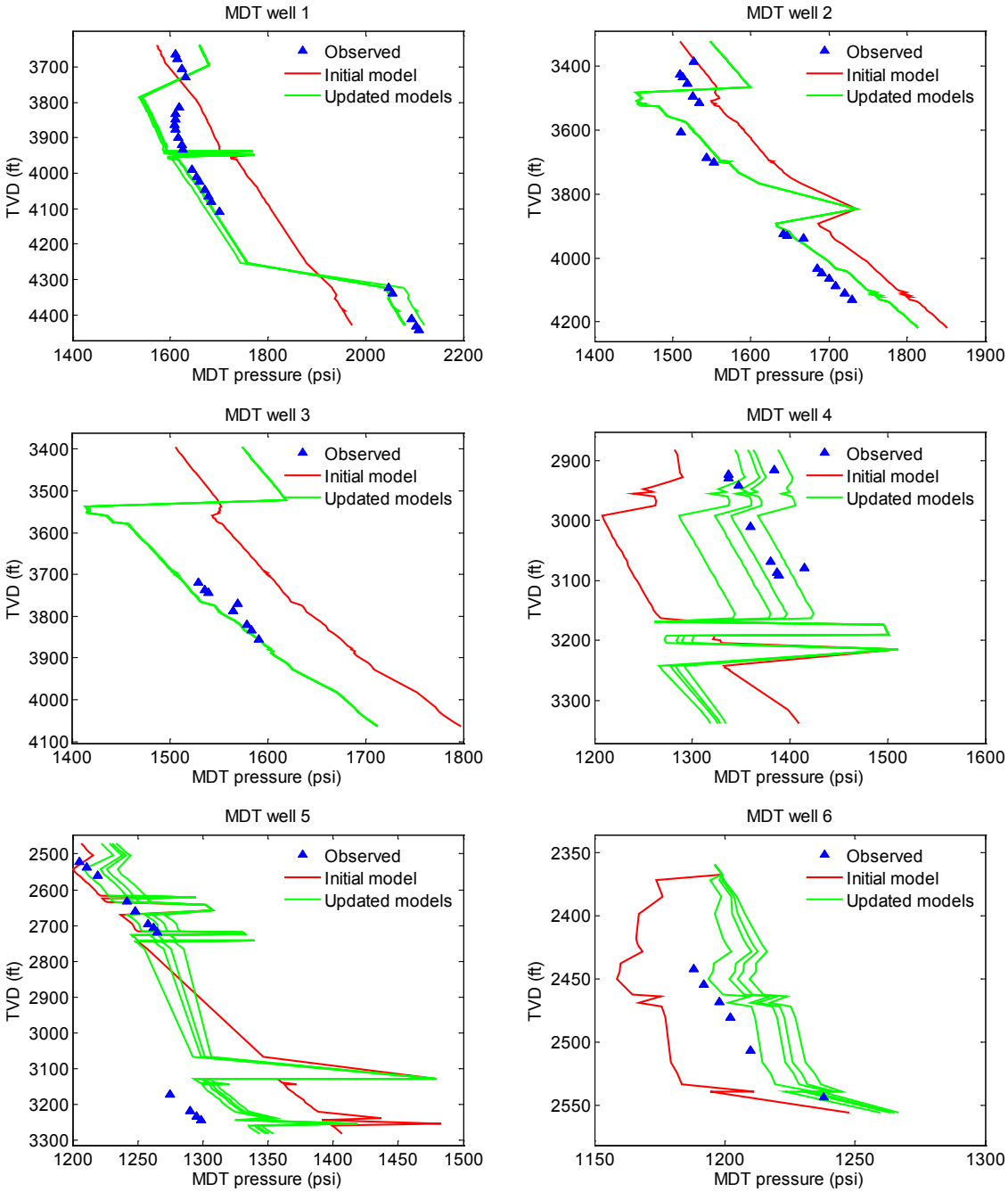

Fig. 2.33 MDT pressure matches from global updates (property modeling)

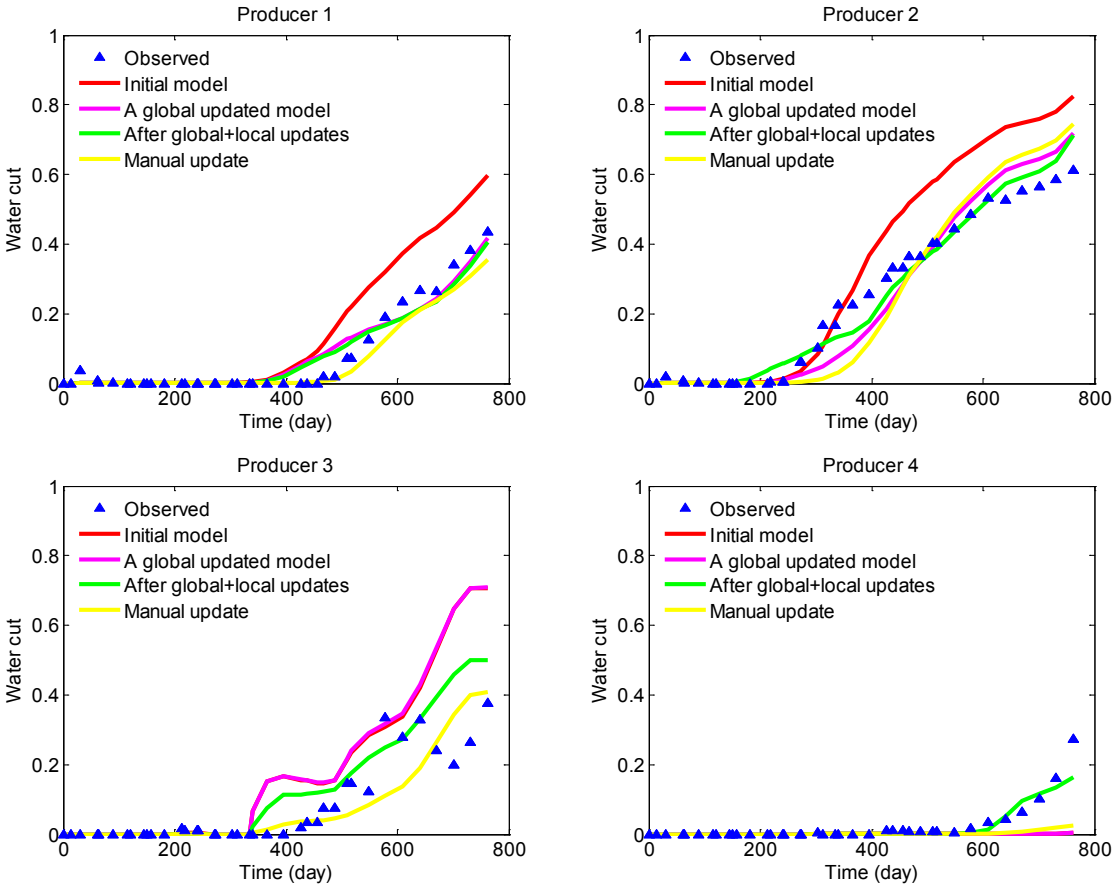

Fig. 2.34 Water-cut of wells from one global updated model

Initial model | A model after global update | After global/local updates

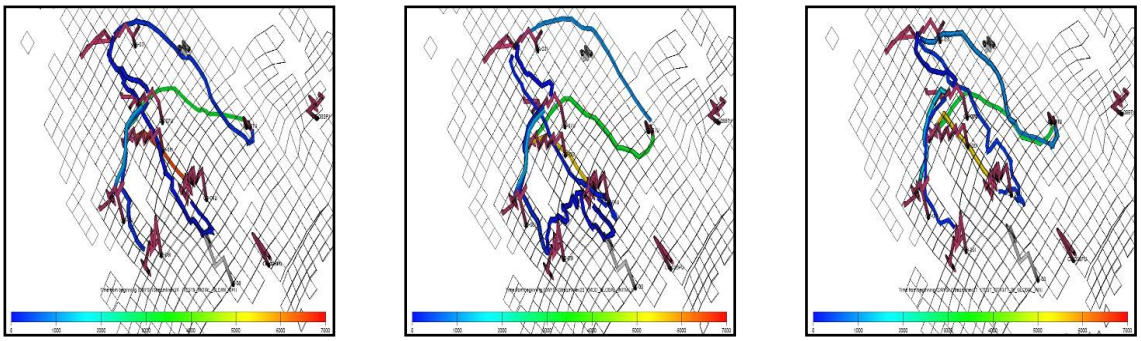

Fig. 2.35 Total liquid flux maps show communications of producers and injectors

Initial model | A model after global update | After global/local updates

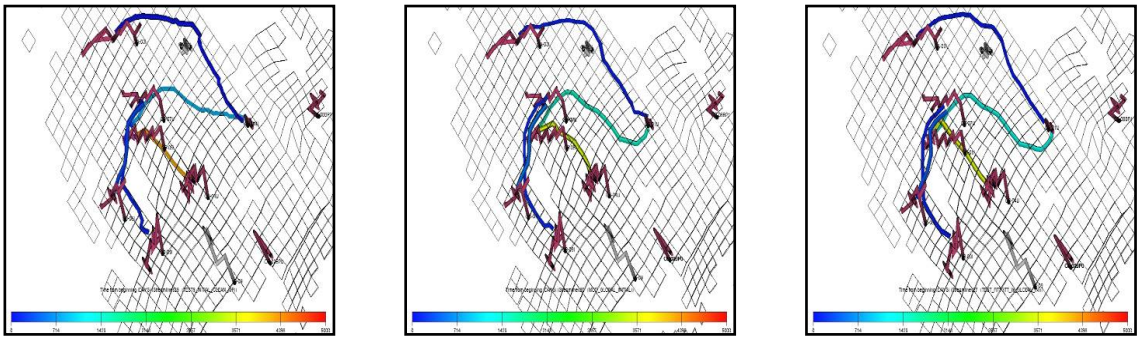

Fig. 2.36 Water flux maps show communications of producers and injectors

Initial model | A model after global update | After global/local updates

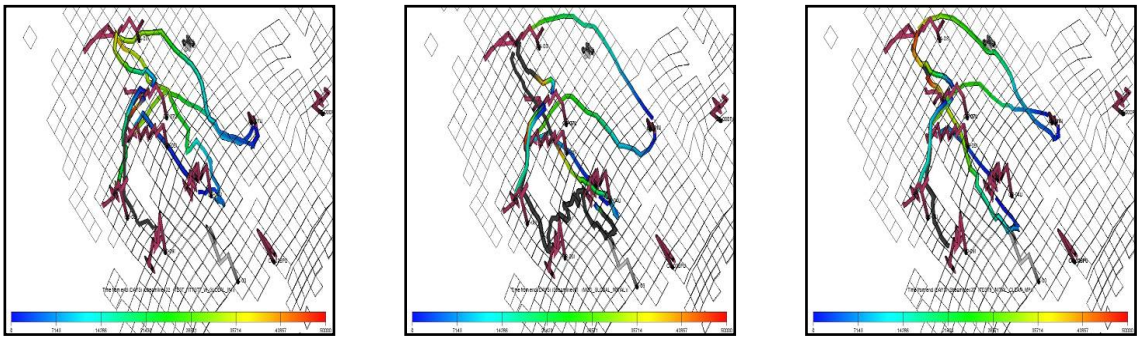

Fig. 2.37 Average TOF maps show different drainage volumes

After global matching, a few selected models are further refined via local updating. For illustration purposes, we will show the detailed results from one of these models. **Fig. 2.34** shows that in terms of water fractional flow, the global update tries to calibrate water-cut in a much larger scale while local update tries to make a finer tuning based on observed production. **Fig. 2.35** and **Fig. 2.36** display total liquid and water flux, respectively, where the value of the flux is used to color the breakthrough streamline. From the comparison of fluxes, we see that the liquid movement was substantially altered by the global update while the local updates focused more on changing the streamline speed. For instance, more streamlines were found in the global updated model between a producer and an injector in the left-bottom corner of Fig. 2.35 (For visualization purpose, the streamlines have been grouped into tubes, while each streamline carries same amount of flux). **Fig. 2.37** shows the average time of flight between wells, which represents the drainage area at a given time. These interpretations were validated against the production response curves in the process of updates.

2.5 Summary

In this chapter, we proposed a streamline-based local update for improving the well-by-well match after the global update as proposed by Cheng et al. (2008). This second step greatly reduces the trial-and-error adjustments of local permeabilities and significantly improves the efficiency of the workflow. We also address effects of local update on global update, which has not been considered by any other structural history matching paper (Cheng et al. 2008; Schulze-Riegert et al. 2003). As explained in this chapter, a norm constraint ensures that local update will not dramatically change globally updated models. In contrast, manual local update or independent local updates without considering the global updates can result in permeability changes that are inconsistent with large-scale global updates. Besides, the convergence of the GA was significantly improved by introduction of the heat bath algorithm. Although heat bath algorithm has

been used in the past (for example in non-linear waveform inversion), in the context of history matching its application is completely new and novel. Moreover, one of the major contributions of this chapter is the assessment of the history match models via the flux-maps. Specifically, the concept of flux map is introduced to identify how each step of the calibration changes the inter-well flux connectivity and flow patterns. Thus, the interaction of the heterogeneity on the flow pattern is clearly visible. In both synthetic and field cases, it was shown that regional fluxes were redistributed among wells after global update, and the local updates altered the streamline paths while maintaining the large-scale fluid movement.

We have shown the power and utility of our proposed method using a large-scale field application. From geological modeling to global update of reservoir fluids in place and regional communications, to local flow calibration (permeability change), each step and its effects were illustrated. The field application was explained to the extent allowed by the operating company. Nonetheless, we are able to illustrate all the major steps and the significant improvement in history matching through the application of our proposed approach.

CHAPTER III

INTEGRATING STIMULATED RESERVOIR VOLUME WITH DYNAMIC PRODUCTION FOR SHALE GAS WELLS*

The rise in the demand of natural gas globally and the application of more sophisticated production technologies in particular, the creation of multiple hydraulic fractures from horizontal wells (Britt and Smith 2009; Cramer 2008; King 2010) have motivated energy companies to increasingly develop harder-to-access natural gas resources such as tight sands, shale gas and coal bed methane. These unconventional reservoirs with ultra-low permeabilities are known to be more abundant throughout the world and are likely to be the dominant suppliers of future natural gas production (Holditch 2006). In this chapter, we will apply the global model calibration in Chapter II to unconventional shale gas reservoirs, with the extension of integrating stimulated reservoir volume as a constraint in the evolutionary algorithm.

Gas flow in shale gas reservoirs occurs primarily from ultra low permeability shale rocks through a complex network of natural and induced hydraulic fractures. Consequently, fracture parameters (conductivity and half length), fracture location and distribution are the dominant factors influencing well drainage volumes and shale gas well performance. Stimulated reservoir volume or SRV, estimated from microseismic event clouds or rate/pressure transient analysis, describes a measurement of overall reservoir volume impacted by fracture treatments. With SRV as well as the dynamic production/pressure response, reservoir simulation models can be calibrated to actual well performance in shale gas reservoirs leading to improved understanding, forecasting and future well placement.

The outline of this chapter is as follows: we first introduce a novel approach for computing well drainage volume for shale gas wells with multistage fractures and fracture clusters. Next, we calibrate the shale gas reservoir model by matching the drainage volume with the SRV within specified confidence limits. The matching of the SRV is done in addition to the traditional history matching of production/pressure response and further constrains the estimation of fracture parameters. An evolutionary algorithm with design of experiments is used for the assisted history matching. Sensitivities to various parameters such as fracture conductivity, fracture half lengths and rock compaction have also been investigated. The proposed approach has been applied to a generic shale gas well designed after a real field case. The results clearly indicate the benefits of including SRV during history matching, leading to improved fracture/matrix parameter estimation and performance forecasting. Our proposed approach provides an important tool that can be used to optimize well placement, fracture treatments and improve the economics of shale gas plays (Yin et al. 2011).

3.1 Introduction

Fluid flow in tight sand and shale gas reservoirs can be analyzed through numerical simulations of the pressure response and saturation distributions just as for conventional reservoirs. Because of the extremely low matrix permeabilites, much of the fluid movement in shale gas and tight gas reservoirs happen in the interconnected networks of natural fractures. The matrix provides the storage for the gas whereas the fractures are the primary flow conduits. Proper modeling of the orientation, distribution and connectivity of the natural fractures is critical to reservoir simulation and forecasting (Cipolla et al. 2009; Olson 2008). In particular, the understanding of the interaction between induced hydraulic fractures and naturally existing fractures is an important key in the successful development and exploitation of these reservoirs (Cipolla et al. 2011; Lee and Hopkins 1994; Weng et al. 2011). Planning an effective field development

strategy requires estimating the drainage capacity of current wells and optimizing well placement so as to minimize the overlapping of drainage volumes of existing wells. Production decline curves have been widely used to compute drainage volumes and estimate ultimate recoveries (EUR) in tight gas reservoirs (Blasingame and Rushing 2005; Cox et al. 1996; Fetkovich 1980; Rushing et al. 2008). Also, pressure transient tests are commonly used in determining the well productivity and the benefits of hydraulic fracturing in tight gas reservoirs (Lee and Hopkins 1994). Whereas both decline curve analysis and pressure transient tests have played a vital role in the exploitation of tight gas reservoirs, the interpretation of such analytical tools can be considerably complicated in the presence of complex spatial heterogeneity and natural fractures. In particular, the interactions between the hydraulic fracture and natural fractures and their implications on well drainage volumes cannot be adequately accounted for by existing analytic methods. We need to resort to numerical reservoir simulation for these purposes. However, such simulations can be severely limited because of the uncertainty in matrix and fracture parameters.

One of the most common and effective ways to develop and exploit unconventional reservoirs, in particular shale gas reservoirs is horizontal wells with multistage fractures. In fact, improvements in hydraulic fracturing and completion technologies have been the primary driving force behind the economic recovery of shale gas resources. However, in a typical application to develop tight or shale gas reservoirs, the cost of completing a horizontal well can be about half (or sometimes more) of the total well cost. Hence, there is a tremendous need to improve our understanding of the effectiveness of the completion strategy so as to optimize the number of hydraulic fracture stages needed to drain the gas-in-place. In many shale gas reservoirs, natural fractures are healed by calcite cementation (Fan et al. 2010). Hydraulic fracturing with proppant and water will not only create high conductivity primary hydraulic fractures but also stimulate and/or reopen natural fractures in the vicinity of hydraulic fractures. This will ultimately generate a complex fracture network or stimulated reservoir volume (SRV) surrounding each stage of primary hydraulic fracture. The growth and final pattern of SRV, which

depends on rock properties and fracturing, are typically complex and unpredictable. Though recently microseismic mapping has been widely used to measure the geometry and location of complex fracture systems (Fisher et al. 2002; Mayerhofer et al. 2010), it does not provide insights into the conductivity of the fracture network or the "effective" drainage volume/area of the stimulated region, mainly due to lack of sufficient data to locate proppant distribution and conductivity distribution in the fracture network. More recently, the use of rate normalized pressure data (Bello and Wattenbarger 2010; Song and Ehlig-Economides 2011) have been proposed to obtain estimates of SRV that actually contribute to the flow. Fig. 3.1 shows a microseismic image of hydraulically fractured horizontal well in a shale gas reservoir.

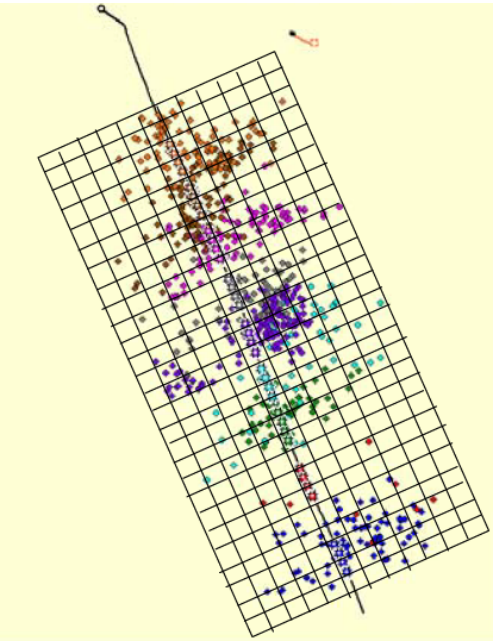

Fig. 3.1 Microseismic image of hydraulically fractured horizontal well in a shale gas reservoir (Bello and Wattenbarger 2010)

Numerous efforts have been undertaken to optimize hydraulic fracture stages in the past. These have involved a combination of numerical simulation and analytical

computations using rate and pressure transient analysis. An important aspect of any simulation study is model calibration, also known as history matching. Previous works related to history matching in shale gas reservoirs has been done by adjusting primarily fracture parameters viz. fracture length, fracture density, and fracture conductivity. History matching applications for both the Barnett shale (Cipolla et al. 2009; Mayerhofer et al. 2006) and the Haynesville shale (Wang and Liu 2011) have involved integration of flowing bottom-hole pressure or phase rates to infer fracture parameters in a manual and deterministic manner. Such deterministic approaches lead to a single set of fracture parameters of unknown reliability. Specifically, no quantification of uncertainty in fracture parameters is available from these deterministic approaches. Stochastic approaches such as genetic or evolutionary algorithms and Ensemble Kalman Filters result in an ensemble of history matched models. By careful analysis of multiple history matched models, we can obtain a sense of non-uniqueness and uncertainty in fracture parameters derived through history matching. Whereas the use of stochastic methods in history matching is now very routine for conventional reservoirs, their applications to unconventional reservoirs have been very few and far between (Ghods and Zhang 2010).

The objectives of this chapter are threefold. First, we draw upon the recent developments in history matching in conventional reservoirs to develop a workflow for calibrating shale gas reservoir models to infer fracture and matrix parameters. Second, we propose a novel approach to estimating well drainage volumes in shale gas reservoirs. Third, we use the drainage volume to calibrate reservoir models with SRV information derived from microseismic or rate/pressure transient analysis. The use of SRV in addition to the production and pressure data provides an additional degree of constraint during history matching and is thus expected to improve estimates of matrix/fracture parameters and reduce associated uncertainties.

3.2 Approach Outline

Our goal here is to calibrate static parameters such as fracture conductivity, fracture half length, matrix permeability and geomechanical/compaction parameters in order to match the dynamic data from shale gas wells viz. flowing bottom-hole pressures and production rates of phases (gas and water) in wells. We adopt the stochastic approach in Chapter II to model calibration,using a modified genetic algorithm(GA) (Yin et al. 2010) to adjust shale gas reservoir and fracture parameters because of the discrete nature of the parameter space. The genetic algorithm imitates biological principals of evolution – survival of the fittest. It has been extensively applied to the history matching problem (Bittencourt and Horne 1997; Floris et al. 2001; Romero and Carter 2001; Schulze-Riegert et al. 2002; Williams et al. 2004). Because the GA works with a population of model parameters, rather than a single set of model parameters, it simultaneously allows for history matching as well as quantification of uncertainty and non-uniqueness in the solution. Previous history matching applications in shale gas reservoirs have primarily used rate and pressure information to infer fracture parameters. In this chapter, we include the estimated SRV as an additional constraint during the history matching process. By incorporating the SRV as the ultimate drained volume, it is shown that history matching results are improved in the sense that the uncertainties in the estimated parameters considerably are reduced without sacrificing the match quality. Before going into details, we first briefly discuss the major steps in our approach followed by an outline of the workflow.

- ***Construction of an objective function***. To start with, an objective function is defined as the mismatch between the observed well response (rate or pressure) and the simulated well response. The goal of the model calibration will be to minimize the objective function by changing a set of fracture and matrix parameters.

- ***Sensitivity analysis.*** A small set of key parameters are first identified via a sensitivity analysis using high-low values for each of potential fracture/matrix parameters. This step involves flow simulations changing one parameter at a time and examining the objective function to identify the most sensitive parameters and eliminate insensitive parameters.
- ***Proxy construction***. A proxy is a computationally inexpensive surrogate model constructed using limited number of flow simulations and is used to prescreen models during assisted history matching. In this chapter, a proxy of the objective function with respect to selected key parameters is constructed using a space-filling experimental design and response surface methodology (Pan and Horne 1998; Yeten et al. 2002).
- ***Drainage volume estimation.*** For a given set of fracture/matrix parameters, the well drainage volume is computed by identifying the location of the 'pressure front' and summing up the pore volumes enclosed by the front. This drainage volume is compared against the SRV to filter out fracture/matrix parameters that are not plausible.
- ***Model calibration using genetic algorithm (GA).*** A genetic algorithm with a proxy check is used to generate a population of updated parameters conditioned to well pressure response and SRV. From the population of updated models, a set of representative models are selected via a cluster analysis.

A stepwise flow chart of the approach is shown in **Fig. 3.2**.

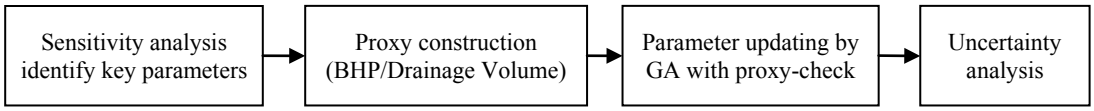

Fig. 3.2 Overview of proxy-assisted history matching for shale gas wells

3.3 Background and Methodology

3.3.1 Evolutionary Algorithm in Unconventional Reservoirs

The majority of our history matching approach follows the method outlined in Chapter II (Cheng et al. 2008; Yin et al. 2010). Similar to in conventional reservoirs, design of experiments (DOE), genetic algorithm (GA) and response surface methodology (RSM) are used for calibrating model parameters, m_i which include both matrix and fracture parameters. The objective (misfit) function is defined as:

$$f(\mathbf{m}_i) = f(m_1, m_2, \cdots, m_N) = \ln|\Delta p| + \ln|\Delta V| + \cdots \quad \text{.....(3.1)}$$

Here multiple objectives are handled by using sum of logarithms of the absolute misfits of simulated well bottom-hole pressure vs. measured pressure, long-term/ultimate drainage volume compared to observed or RTA/PTA derived SRV.

3.3.2 Efficient Drainage Volume Estimation

Pressure Front Equation. One of the objectives in this chapter is to integrate the SRV in addition to well response to reduce model uncertainty. For this, we first introduce an efficient approach to estimate the long-term drained volume for a well. We assume that the SRV represents this long-term drained volume of the well. Thus, by matching the drained volume with the SRV, we are able to further constrain fracture/matrix parameters.

The drainage volume calculations follow the method outlined by Datta-Gupta et al. (2011) and utilize the concept of radius of investigation proposed by Lee (1982) and its generalization to unconventional reservoirs. Lee defines the radius of investigation as the propagation distance of the 'peak' pressure disturbance for an impulse source or sink.

Recently, Datta-Gupta et al. (2011) generalized the concept to arbitrary heterogeneity and well conditions including horizontal wells with multistage factures by solving the propagation equation of the 'peak' disturbance or the pressure 'front'. Specifically, a high frequency asymptotic solution of the diffusivity equation leads to the following equation for a propagating pressure 'front' for an impulse source or sink (Cheng et al. 2007; Vasco et al. 2000):

$$\sqrt{\alpha(\mathbf{x})}\left|\nabla\tau(\mathbf{x})\right| = 1, \alpha(\mathbf{x}) = \frac{k(\mathbf{x})}{\phi(\mathbf{x})\mu c_t} \quad \text{.....(3.2)}$$

In the above equation, $\alpha(\mathbf{x})$ is the diffusivity (consisting of $k(\mathbf{x})$ = permeability, $\phi(\mathbf{x})$ = porosity, μ = fluid viscosity, c_t = total compressibility) which can be function of position and $\tau(\mathbf{x})$ is the propagation time of the pressure 'front', also called a 'diffusive time of flight' (Kim et al. 2009). It simply tells us that the pressure 'front' propagates in the reservoir with a velocity given by the square root of diffusivity and thus it has unit of square root of time and is associate with arrival time of pressure front at **x** through a simple equation for 3D flow (Datta-Gupta and King 2007; Vasco and Finsterle 2004)

$$t(\mathbf{x}) = \tau^2(\mathbf{x})/6 \quad \text{.....(3.3)}$$

The pressure 'front' equation is actually a form of the Eikonal equation which appears in many contexts such as elastic and electromagnetic wave propagation; its properties are well developed in the literature (Sethian 1999). Most importantly, the Eikonal equation can be solved very efficiently (in seconds opposed to hours of simulation time for comparable problems) by a class of solution called Fast Marching Methods (FMM) (Sethian 1999) to obtain the location of the pressure 'front'.

Discretization. To solve Eikonal equation 3.2, we start with discretizing the equation. For illustration purposes, we discretize the Eikonal equation on 2-D Cartesian grid. The gradient in Eq. 3.2 is estimated using the first order approximation.

$$\max\left(D_{ij}^{-x}\tau - D_{ij}^{+x}\tau, 0\right)^2 + \max\left(D_{ij}^{-y}\tau - D_{ij}^{+y}\tau, 0\right)^2 = \frac{1}{\alpha} \quad \text{.....(3.4)}$$

where in x direction, first order finite difference operators are defined (Sethian and Vladimirsky 2000)

$$D_{ij}^{-x}\tau = \frac{\tau_{i,j} - \tau_{i-1,j}}{\Delta x}, D_{ij}^{+x}\tau = \frac{\tau_{i+1,j} - \tau_{i,j}}{\Delta x} \quad \text{.....(3.5)}$$

The operators D^{-y} and D^{+y} in y direction are similar. Higher order finite difference can be used to discretize Eq. 3.4 as well. To improve accuracy along diagonal directions, Hassouna and Farag (2007) proposed Multi-stencils Fast Marching Method (MSFM) using eight stencils with second order approximation on Cartesian grid. And Sethian and Vladimirsky (2000) applied Fast Marching Method to unstructured grid.

Solve Eikonal Equation by Fast Marching Method. Now we could solve $\tau(\mathbf{x})$ by solving quadratic Eq. 3.4. To compute diffusive time of flight $\tau(\mathbf{x})$, we need to define all the grid points into three groups: *accepted*, *considered* and *far away*. Initially, the solution is known at a set of points (for example, at zero time, we know diffusive time of flight equals to zero at producers). These points are denoted as *accepted* points. The points adjacent to *accepted* points are defined as *considered* points and their diffusive time of flights are calculated using Eq.3.4. All other grid points are tagged as *far away* points. Then we start looping until all the points are tagged as *accepted*:

- Pick a *trial* from *considered* points with smallest value of diffusive time of flight, $\tau(\mathbf{x})$. Add it to *accepted* and remove it from *considered*;

- Tag all neighbors of *trial* that are not *accepted* as *considered*. If the neighbor is in *far away*, remove it from the set;
- Re-compute $\tau(\mathbf{x})$ for all *considered* neighbors of *trial* by solving Eq. 3.4.

After calculating diffusive time of flight at all grid points, we could convert it to arrival time and compute drainage volumes at various times by imposing different time cut-offs. We illustrate this in **Fig. 3.3** for a horizontal well with six stages of hydraulic fractures (Datta-Gupta et al. 2011).

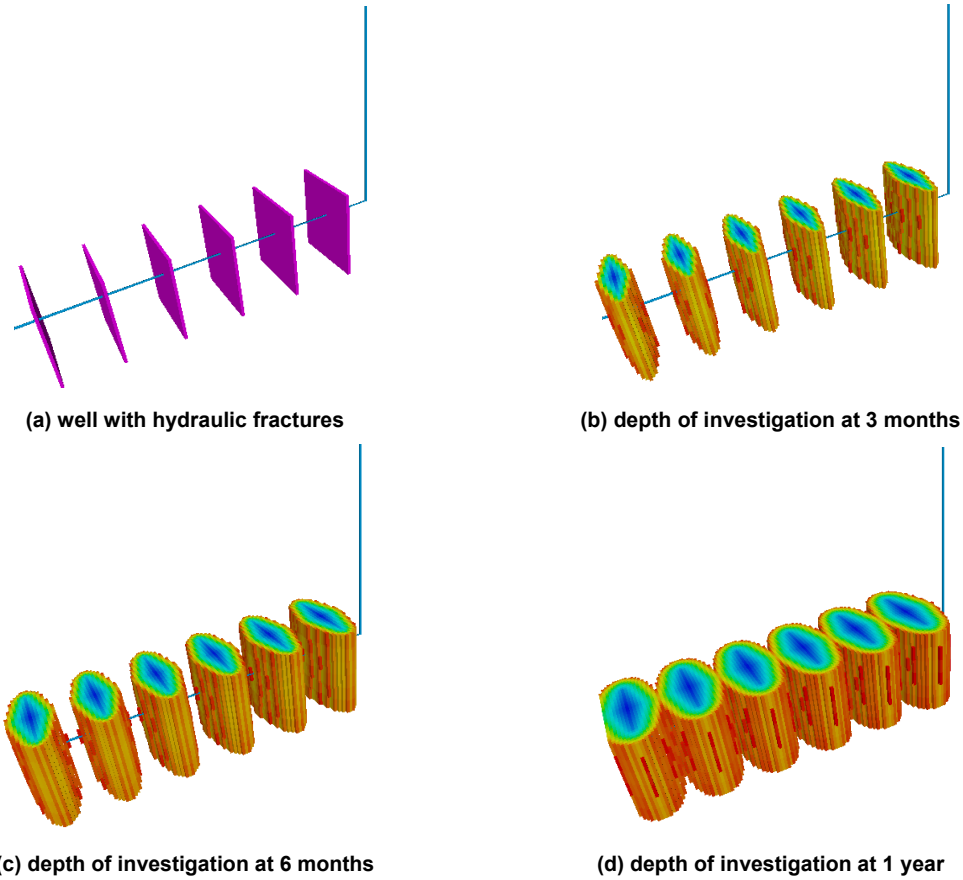

Fig. 3.3 Depth of investigation at various times for a horizontal well with multistage hydraulic fractures

Extension of Eikonal Equation. Eq. 3.2 is under several fundamental assumptions among which two are most important: a) the 'front' is moving monotonically outward; b) diffusivity coefficients don't depend on pressure solution therefore can be considered as static properties. If the well is producing at a bottom-hole pressure control rather than rate control in the example we presented, the method still applies since the pressure front arrival time doesn't depend on rate magnitudes, and only its relative amplitude depends on the rate. For another situation in certain shale rocks, the permeability can depend on pressure, even strongly, especially when geomechanical effects dominate the fluid flow. Under such conditions, a work-around may be to use small timestep, within each timestep permeability is assumed to be unchanged, and at the end of each timestep, we update the permeability according to the pressure and geomechanical effects.

3.3.3 Integration of SRV in Evolutionary Algorithms

For our purposes, the drainage volume is defined as the reservoir volume enclosed by the pressure ‘front’ at any given time. A typical evolution of a well drainage volume with time in previously mentioned illustration example is shown in **Fig. 3.4**.

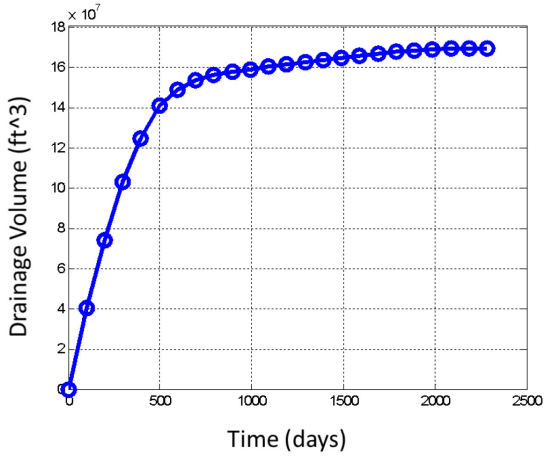

Fig. 3.4 Well drainage volume vs. time

We define the SRV as the volume when the drainage volume curve in Fig. 3.4 reaches an asymptote as shown. Given an estimate of SRV either from rate or pressure transient analysis or microseismic, we can compare the SRV with the computed well drainage volume to further screen the matrix and fracture parameters. The steps are as follows:

- Given a set of fracture and matrix parameters, we first compute the long-time drainage volume using the method as outlined above. It must be emphasized that the computation of drainage volume is extremely fast and requires only a few seconds of computer time.
- We compare the long-term drainage volume with the estimated SRV from an independent source.
- If the difference is substantial as determined by a threshold measure, then the given matrix fracture parameters are rejected and a new set of parameters are proposed.
- If the difference is within the threshold limit, then the parameters are accepted and the next step of calculations begins. This next step involves integration of rate/pressure response via proxy check and flow simulation.

The inclusion of SRV not only constrains the parameter space but also substantially reduces the number of flow simulations by pre-screening undesirable sets of fracture and matrix parameters.

3.4 Results and Discussions

In this section we illustrate our approach using a 3D synthetic example designed after a real field case. Two different cases are considered. First, we history match the well BHP to infer fracture and matrix parameters in a shale gas reservoir with a horizontal well with multistage fractures. Next, we assume that an estimate of the SRV is available through an independent measurement, for example microseismic or rate/pressure transient analysis. We then incorporate the SRV during history matching along with the well BHP response. The results clearly show the benefits of incorporating SRV in reducing the uncertainties in estimates of fracture/matrix parameters via history matching.

3.4.1 A 3D Synthetic Example

The reference model for this case is a 3D single-phase gas shale reservoir represented using single porosity compositional model designed after a Haynesville field case. The size of the grid is 264×64×5. The matrix permeability ranges from 80 nano-darcy to 150 nano-darcy. A horizontal well is completed in the center of the reservoir with 4 transverse fractures (**Fig. 3.5**). We assume that the fracture locations are known and are as shown in **Fig. 3.6**. The fracture heights fully penetrate the pay zone. Each fracture is considered surrounded by an enhanced permeability area (EPA) (Kundert and Mullen 2009; Wang and Liu 2011) that represents natural fracture and/or hydraulic fracture induced permeability enhancements as shown in **Fig. 3.7**. The parameters to be estimated via history matching and the associated uncertainties for this example are listed in **Table 3.1**. The horizontal well is first produced at a constant rate of 2

MMSCF/day, until bottom-hole pressure (BHP) drops to 1000 psi when the well control switches to BHP control. In this synthetic case, the first 295 days of BHP history will be integrated to predict BHP and gas production for the following 435 days. The objective function is defined as the sum of squared differences of BHP between simulation results and the reference ('true') case for first 295 days.

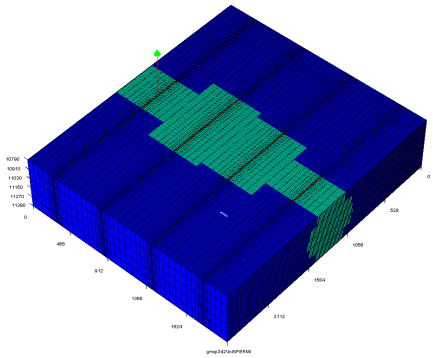

Fig. 3.5 Reservoir and grid

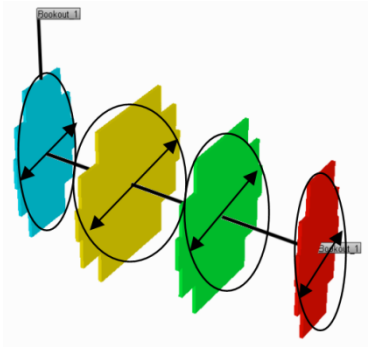

Fig. 3.6 Elliptical fractures

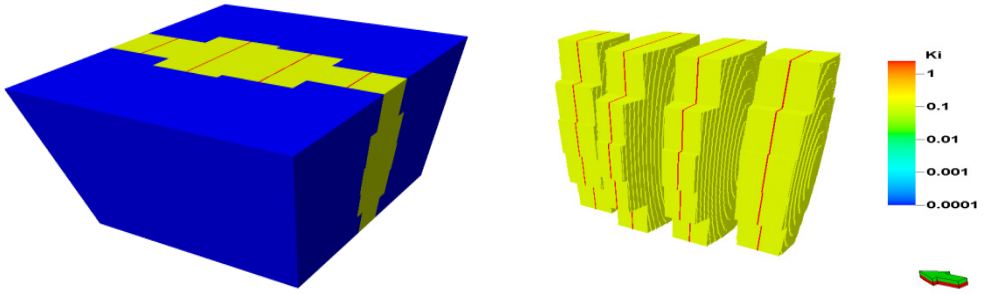

Fig. 3.7 Stimulated reservoir volume defined by enhanced permeability area

Table 3.1 Parameter uncertainties for sensitivity and history matching

Uncertainty	Base	Low	High	Reference
Matrix permeability (k_M)	80.0E-6 md	70.0E-6 md	150E-6 md	100E-6 md
EPA permeability (k_E)	0.15 md	0.05 md	0.25 md	0.12 md
Fracture perm (k_F)	3.50 md	1.00 md	5.00 md	2.50 md
Matrix compaction factor (C_M)	3.00E-4 /psi	2.00E-4 /psi	5.00E-4 /psi	4.00E-4 /psi
EPA compaction factor (C_E)	5.00E-4 /psi	4.00E-4 /psi	6.50E-4 /psi	5.50E-4 /psi
Fracture compaction factor (C_F)	3.00E-4 /psi	2.00E-4 /psi	4.50E-4 /psi	3.50E-4 /psi
Fracture 1 half long axis (X_{F1})	200 ft	100 ft	300 ft	190 ft
Fracture 2 half long axis (X_{F2})	300 ft	200 ft	450 ft	350 ft
Fracture 3 half long axis (X_{F3})	300 ft	200 ft	450 ft	300 ft
Fracture 4 half long axis (X_{F4})	200 ft	100 ft	300 ft	150 ft

The compaction factors C_M, C_E, C_F describe how rock permeability changes with pressure in a form of $k=k_{ref} \exp(C (p-p_{ref}))$. To evaluate the impact of various parameters on the well production performance, a sensitivity analysis was first performed on a set of preselected parameters including hydraulic fracture conductivity, fracture half length, rock compaction factors and matrix permeability. The initial distributions of the parameters are considered to be uniform. The parameter ranges and reference values are

summarized in Table 3.1. **Fig. 3.8** shows a tornado diagram of the objective function (logarithm of BHP misfit) with respect to various parameters generated by perturbing each parameter from the base model to the lower or upper bounds. From Fig. 3.8 it can be seen that fracture permeability and EPA permeability and their compaction factors have major impacts on the BHP misfit, while matrix permeability and its compaction have relatively low impacts. This can be explained from the fact that for the time period of interest, the flow mainly happens inside SRV (fracture and EPA). Based on the sensitivity analysis, the k_M and C_M are removed as history matching parameters.

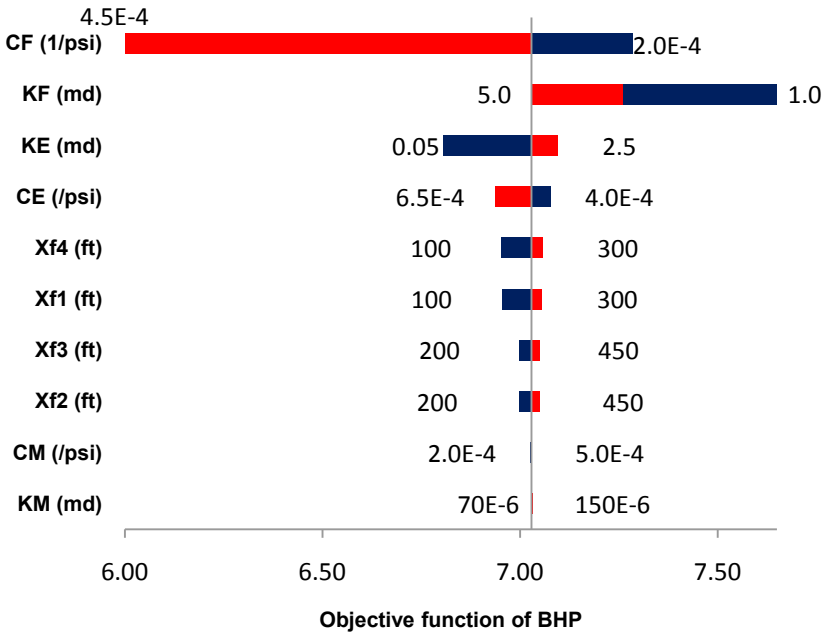

Fig. 3.8 Sensitivity analysis of BHP objective

3.4.2 Integration of BHP Only

Initially, we perform a history matching of the well BHP only in order to estimate the fracture/matrix parameters as identified by the sensitivity analysis. The top eight parameters shown in Fig. 3.8 are used for the history matching. As discussed above, the

history matching was done by genetic algorithm with response surface proxy (Yin et al. 2010). The history matching was followed by predictions. **Fig. 3.9** compares the well responses for the initial population of GA models before and after history matching. The reference model response is shown in blue and is treated as observed data. Before history matching, a large discrepancy is observed in the production history between the reference model and the initial models reflecting the large uncertainty in the fracture/matrix parameters. After model calibration, uncertainties in parameter distributions are greatly reduced.

The effects of history matching BHP data in reducing the parameter uncertainties are shown using the box plots in **Fig. 3.10**. Here, all the parameter ranges have been normalized to fall between zero and unity. The range of model parameters in the population is indicated by the blue box with the reference case indicated by the triangle. Clearly, after history matching it can be seen that the parameter ranges in the population are considerably tightened and some of them tend to converge to the reference value. However, because of the limited data and the inherent non-uniqueness, a large bias can be seen in the estimate of some of the parameters.

In Fig. 3.10 we have also shown the distribution of drainage volumes of the initial models and the final models after history matching. For comparison purposes, the drainage volume for the reference model is also shown in these figures. The bias in the parameter estimation as observed before is also evident here. All the history matched models seem to systematically over-estimate the drainage volume compared to the reference model. Part of the reason for this overestimation is the drainage volume distribution of the initial models. A large majority of the initial models (>80%) had drainage volumes more than the reference model. Another reason can be the use of response surface as a surrogate model which can introduce bias because of lack of coverage of the complete parameter space. In the next section, we will see that such bias and non-uniqueness in the parameter estimation can be considerably reduced by incorporating additional information during history matching viz. the SRV estimate.

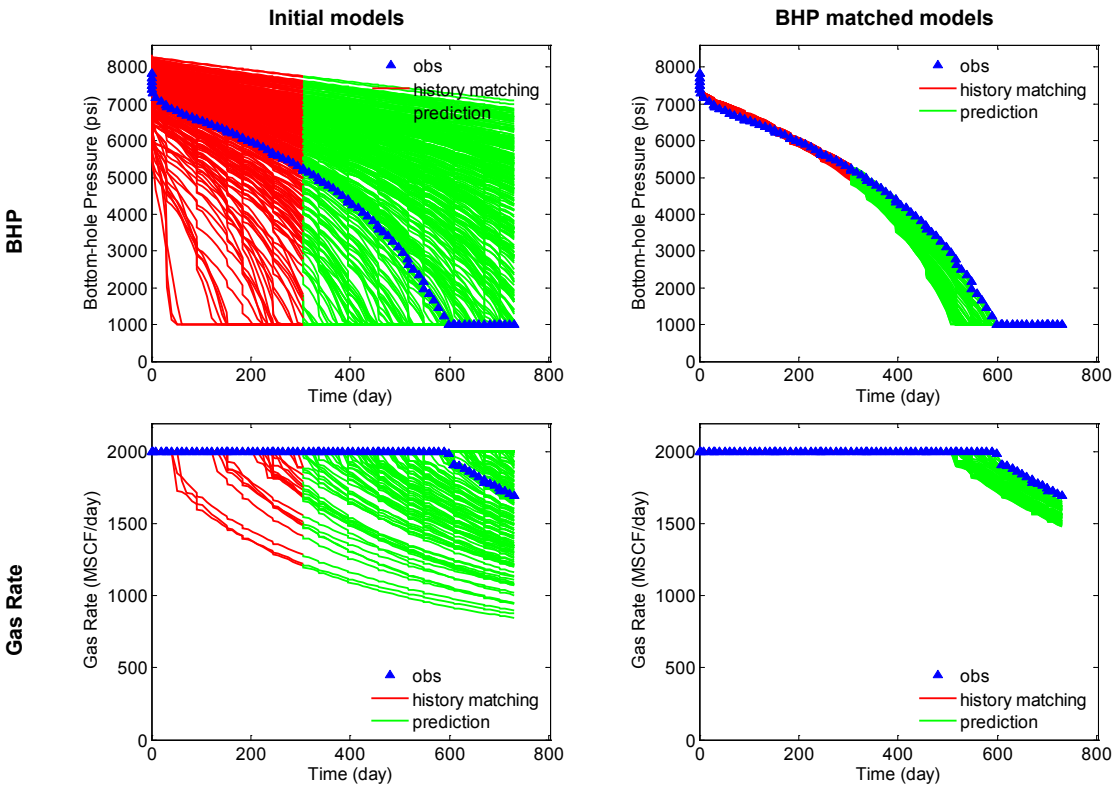

Fig. 3.9 History matching and predictions by GA with response surface proxy

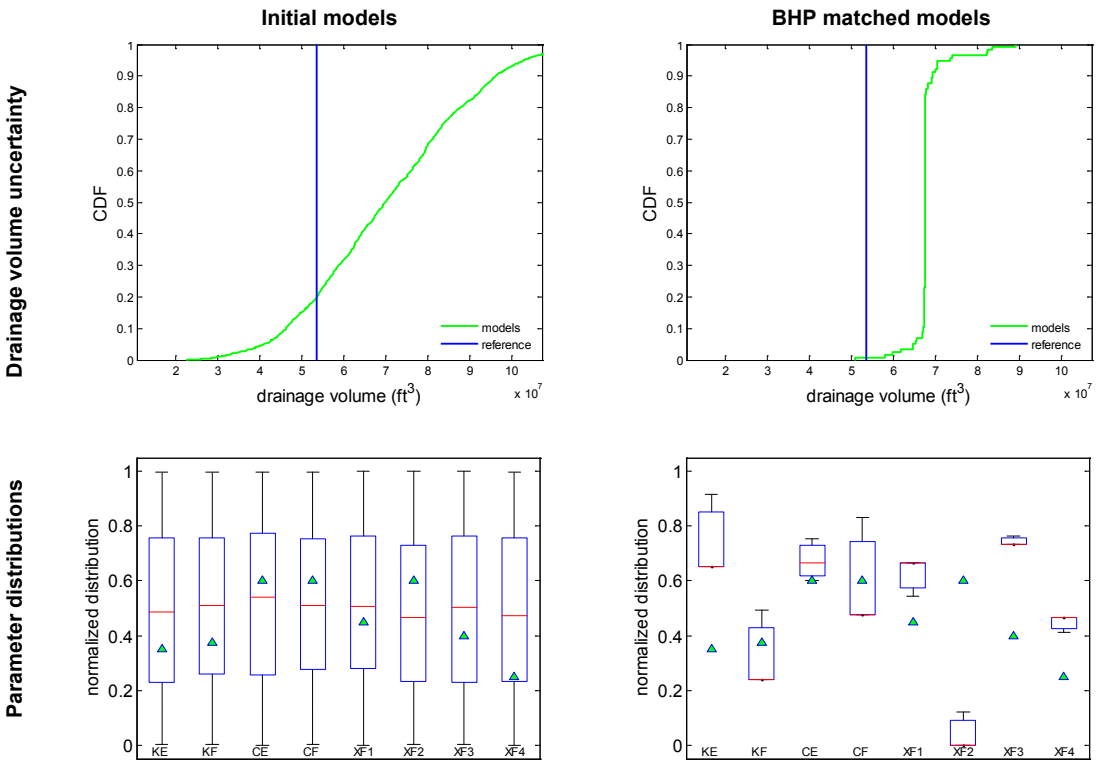

Fig. 3.10 Uncertainty analysis of models by GA with response surface proxy

3.4.3 Integration of SRV and BHP

In order to improve the fracture/matrix parameter estimation, next we incorporate SRV information during history matching. Though the SRV is a static measure controlled by fracture connectivity and associated EPA, it can be approximated at a time when drainage volume defined by radius of investigation reaches pseudo-steady state, that is, the boundary effects become predominant and no dramatic increase in the well drainage volume occurs. The situation is illustrated in **Fig. 3.11** and **Fig. 3.12** which show the evolution of the drainage volume as depicted by the location of the pressure 'front' at various times (color represents pressure front arrival time in log10 scale). Clearly, at

early times the drainage volume increases rapidly and eventually stabilizes to SRV when pseudo steady state is reached and also fracture interference is observed.

Before history matching, we first examine the impact of various fracture/matrix parameters on the SRV. In **Fig. 3.13** we have shown log-log plots of drainage volume with time and its sensitivity to various parameters. It can be seen that the drainage volume reaches plateau about 100 days-1000 days (corresponds to Fig. 3.11c-Fig. 3.11e). Fracture permeability (k_F) and EPA permeability (k_E) have dominant impacts in the early drainage volume development, while fracture lengths tend to influence the final values of the drainage volume. This observation is consistent with the sensitivity of the BHP as seen in Fig. 3.8. Matrix permeability has a noticeable impact only after the whole SRV has been drained (1.0E3 days-1.0E4 days, corresponds to Fig. 3.11e-Fig. 3.11f), which is typically way beyond the production schedule.

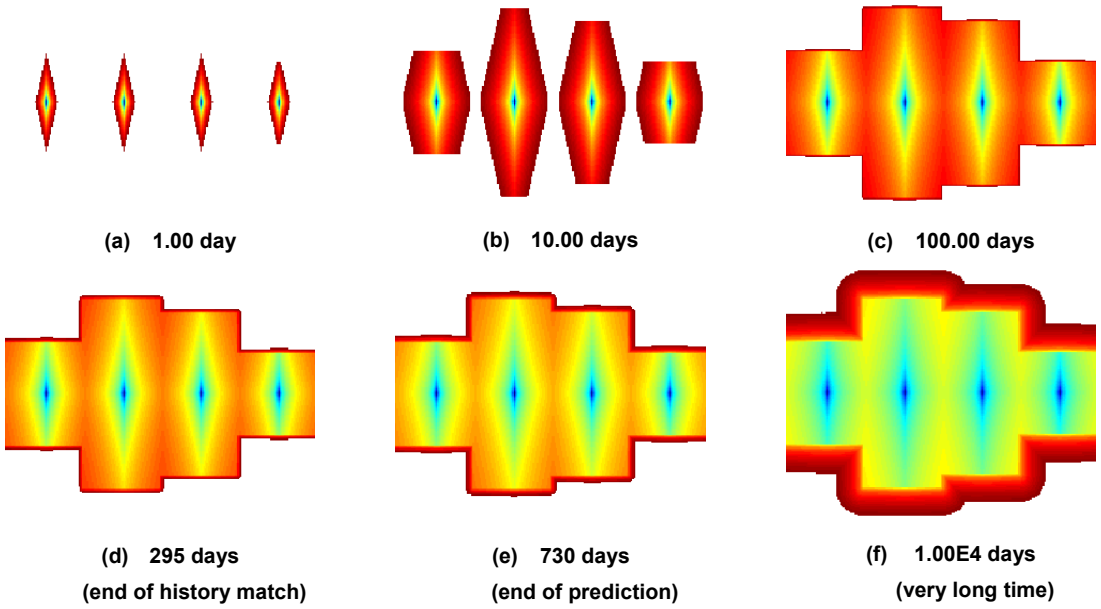

Fig. 3.11 Development of drainage volume defined by radius of investigation (center layer), colored by pressure front arrival time

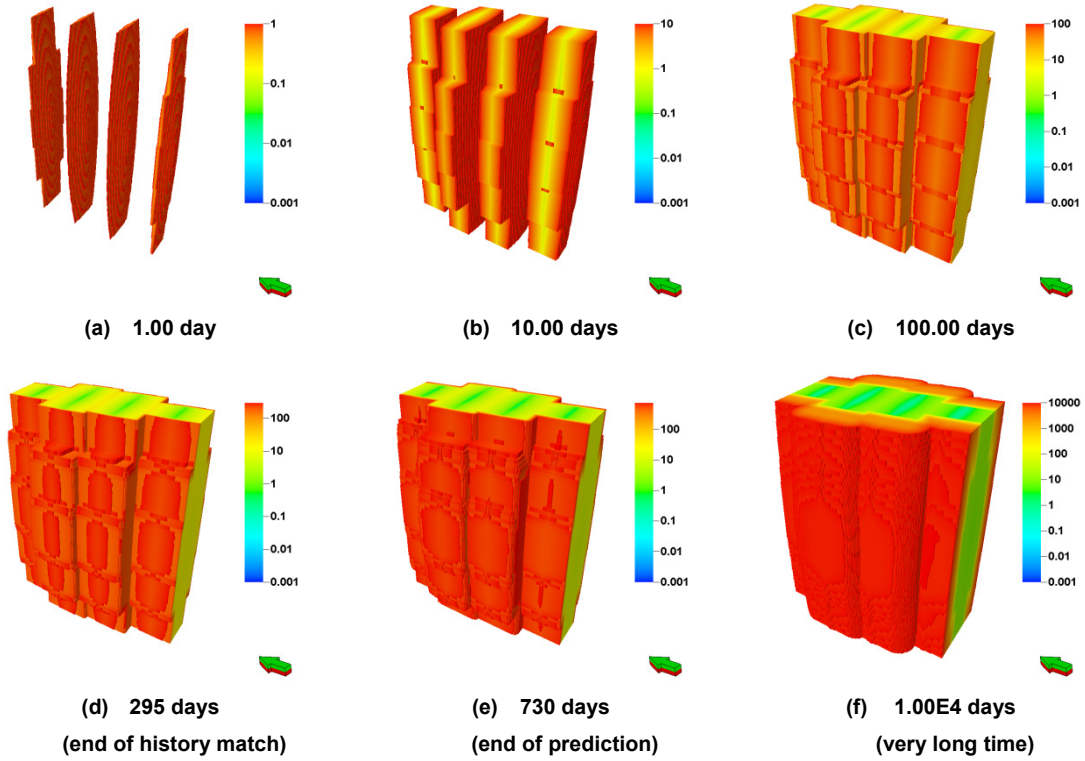

Fig. 3.12 3D drainage volume defined by radius of investigation, colored by pressure front arrival time

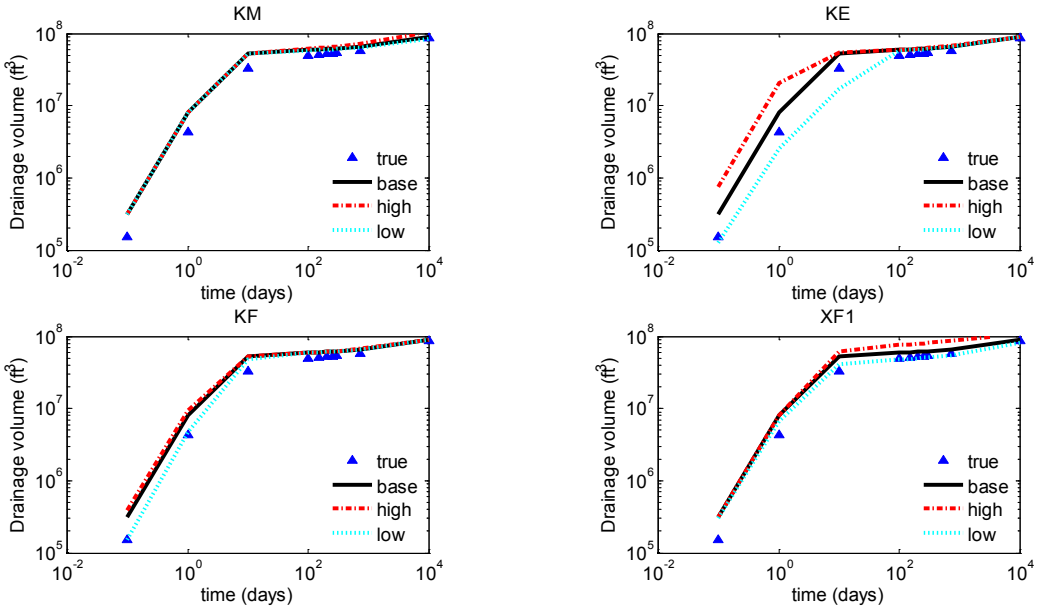

Fig. 3.13 Sensitivity of drainage volume to different input parameters

Next we carry out the history matching using the SRV and the BHP data. During history matching, the SRV data is incorporated as a single value that corresponds to the long-term drained volume of the well. The drainage volume is computed using the pressure 'front' propagation as discussed before. The history matching proceeds as follows:

- For each set of fracture/matrix parameters in the GA population, we first compute the drainage volume. Recall that the drainage volume computation does not require flow simulation and can be done in seconds. The drainage volume is compared with the well SRV. If the difference is less than 10%, then the parameter set is accepted for flow simulation and BHP calculation; otherwise, the parameter set is rejected and a new set of parameters are generated by sampling the corresponding distribution.

- Once a parameter set passes the prescreening step above, the parameter combination is used to carry out a flow simulation and compute the well BHP. An objective function is constructed based on the misfit between the observed and computed BHP as well as SRV as defined in Eq. 1.
- The above steps are repeated for all the members of the GA population which is then resampled to create a new generation based on the selection probability as given in Eq. 2. The usual GA steps of crossover and mutation then follow.
- The process is repeated until the data misfit reaches a satisfactory level or we exceed a preset number of generations.

History matching and prediction results are shown in **Fig. 3.14**. The results show that matching the SRV with the drainage volume did not improve the quality of the BHP or gas rate match and there is still a large discrepancy between the models pre-screened using SRV and the reference model response. This is expected because the SRV, as used here, is a single integrated estimate and does not provide any spatial detail. However, in **Fig. 3.15** we can see the impact of SRV matching. As expected, the uncertainty in final drained volume is substantially reduced compared to the initial population. More importantly, the uncertainties in k_E, k_F, X_{F1}-X_{F4} are also greatly reduced as seen in the box plots in Fig. 3.15. Finally, from Fig. 3.14 after calibrating the models with BHP using GA, we can see that both BHP and gas rate matches are improved substantially. Also, the parameter ranges are also narrowed considerably as seen in Fig. 3.15. In **Fig. 3.16** we have shown the drainage volume at 295 days for a selected set of history matched models. For comparison purposes, we have also shown the SRV for the reference model. Recall that we only matched the SRV with the drainage volume, not the specific shape of the SRV. However, the results in Fig. 3.16 show a reasonable correspondence with the shape of the reference SRV within the levels of non-uniqueness to be expected for the history matching process.

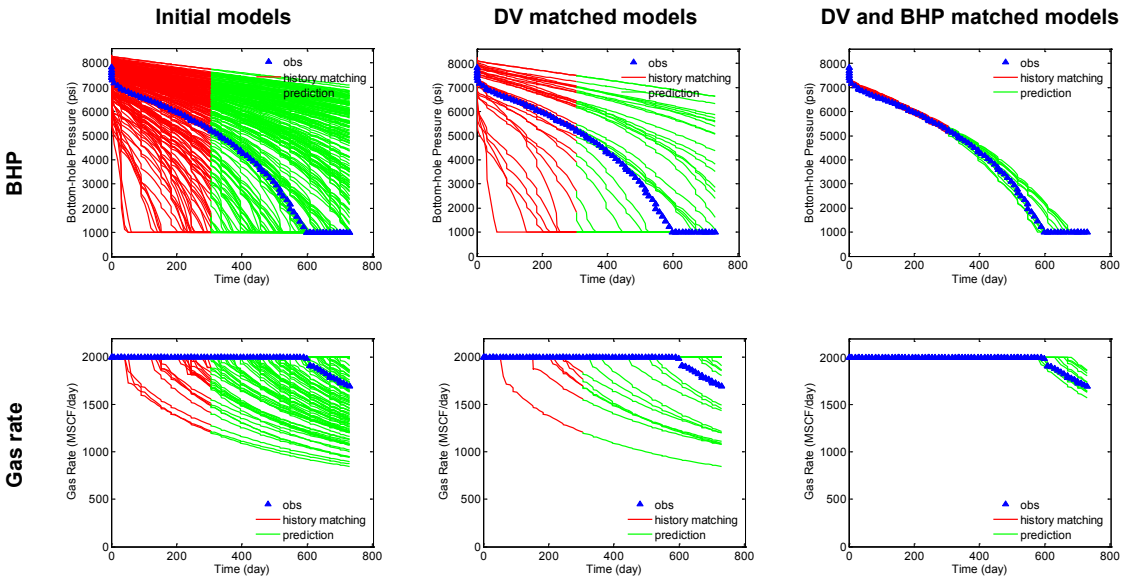

Fig. 3.14 History matching and predictions by GA with SRV proxy

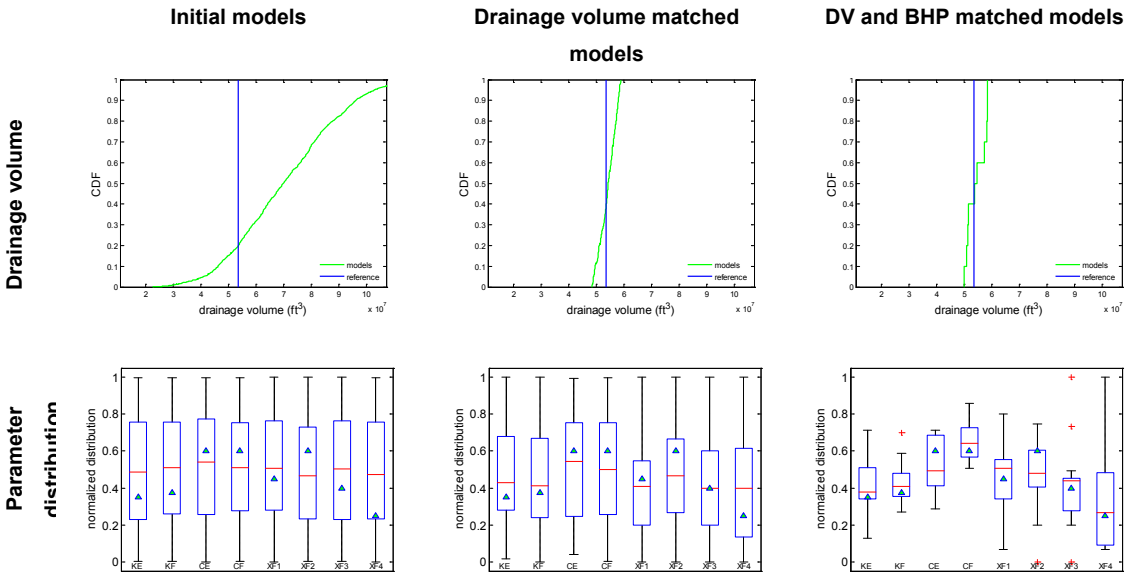

Fig. 3.15 Uncertainty analysis of models by GA with SRV proxy

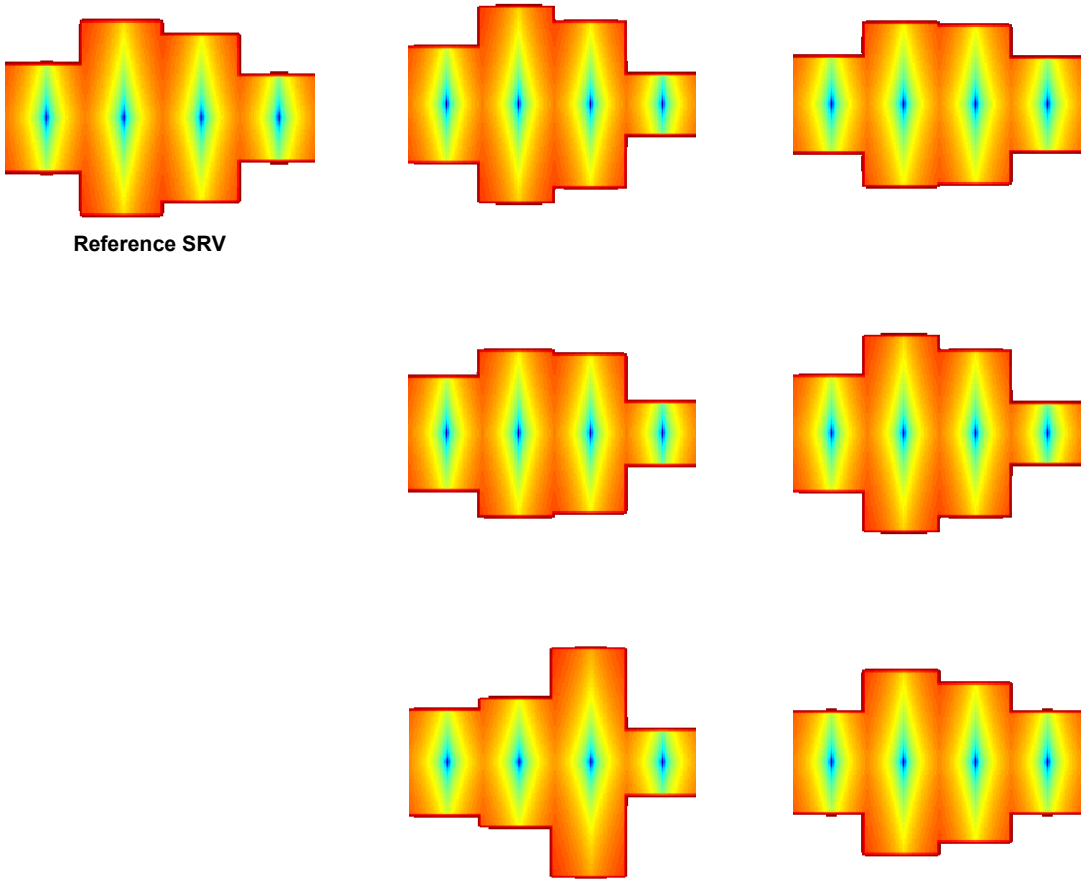

Fig. 3.16 SRV of models integrated with both DV and BHP

In order to further resolve uncertainty and non-uniqueness of updated models in Fig. 3.16, additional information can be added, such as well-log measurements, downhole pressure or temperature sensor data, rate measurements and/or acoustic data etc. In Chapter IV, integration of temperature measurements into reservoir characterization will be introduced to show how additional information is assimilated during geological modeling stage so that uncertainty in reservoir model can be reduced.

3.5 Summary

In this chapter, we have proposed a systematic method for assisted history matching of shale gas wells. Specifically, we build upon our expertise in conventional reservoir history matching to propose a workflow based on the use of experimental design and the genetic algorithm. The outcome of the history matching results in multiple sets of fracture/matrix parameter combinations that match both the well response such as the BHP and the SRV within specified limits and at the same time provide a measure of uncertainty in the parameter estimates. Some specific conclusions from this chapter are as follows:

- We have discussed a novel and efficient way of computing the drainage volume for unconventional wells that is based on the propagation of pressure 'front' and do not require flow simulation. The drainage volume calculations require only a few seconds of computation time as opposed to several hours of simulation time for comparable problems.
- We have shown the correspondence between the drainage volume and the SRV. By comparing the drainage volume with SRV estimates, we are able to incorporate SRV during history matching in addition to well BHP as is done in traditional history matching.
- Using a 3D synthetic example designed after a real field case, we are able to demonstrate the benefits of incorporating the SRV during the history matching process. Specifically, our results show that the uncertainty in the fracture/matrix parameters are reduced significantly when SRV was incorporated in addition to BHP during history matching as compared to BHP matching only.
- We have restricted our analysis to a rate constrained well. However, the arrival time of a pressure front doesn't depend on rates, but rather only its amplitude does. Therefore, the fast marching method still applies to BHP controlled wells.
- In our drainage volume calculations, we do not take into account change in permeability because of rock compactions. This can be solved by recomputing the

drainage volume at discrete time intervals, and by the end of each interval permeability is updated according to latest pressure solution from fast marching method.

CHAPTER IV

USING DOWNHOLE TEMPERATURE MEASUREMENTS TO ASSIST RESERVOIR CHARACTERIZATION*

In Chapter III, we integrated SRV as a constraint to pre-check evolutionary algorithm generated stochastic models. We have shown that by including microseismic-derived SRV, history matching was improved, parameter uncertainty was reduced, and dynamic production data prediction range was narrowed down. In this chapter, we will present another idea of incorporating a different data source to reservoir characterization - downhole temperature log data. Like inclusion of SRV, inclusion of temperature data greatly reduces model uncertainty and improves quality of history matching and prediction. However, unlike SRV in Chapter III, in this chapter we will integrate temperature data in a different stage of reservoir characterization: prior geological model construction, which is done before dynamic data assimilation.

We will primarily look at downhole temperature measurements in horizontal wells, which can be an important source of information that helps us characterize the reservoir and understand the bottom-hole flow conditions. The temperature measurements are obtained from permanent monitoring systems such as downhole temperature gauges and fiber optic sensors. Also, production history and bottomhole pressures are usually readily available and are routinely used for history matching to improve the initial geological models. Combining the downhole temperature distribution and the production history, we can extract more reliable information about the reservoir permeability distribution and bottomhole flow conditions that help us optimize the wellbore performance, particularly in horizontal wells.

In this chapter, we use a thermal model and a transient, 3D, multiphase flow reservoir model to calculate the wellbore temperature distribution in horizontal wells. By comparing the simulated temperature and the observed data, we first derive large-scale permeability trends in the reservoir. These permeability trends are then incorporated as 'secondary' information in the geologic model building and history matching. Finally, the updated permeability models from history matching are used to infer the downhole flow conditions along horizontal wells. The final outcome is a geologic model that is consistent with reservoir static and dynamic information, and also the wellbore temperature measurements.

We present several synthetic cases to illustrate the procedure. The results show that with only production history matching without distributed data along the wellbore, the water entry location in horizontal wells cannot be detected satisfactorily. Combining production history matching with the temperature distribution in the wellbore, we can get an improved geological model that can match not only dynamic production history but also, locate the water entry correctly. Therefore, based on prediction from the downhole flow conditions and the updated geological model, we can now optimize the well performance by controlling the inflow rate distribution, such as shutting inflow control devices (ICD) of high water inflow sections (Li et al. 2011).

4.1 Introduction

Horizontal wells are now routinely applied as part of the oil and gas field development strategy. Inferring reservoir and downhole flow conditions are important aspects of production and recovery optimization of horizontal wells. The commonly used method to obtain downhole flow conditions is production logging, and more recently, downhole temperature and pressure sensors become a valuable addition for accessing downhole flow conditions. Many studies have been presented in analyzing these data for production optimization. Alaeddin and Maizeret (2003) used production logging

technology to evaluate the contribution of two horizontal legs and possible water entry locations. This information can help to manage reservoir for optimizing the re-development plan of the field. Alhuthali et al. (2007) provided an optimal waterflood reservoir management by rate control. Their results show that the correct rate control for horizontal well with ICV completions can delay the water breakthrough time and significantly increase the reservoir recovery. Real time production data is also used for optimizing oil recovery in multilateral wells (Alghareeb et al. 2009). Based on the production history data and reservoir permeability distribution, an optimum ICV configuration can be obtained so as to minimize water cut and maximize net present value.

Much of the previous optimization works are based on known reservoir geologic models. Then, the downhole flow condition in horizontal wells can be predicted via forward modeling followed by data integration. Production history matching is routinely used to update the geologic models. Based on the refined reservoir information, we can optimize well performance by relocating the inflow rate along horizontal wells. However, because of the hydrodynamic connections or fluid mixture in horizontal wells, the reservoir information is often difficult to extract. In such situations, collecting additional information about well and reservoir, such as downhole temperature data, and interpreting them correctly, will help us understand reservoir and well performance more clearly.

Horizontal temperature data is usually measured by either production logging or distributed temperature sensor (DTS). Because these transient temperature data are distributed along the well, they can provide more information about the wellbore and the reservoir. Li and Zhu (2010) developed a detailed thermal model to interpret temperature data to obtain downhole flow conditions. In addition, this model also reveals some relations between the transient inflow fluid temperature and the reservoir permeability characteristics. Specifically, their results showed the possibility to obtain a coarse-scale reservoir permeability distribution based on the interpretation of the observed temperature data. This coarse-scale permeability distribution can provide guidance for

generating detailed permeability model conditioned to well data and geologic information for use in production history matching.

In this chapter, we develop an integrated workflow for including the downhole temperature information during production history matching. The organization of the chapter is as follows. First of all, we introduce the fundamentals of temperature interpretation, aimed at how the temperature information can be translated to a coarse-scale permeability distribution. Next, we utilize the coarse-scale permeability as constraints in generating high resolution geological models using geostatistical methods, viz. sequential Gaussian simulation with block kriging. Finally, we further calibrate these models to production data using streamline-based generalized travel time inversion. We use synthetic water-oil examples with two horizontal wells to illustrate our approach and how the proposed method can help optimize production.

4.2 Methodology

Earlier work has shown that downhole temperature interpretation can provide a coarse-scale reservoir permeability distribution (Li and Zhu 2010). The question we address here is how to incorporate this information for geologic modeling and production history matching. There are two potential approaches, possibly among others. The first one is to incorporate the coarse-scale permeability information as 'secondary' information while constructing the prior geologic model. This model can then be history matched to further update the geologic model. Another approach would be to include the temperature-derived coarse-scale permeability as a penalty function during the history matching process. In this chapter, we adopt the former approach.

Fig. 4.1 shows an outline of an integrated approach that combines the temperature interpretation and production history matching for dynamic reservoir characterization and modeling. It includes four major steps as follows.

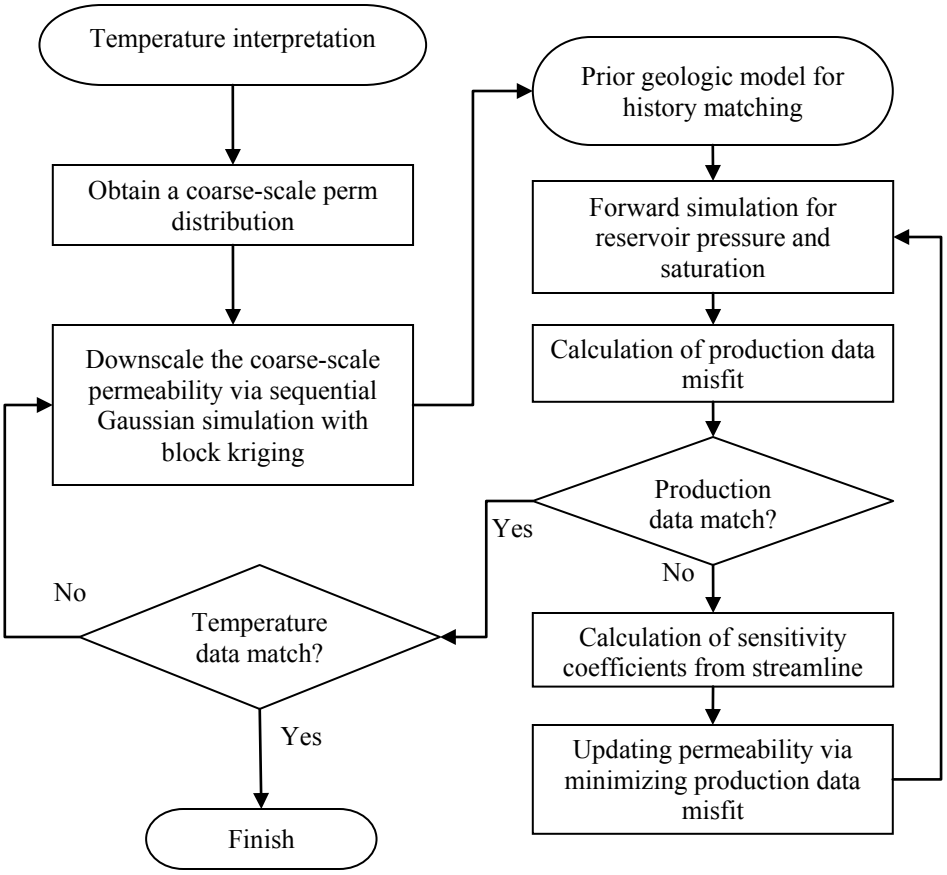

Fig. 4.1 Integrated workflow for incorporating temperature data into history matching

Step 1: Use of temperature interpretation method to match the observed temperature data, and obtain a coarse-scale permeability distribution.

Step 2: Generating high-resolution geologic model constrained to the coarse-scale permeability estimate. This is accomplished using sequential Gaussian simulation (SGS) with Block Kriging (BK), much along the line of seismic data integration into geologic models.

Step 3: Use of the geologic model from step 2 as the prior model for production history matching. The history matching is carried out using a fast streamline-based approach that is well-suited for the high resolution model.

Step 4: Forward modeling of wellbore temperature to cross-check that the history matched model reproduces the temperature data. If the updated model reproduces the wellbore temperature measurements within pre-specified tolerance, we accept the refined permeability distribution. Otherwise, we go back to step 2 and repeat the process.

4.2.1 Temperature Interpretation Method

The temperature interpretation method infers downhole flow conditions using the measured temperature and pressure data, and includes a forward model and an inversion method. The forward model consists of a reservoir model and a wellbore model. It can be used for 3D multiphase flow in the reservoir. The inversion method matches the observed temperature data to generate downhole flow conditions in the horizontal well and also, a coarse permeability distribution.

Reservoir Model. We have utilized a streamline simulator to generate reservoir pressure and saturation distribution (Datta-Gupta and King 2007). These pressures and saturations are then utilized to solve temperature equation. Including the thermal expansion and viscous dissipation effects, the reservoir temperature equation is given by Yoshioka et al. (2007)

$$-\left[\sum_i \left(\phi S_i \rho_i C_{pi}\right) + (1-\phi)\rho_s C_{ps}\right]\frac{\partial T}{\partial t} + \sum_i \left(\phi S_i \beta_i T \frac{\partial p_i}{\partial t}\right)$$
$$= \sum_i \rho_i \vec{u}_i \cdot C_{pi} \nabla T + \sum_i \vec{u}_i \cdot \nabla p_i - \sum_i \beta_i T(\vec{u}_i \cdot \nabla p_i) - \nabla \cdot (K_{Tt} \nabla T) + \sum_i \rho_i \vec{u}_i \cdot \nabla(gD) \quad \text{.....} \tag{4.1}$$

Eq. 4.1 is solved by finite difference method. The total heat conductivity K_{Tt} is treated as a constant. The heat transfer between the reservoir grid and the wellbore segment is given by Li and Zhu (2010)

$$\dot{Q}_h\Big|_{res-well} = -K_{Tt}\frac{\partial T}{\partial r}\Big|_{r=r_w} + \sum_{i=1}^{N_p}\left(\rho\bar{u}C_p\right)_i \cdot \left(T_{res} - T_I\right)_{well-located} \quad \text{.....} \quad (4.2)$$

In the right hand side of the above equation, the first term represents the heat conduction at the outside of wellbore, and the second term represents the heat convection from reservoir to wellbore.

Wellbore Model. We use the horizontal well model developed by Yoshioka et al. (2005; 2007) to calculate the temperature and pressure in the wellbore. The pressure equation is derived from momentum balance and is given by

$$\frac{dp}{dx} = -\frac{\rho v^2 f}{R} - \frac{d\left(\rho v^2\right)}{dx} - \rho g \sin\theta \quad \text{.....} \quad (4.3)$$

And, the temperature equation from energy balance gives

$$\frac{dT}{dx} = \frac{\left(\rho v C_p K_{JT}\right)_T}{\left(\rho v C_p\right)_T}\frac{dp}{dx} + \frac{2}{R}\frac{\gamma\left(\rho v C_p\right)_{T,I} + (1-\gamma)\alpha_T}{\left(\rho v C_p\right)_T}\left(T_I - T\right) - \frac{(\rho v)_T}{\left(\rho v C_p\right)_T} g\sin\theta \quad \text{.....} \quad (4.4)$$

where the subscript T denotes the total average number of all phases. The solutions of **Eq. 4.3** and **Eq. 4.4** provide the temperature and pressure distribution in the wellbore.

Coupled Reservoir and Wellbore Temperature. To solve for temperature distribution in the wellbore, we need to solve the coupled reservoir and well bore equations, Eq. 4.2 and Eq. 4.4. For this, we must know the arriving temperature T_I, which is the link between the reservoir grid temperature and wellbore temperature. The T_I is assumed to have the form

$$T_I = c_1 r_w^{\,n_1} + c_2 r_w^{\,n_2} + b \quad \text{.....} \quad (4.5)$$

The details of the coefficients of T_I can be found in the previous work (Li and Zhu 2010). These coefficients are obtained from fluid properties, reservoir permeability, grid geometry, and drawdown pressure from grid to wellbore.

Temperature Inversion Method. Our available data for inversion is the temperature distribution along horizontal wells. The goal of the inversion is to infer downhole flow conditions and a coarse-scale permeability distribution based on the temperature data. For this purpose, our objective function is defined as follows,

$$E(w) = D_T \sum_j \left(T^{cal} - T^{obs}\right)_j^2 \quad \text{..... (4.6)}$$

where D_T is the weighting term that is related to measurement errors.

The horizontal well temperature can be obtained from the forward model for a given set of conditions. When the temperature calculated from the forward model agrees with the observed data, that is, the objective function reaches a minimum, we conclude that the wellbore flow profile is identified under these conditions. A primary unknown here is the reservoir permeability distribution which is obtained via the inversion process.

The reservoir permeability is parameterized using a very coarse-scale distribution and is adjusted to match the observed and simulated temperature response. We use another stochastic algorithm Metropolis-Hastings MCMC algorithm to minimize the objective function (Ma et al. 2008). At state n, for a given initial permeability distribution, k_n , we calculate $E(k_n)$ using Eq. 4.6. Next, we generate k_{n+1} from a pre-specified proposal distribution $q_d(k \mid k_n)$. With the proposed permeability distribution k_{n+1}, we calculate $E(k_{n+1})$. The proposed permeability distribution, k_{n+1} is accepted according to the probability,

$$\rho_{prob}(k_n, k_{n+1}) = \min\left(1, \frac{q_d(k_{n+1} \mid k_n) E(k_{n+1})}{q_d(k_n \mid k_{n+1}) E(k_n)}\right) \quad \text{..... (4.7)}$$

After a series of sampling (known as burn-in), we collect samples $k_0, k_1, \ldots k_n, k_{n+1}, \ldots$, which are possible solutions to the inverse problem.

The temperature inversion process results in a very coarse-scale estimate of the reservoir permeability distribution. In our approach, we treat this information as 'soft' or 'secondary' data and incorporate the coarse-scale permeability into high resolution geologic modeling using downscaling techniques, viz. the Sequential Gaussian Simulation with Block Kriging. The high-resolution model is then history matched to further update the permeability distribution by matching the production history.

4.2.2 Downscaling Coarse-scale Permeability from Temperature

The coarse-scale permeability distribution obtained from inversion of the temperature data is integrated into geologic modeling using Sequential Gaussian Simulation with Block Kriging (SGSBK). The SGSBK was originally introduced by Behrens et al. (1998) to integrate seismic data into geologic modeling. The method provides a systematic framework for static data integration accounting for the varying scales and precisions of the data. A brief summary of the SGSBK is given as follows:

The simple kriging estimator conditioned to both point data and block data (Liu and Journel 2009) is

$$Z_{SK}(\mathbf{u}) = \mathbf{m}_0 + \Lambda^T \mathbf{D} \quad \text{.....} \quad (4.8)$$

where $\Lambda^T = [\boldsymbol{\lambda}_P, \boldsymbol{\lambda}_B]$ denotes the kriging weights for point data P and block data B, $\mathbf{D}^T = [\mathbf{P}, \mathbf{B}]$ denotes the data value vector, P denotes known data points, B denotes known block data, $\mathbf{m}_0$ denotes stationary means and **u** means the point.

Therefore the kriging system is

$$\mathbf{K}\Lambda = \mathbf{k}\text{, with } \mathbf{K} = \begin{bmatrix} \mathbf{C}_{PP'} & \overline{\mathbf{C}}_{PB} \\ \overline{\mathbf{C}}^{T}_{PB} & \overline{\overline{\mathbf{C}}}_{BB'} \end{bmatrix} \text{ and } \mathbf{k} = \begin{bmatrix} \mathbf{C}_{P_0P} \\ \overline{\mathbf{C}}_{P_0B} \end{bmatrix} \quad (4.9)$$

where P_0 is point to be estimated. **K** denotes data-to-data covariance matrix, **k** denotes the data-to-unknown covariance matrix, **C** denotes point-to-point covariance matrix, $\overline{\mathbf{C}}$ denotes point-to-block covariance matrix, $\overline{\overline{\mathbf{C}}}$ denotes block-to-block covariance matrix. Symbols in bold denote vectors or matrices. The point-to-block and block-to-block covariances can be approximated by discretizing the following integral forms respectively

$$\overline{C}(P,B) = \frac{1}{V}\sum_{P'\in B} C(P,P')\Delta V \quad (4.10)$$

$$\overline{\overline{C}}(B,B') = \frac{1}{VV'}\sum_{P\in B,P'\in B'} C(P,P')\Delta V\Delta V' \quad (4.11)$$

These point-to-point, point-to-block, block-to-block covariances are obtained from variogram models with SGSBK, which ensures generated fine scale model are not only smooth but also physically reasonable.

The kriging variance is

$$\sigma^2_{SK}(\mathbf{u}) = C(0) - \Lambda^T\mathbf{k} \quad (4.12)$$

where $C(0)$ is the stationary variance of point **u**.

Using Eqs. 4.8 to 4.12, we can generate a new Gaussian permeability distribution. More details of the block sequential simulation algorithm is introduced by Remy et al. (2008).

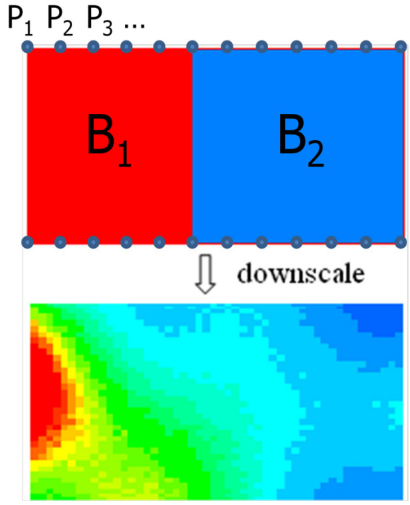

Fig. 4.2 Downscaling of the temperature inverted coarse-scale permeability

Fig. 4.2 illustrates the method by a simple example of downscaling two-value coarse permeability. We downscale the block data and then assign fine-scale permeabilities to grid cells, conditioned to permeability at well locations.

4.2.3 Production Data Integration by Streamline Sensitivity

The fine-scale permeability distribution derived from the SGSBK is now further updated via history matching of production data. This step involves minimization of a penalized misfit function as given by Chapter II local model calibration and results in an updated permeability model that matches the production data and also preserves the features of the prior permeability model. By incorporating the norm penalty and staying close to the prior model, we expect that the final updated model will still maintain the matches to the temperature data. We verify this by forward modeling of the wellbore temperature using the final updated permeability. Our experience shows that for most cases the temperature matches are preserved. In rare cases when the temperature matches are not satisfied within specified tolerance, an alternative would be to start with another realization of the prior permeability distribution obtained from the SGSBK.

4.3 Results and Discussions

4.3.1 A Synthetic Case with Horizontal Wells

We use a synthetic case to illustrate our procedure. **Fig. 4.3** and **Fig. 4.4** are the reservoir geometry and the reference permeability distribution. The reservoir has a horizontal injection well and a horizontal production well, both located in the middle of the pay zone. The production well has a constant production rate, 6000 stb/d. We assume the observed data to be the water cut and downhole temperature at the production well. For the synthetic example, the observed data are generated from the forward model with the known permeability distribution. They are plotted in **Fig. 4.5** and **Fig. 4.6**.

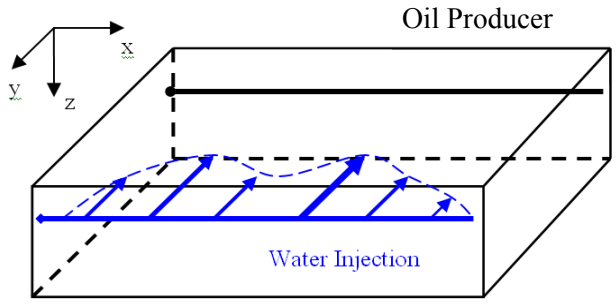

Fig. 4.3 Reservoir geometry and horizontal wells

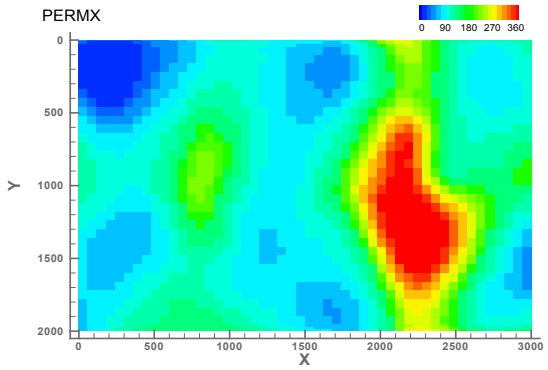

Fig. 4.4 Reference permeability distribution

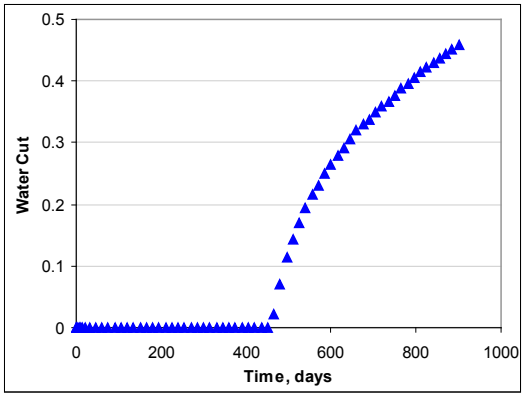

Fig. 4.5 Observed horizontal well water-cut history

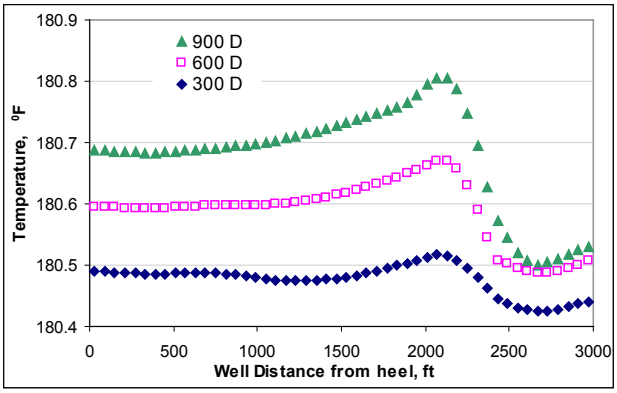

Fig. 4.6 Downhole temperature distribution

4.3.2 Production History Match Only

As a base case, we do not incorporate the temperature data to start with. Our initial permeability model is generated using sequential Gaussian simulation with well data only and no secondary information. The permeability distribution is then updated using the water-cut data at the well.

Fig. 4.7a shows water-cut history matching results in which only production history is considered in data integration. **Fig. 4.8** shows the updated model. As expected, the updated model is able to reproduce the production history but fails to match the observed temperature data, as shown in **Fig. 4.7b**. The downhole flow rates in tubing, particularly the water entry points, also exhibit large deviations as shown in **Fig. 4.7c**.

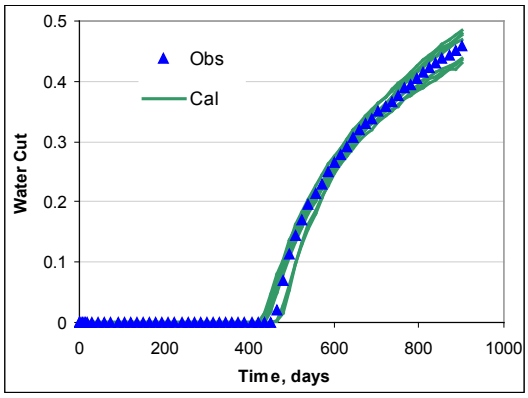

(a)

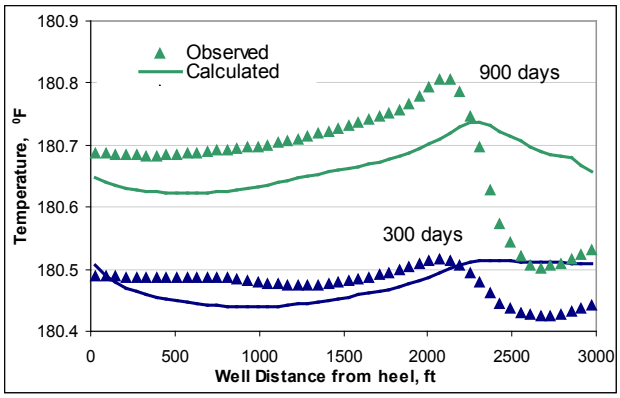

(b)

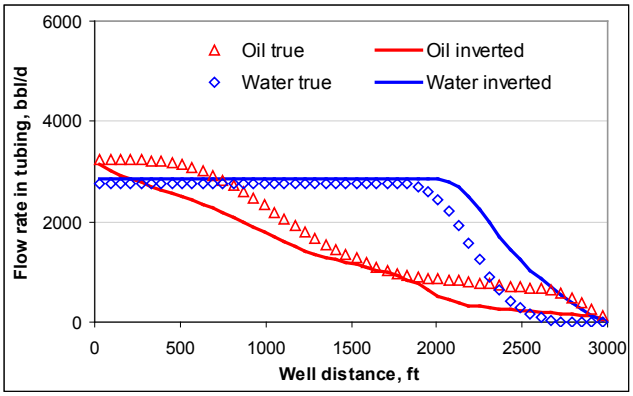

(c)

Fig. 4.7 Water-cut history get matching, but temperature data is not matching and downhole flow rates may not be predicted correctly

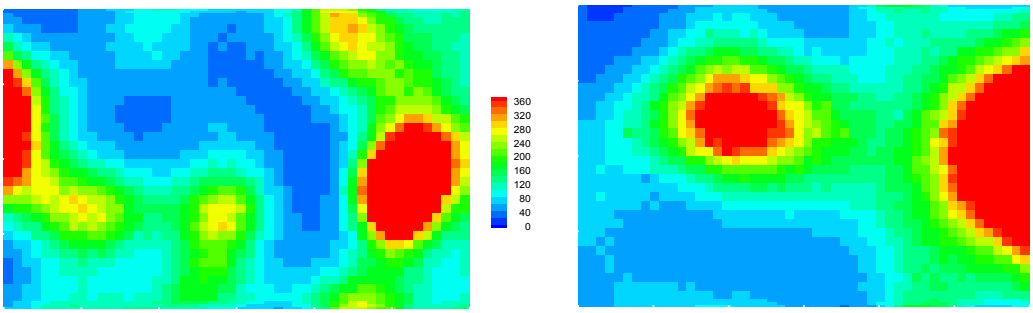

Fig. 4.8 Permeability distributions derived from water cut and well data only

4.3.3 Temperature Interpretation Only

In this example, we only use the temperature interpretation to diagnose the downhole flow condition. To start with, we subdivide the reservoir to several sections according to the temperature trend or temperature derivative. **Fig**. 4.9**a** shows reservoir sections inferred based on the temperature data. In each section, the permeability is assigned a constant value. The permeabilities are considered unknown variables that need to be determined during the inversion process. Because the measured temperature is only along the horizontal well (x direction), the estimated reservoir permeability distribution is aligned along the well as shown in **Fig**. 4.9**b**.

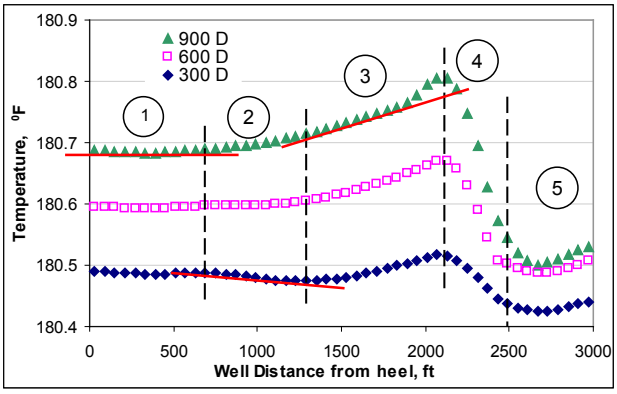

(a)

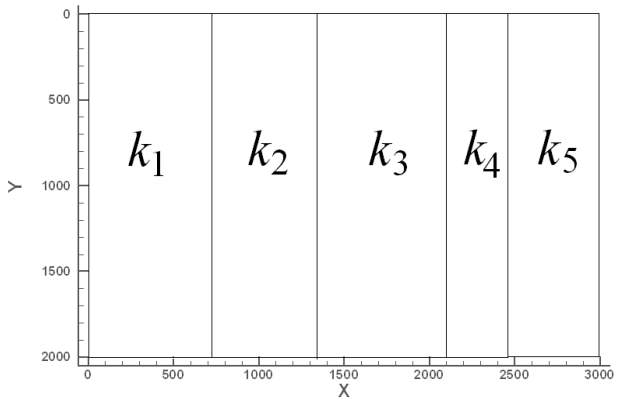

(b)

Fig. 4.9 Estimated reservoir permeability sections by temperature trend or derivative by temperature inversion

We first calculate the horizontal well temperature from the forward model by adjusting the permeability value in each section, until the calculated temperature match the observed data, as in **Fig. 4.10b**. The inverted permeability at this temperature matching condition is shown in **Fig. 4.11a,** and compared with the true permeability distribution in **Fig. 4.11b**. Although the temperature does not match perfectly, the simulated results follow the trend of the observed data. Using the temperature inverted permeability distribution, we also obtain water-cut history in **Fig. 4.10a**, and the flow rate profiles for oil and water along the horizontal well at time 900 days in **Fig. 4.10c**. The interpreted results of the flow rate profiles are acceptable. The water entry location is detected correctly, and the water and oil flow rate distributions are close to the reference case.

The simulated water-cut history with this inverted permeability distribution follows the trend of the observed data, but still shows significant mismatch. We can also see that the inverted temperature at the high permeability section increases faster than the observed data. Some of these discrepancies arise from the fact that the inverted

permeability is only 1D, which is an approximation of the 2D true permeability. Next, to improve the water cut and temperature data matching, we combine the temperature interpretation method and production history matching.

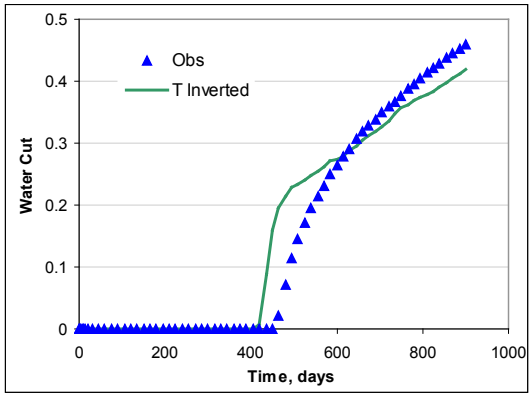

(a)

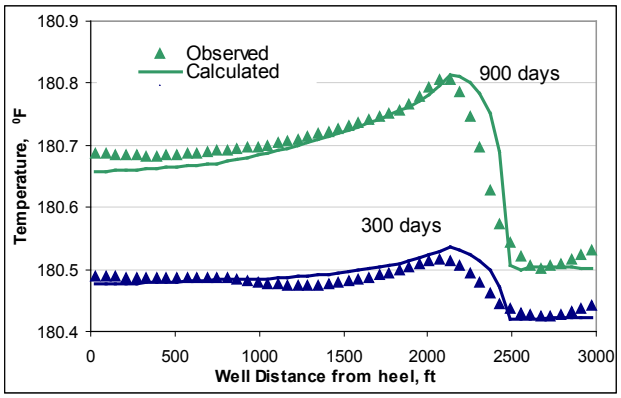

(b)

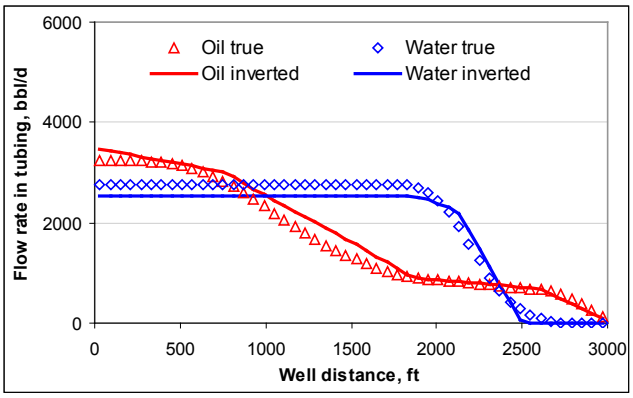

(c)

Fig. 4.10 Temperature inverted reservoir permeability for water cut matching is not very accurate, but the inverted flow rates at 900 days are acceptable and the water entry location is detected correctly

As mentioned above, we want to use the temperature inverted permeability distribution as a coarse-scale initial model. To verify that this temperature inverted permeability distribution indeed represents the average of the true 2D permeability, we calculate the arithmetic, geometric and harmonic mean of the inverted regions for the reference permeability distribution. **Fig. 4.11c** shows the comparison between the temperature-inverted permeabilities and the corresponding averages of the true permeability. The results indicate that the 1D temperature inverted permeability, indeed, captures the basic characteristics of the true permeability field, such as the low and the high permeability ranges.

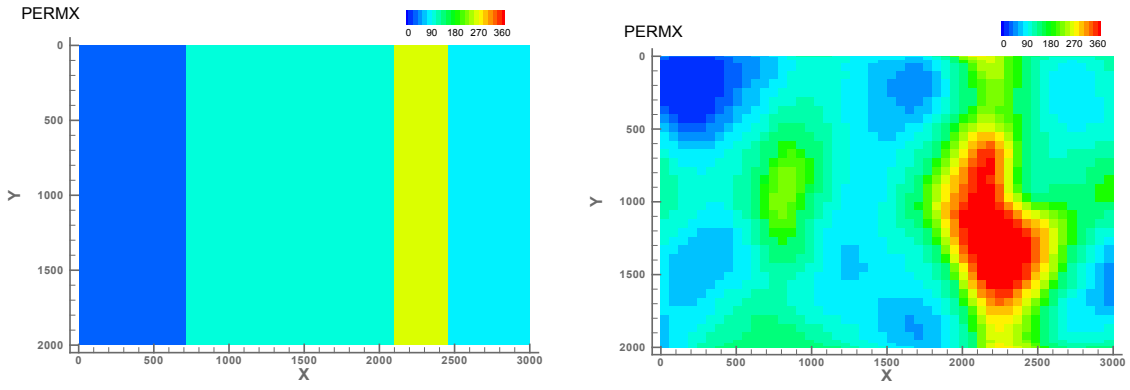

a b

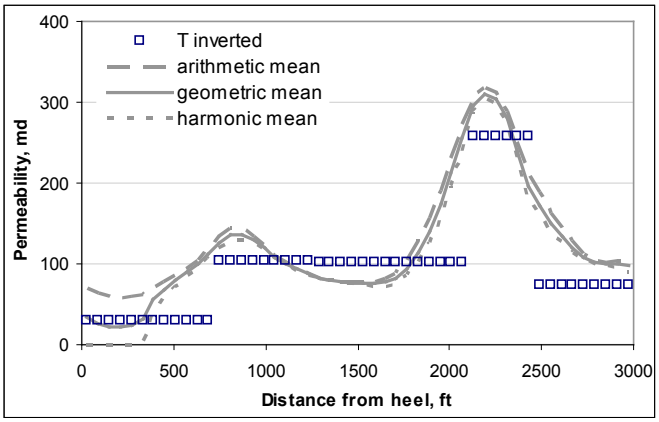

c

Fig. 4.11 Temperature inverted reservoir perm compares with average of true perm

4.3.4 Result of Integrated Approach

For this case, we generate initial permeability models from sequential Gaussian simulation with block kriging. Block definition and average permeabilities are from the interpretation of the observed temperature data. The permeability distribution is conditioned to hard data at well locations. Any other geologic information can be easily

incorporated at this stage. For each model, we perform a streamline-based GTTI to match the water cut data at the well. In this way we are able to take into consideration both temperature data and production history. **Fig. 4.12** shows one realization of permeability distribution resulting from our integrated approach, and **Fig. 4.13** shows the corresponding water cut, fluid flow rates in tubing, and calculated temperature distribution. Compared with only temperature interpretation results, the water-cut history matching has significantly improved, the temperature match is still retained, and the calculated temperature at the high permeability section shows improved behavior. The water entry location is found correctly and the calculated water and oil flow rates in tubing are very close to that of the true data.

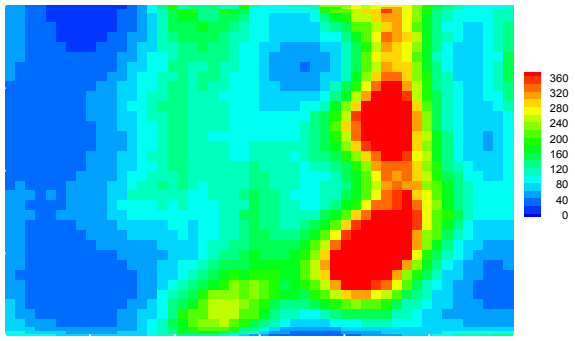

Fig. 4.12 A sample of final updated permeability from the integrated approach

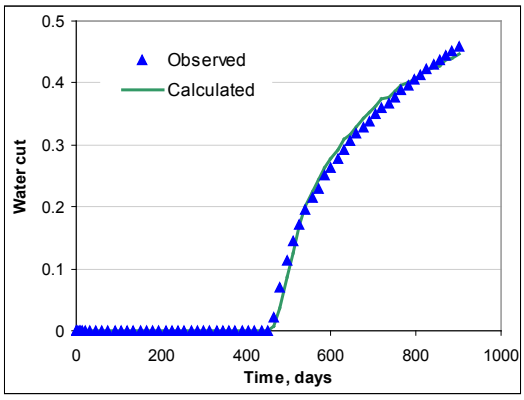
Observed
Calculated
Water cut
Time, days
0.5
0.4
0.3
0.2
0.1
0
0
200
400
600
800
1000

(a)

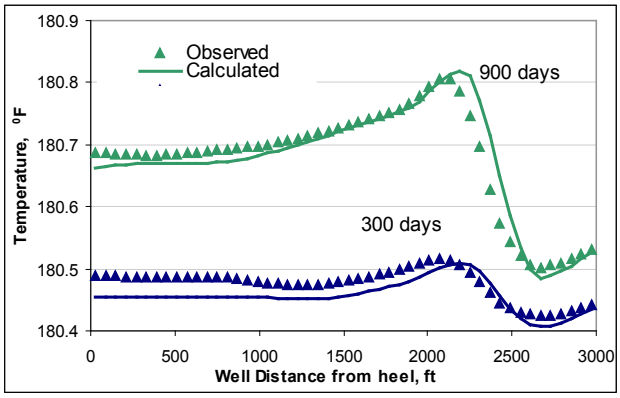
Observed
Calculated
900 days
300 days
Temperature, °F
Well Distance from heel, ft
180.9
180.8
180.7
180.6
180.5
180.4
0
500
1000
1500
2000
2500
3000

(b)

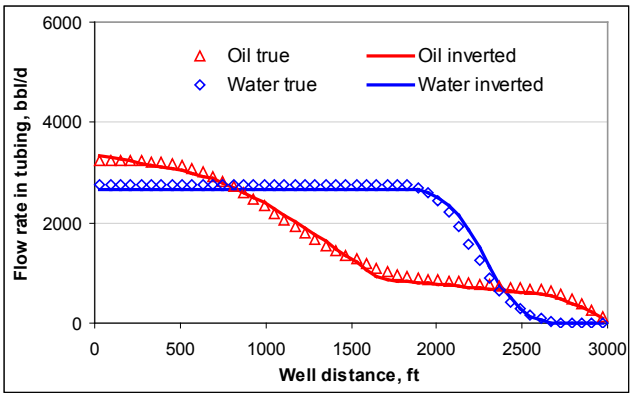

(c)

Fig. 4.13 Water-cut history from refined perm matches the observed data, and the inflow rate distribution is also better

Once we detect the water entry location correctly, we can decide whether we need shut in the water producing zone (2100 ft to 2460 ft). After our procedure, to make sure we correctly determine the phase influx along the horizontal well, other measurement may be required. By shutting in this zone to restrict the water entry, the well performance can be improved.

4.4 Summary

In this chapter, we developed a procedure to combine the temperature interpretation method and production history matching to diagnose reservoir characteristics and horizontal well flow conditions. Our results show that the downhole temperature measurements can assist to improve the understanding of reservoir characteristics. The outcome is a geologic model that is consistent with the prior static model and dynamic information, and also the wellbore temperature measurements. The updated model can then be used to predict the downhole flow conditions in the horizontal well operation. By shutting the unwanted phase entry sections, we can optimize the well performance. Some specific conclusions from this chapter are summarized as follows:

1. We have presented an integrated framework for incorporating temperature data and production history for improved reservoir characterization and optimization of horizontal well performance.
2. Our approach involves obtaining a coarse-scale permeability distribution from the temperature interpretation which is incorporated into the prior geologic model construction. This model is further updated though production history matching along with a ‘norm’ constraint to preserve the temperature matching.
3. We have illustrated our approach using synthetic examples. The results clearly demonstrate the benefits of the integrated approach over either the temperature interpretation only or the production history matching only.

CHAPTER V

CONCLUSIONS AND RECOMMENDATIONS

In this work, we have presented a hierarchical workflow for assisted history matching that integrates not only static data including modular dynamic tester pressures, shut-in bottom-hole pressures, stimulated reservoir volumes, and downhole distributed temperature measurements etc., but also dynamic production data including water-cut, and flowing bottom-hole pressures. The proposed approach generally consists of two steps: global update and local update. In global model calibration, stochastic algorithm is used to calibrate large-scale geological features related to reservoir energy, while in local model calibration we use an efficient streamline-based sensitivity technique to calibrate high resolution reservoir permeability heterogeneity. Our proposed method leads to a significant reduction in computation time and has been demonstrated using both synthetic and field applications.

5.1 Conclusions

Some specific conclusions that can be made from this work are as follows:

The combination of structured global and local history matching procedures has worked quite well. The global match is used to calibrate the models for reservoir energy and reservoir connectivity and is based on total fluid production and reservoir pressures. Local updates calibrate the models to the fractional flow of water or gas and/or bottom-hole pressures consistent with the production data.

A stochastic global search approach based upon the genetic algorithm combined with a proxy model for the objective function provided an effective means to match the global parameters and produce an ensemble of preliminary solutions for the local update.

Streamline-based sensitivity and generalized travel time inversion algorithms are very useful for local updates. Given the reservoir energy has been calibrated to

reasonable level by global updates, this local search algorithm will find solutions very fast for each globally updated model. Flux connectivity and TOF displays can easily identify changes before and after global/local updates. Typically the structured global-local approach was shown to be stable in that the local updates preserved the global match for reservoir energy.

We have discussed a novel and efficient way of computing the drainage volume for unconventional wells that is based on the propagation of pressure 'front' and does not require flow simulations. The drainage volume calculations require only a few seconds of computation time as opposed to several hours of simulation time for comparable problems. We have shown the correspondence between the drainage volume and the SRV. By comparing the drainage volume with SRV estimates, we are able to incorporate SRV during history matching in addition to well BHP as is done in traditional history matching.

Using a 3D synthetic example designed after a real field case, we are able to demonstrate the benefits of incorporating the SRV during the history matching process. Specifically, our results show that the uncertainty in the fracture/matrix parameters are reduced significantly when SRV was incorporated in addition to BHP during history matching as compared to BHP matching only.

We have presented an integrated framework for incorporating temperature data and production history for improved reservoir characterization and optimization of horizontal well performance.

Our approach involves obtaining a coarse-scale permeability distribution from the temperature interpretation which is incorporated into the prior geologic model construction. This model is further updated though production history matching along with a 'norm' constraint to preserve the temperature matching.

We have illustrated our approach using synthetic examples. The results clearly demonstrate the benefits of the integrated approach over either the temperature interpretation only or the production history matching only.

5.2 Recommendations and Future Work

Proxy Model. Though the genetic algorithm can calibrate taking into account uncertainty almost all sorts of reservoir model parameters, it is costly due to its stochastic search nature. It can be speeded up by using proxy models, either response surface proxy in Chapter II or SRV proxy in Chapter IV. However, the inclusion of any proxy model may bring in bias or errors, compared to flow simulations. Therefore, one should pay special attention on how much we should rely on the proxy model. More investigations are needed on this aspect.

GA Parameters. Another tricky part of the evolutionary algorithm is how to set GA parameters. A rule of thumb is that for a larger number of variable, a larger population should be used, for instance ten to twenty times variable number. Uniform crossover is preferred since it provides fast hill-climbing and introduces more diversity at the same time. One can adjust uniform mutation rate from 0.1 percent to 1 percent according to dynamic check of the similarity and dissimilarity of the populated models. Proper choice of GA parameters can be an area of future research.

Integration of Various Types of Data. One may conclude that any data, either static or dynamic can be included to history matching work, either in a structured way, for instance use one as pre-check and the rest as second step objective function, or include them all in an overall objective function. According to this work, a better way would be analyze the data types first and integrate in a hierarchical manner according to its nature, and scale of influence. However, parameterization of the uncertainty is extremely important and needs more investigations.

Considerations of Fast Marching Method. In order to consider geomechanical

effects on the fast marching solution, a future consideration will be to include pressure effects on the fast marching solution. Time can be divided into small intervals, and within each time interval permeability can be updated according to the latest pressure solution.

REFERENCES

Alaeddin, E., and Maizeret, P.-D. 2003. Using Production Logging Technology for Reservoir Management in the Persian Gulf Paper SPE 85667 presented at Nigeria Annual International Conference and Exhibition, Abuja, Nigeria, 4-6 August 2003. DOI: 10.2118/85667-MS.

Alghareeb, Z.M.,Horne, R.N.,Yuen, B.B., and Shenawi, S.H. 2009. Proactive Optimization of Oil Recovery in Multilateral Wells Using Real Time Production Data. Paper SPE 124999 presented at SPE Annual Technical Conference and Exhibition, New Orleans, Louisiana, USA, 4-7 October 2009. DOI: 10.2118/124999-MS.

Alhuthali, A.,Oyerinde, D., and Datta-Gupta, A. 2007. Optimal Waterflood Management Using Rate Control. *SPE Reservoir Evaluation & Engineering* **10** (5): 539-551. SPE-102478-PA. DOI: 10.2118/102478-PA.

Behrens, R.A.,MacLeod, M.K.,Tran, T.T., and Alimi, A.C. 1998. Incorporating Seismic Attribute Maps in 3D Reservoir Models. *SPE Reservoir Evaluation & Engineering* **1** (2): 122-126. SPE-36499-PA. DOI: 10.2118/36499-PA.

Bello, R.O., and Wattenbarger, R.A. 2010. Multi-stage Hydraulically Fractured Horizontal Shale Gas Well Rate Transient Analysis. Paper SPE 126754 presented at North Africa Technical Conference and Exhibition, Cairo, Egypt, 14-17 February. DOI: 10.2118/126754-MS.

Beres, D.L., and Hawkins, D.M. 2001. Plackett-Burman Technique for Sensitivity Analysis of Many-parametered Models. *Ecological Modelling* **141** (1-3): 171-183. DOI: 10.1016/s0304-3800(01)00271-x.

Bhark, E.W.,Jafarpour, B., and Datta-Gupta, A. 2011a. An Adaptively Scaled Frequency-domain Parameterization for History Matching. *Journal of Petroleum Science and Engineering* **75** (3-4): 289-303. DOI: 10.1016/j.petrol.2010.11.026.

Bhark, E.W.,Jafarpour, B., and Datta-Gupta, A. 2011b. A Generalized Grid Connectivity-based Parameterization for Subsurface Flow Model Calibration. *Water Resources Research* **47** (6): W06517. DOI: 10.1029/2010wr009982.

Bissell, R.,Killough, J.E., and Sharma, Y. 1992. Reservoir History Matching Using the Method of Gradients on a Workstation. Paper SPE 24265 presented at European Petroleum Computer Conference, Stavanger, Norway, 24-27 May. DOI: 10.2118/24265-MS.

Bittencourt, A.C., and Horne, R.N. 1997. Reservoir Development and Design Optimization. Paper SPE 38895 presented at SPE Annual Technical Conference and Exhibition, San Antonio, Texas, USA, 5-8 October. DOI: 10.2118/38895-MS.

Blasingame, T.A., and Rushing, J.A. 2005. A Production-Based Method for Direct Estimation of Gas in Place and Reserves. Paper SPE 98042 presented at SPE Eastern Regional Meeting, Morgantown, West Virginia, USA, 14-16 September. DOI: 10.2118/98042-MS.

Britt, L.K., and Smith, M.B. 2009. Horizontal Well Completion, Stimulation Optimization, and Risk Mitigation. Paper SPE 125526 presented at SPE Eastern Regional Meeting, Charleston, West Virginia, USA, 23-25 September. DOI: 10.2118/125526-MS.

Cheng, H.,Datta-Gupta, A., and He, Z. 2005. A Comparison of Travel-Time and Amplitude Matching for Field-Scale Production-Data Integration: Sensitivity, Nonlinearity, and Practical Implications. *SPE Journal* **10** (1): 75-90. SPE-84570-PA. DOI: 10.2118/84570-PA.

Cheng, H.,Dehghani, K., and Billiter, T. 2008. A Structured Approach for Probabilistic-Assisted History Matching Using Evolutionary Algorithms: Tengiz Field Applications. Paper SPE 116212 presented at SPE Annual Technical Conference and Exhibition, Denver, Colorado, USA, 21-24 September. DOI: 10.2118/116212-MS.

Cheng, H.,Osako, I.,Datta-Gupta, A., and King, M.J. 2006. A Rigorous Compressible Streamline Formulation for Two- and Three-Phase Black-Oil Simulation. *SPE Journal* **11** (4): 407-417. SPE-96866-PA. DOI: 10.2118/96866-PA.

Cheng, H.,Oyerinde, A.,Datta-Gupta, A., and Milliken, W.J. 2007. Compressible Streamlines and Three-Phase History Matching. *SPE Journal* **12** (4): 475-485. 99465-PA. DOI: 10.2118/99465-PA.

Cheng, H.,Wen, X.-H.,Milliken, W.J., and Datta-Gupta, A. 2004. Field Experiences with Assisted and Automatic History Matching Using Streamline Models. Paper SPE 89857 presented at SPE Annual Technical Conference and Exhibition, Houston, Texas, USA, 26-29 September. DOI: 10.2118/89857-MS.

Cipolla, C.L.,Lolon, E.,Erdle, J., and Tathed, V.S. 2009. Modeling Well Performance in Shale-Gas Reservoirs. Paper SPE 125532 presented at SPE/EAGE Reservoir Characterization and Simulation Conference, Abu Dhabi, UAE, 19-21 October. DOI: 10.2118/125532-MS.

Cipolla, C.L., Weng, X., Mack, M.G., Ganguly, U., Gu, H. et al. 2011. Integrating Microseismic Mapping and Complex Fracture Modeling to Characterize Hydraulic Fracture Complexity. Paper SPE 140185 presented at SPE Hydraulic Fracturing Technology Conference, The Woodlands, Texas, USA, 24-26 January. DOI: 10.2118/140185-MS.

Cox, D.O.,Kuuskraa, V.A., and Hansen, J.T. 1996. Advanced Type Curve Analysis for Low Permeability Gas Reservoirs. Paper SPE 35595 presented at SPE Gas Technology Symposium, Calgary, Alberta, Canada, 28 April-1 May. DOI: 10.2118/35595-MS.

Cramer, D.D. 2008. Stimulating Unconventional Reservoirs: Lessons Learned, Successful Practices, Areas for Improvement. Paper SPE 114172 presented at SPE Unconventional Reservoirs Conference, Keystone, Colorado, USA, 10-12 February. DOI: 10.2118/114172-MS.

Datta-Gupta, A., and King, M.J. 2007. *Streamline Simulation: Theory and Practice*. SPE Textbook Series. Richardson, Texas: Society of Petroleum Engineers. ISBN 9781555631116.

Datta-Gupta, A.,Kulkarni, K.N.,Yoon, S., and Vasco, D.W. 2001. Streamlines, Ray Tracing and Production Tomography: Generalization to Compressible Flow. *Petroleum Geoscience* **7** (S): S75-S86. DOI: 10.1144/petgeo.7.S.S75.

Datta-Gupta, A.,Xie, J.,Gupta, N.,King, M.J., and Lee, W.J. 2011. Radius of Investigation and its Generalization to Unconventional Reservoirs. *Journal of Petroleum Technology* **63** (7): 52-55.

Fan, L.,Thompson, J.W., and Robinson, J.R. 2010. Understanding Gas Production Mechanism and Effectiveness of Well Stimulation in the Haynesville Shale Through Reservoir Simulation. Paper SPE 136696 presented at Canadian Unconventional Resources and International Petroleum Conference, Calgary, Alberta, Canada, 19-21 October. DOI: 10.2118/136696-MS.

Fetkovich, M.J. 1980. Decline Curve Analysis Using Type Curves. *SPE Journal of Petroleum Technology* **32** (6): 1065-1077. SPE-4629-PA. DOI: 10.2118/4629-PA.

Fisher, M.K., Wright, C.A., Davidson, B.M., Goodwin, A.K., Fielder, E.O. et al. 2002. Integrating Fracture Mapping Technologies to Optimize Stimulations in the Barnett Shale. Paper SPE 77441 presented at SPE Annual Technical Conference and Exhibition, San Antonio, Texas, USA, 29 September-2 October. DOI: 10.2118/77441-MS.

Floris, F.J.T.,Bush, M.D.,Cuypers, M.,Roggero, F., and Syversveen, A.R. 2001. Methods for quantifying the uncertainty of production forecasts: a comparative study. *Petroleum Geoscience* **7** (S): S87-S96. DOI: 10.1144/petgeo.7.S.S87.

Galassi, M., Davies, J., Theiler, J., Gough, B., Jungman, G. et al. 2009. *GNU Scientific Library Reference Manual*. UK: Network Theory Ltd. ISBN 0954612078.

Ghods, P., and Zhang, D. 2010. Ensemble Based Characterization and History Matching of Naturally Fractured Tight/Shale Gas Reservoirs. Paper SPE 133606 presented

at SPE Western Regional Meeting, Anaheim, California, USA, 27-29 May. DOI: 10.2118/133606-MS.

Gill, P.E.,Murray, W., and Wright, M.H. 1981. *Practical Optimization*: Academic Press. ISBN 0122839528.

Hassouna, M.S., and Farag, A.A. 2007. MultiStencils Fast Marching Methods: A Highly Accurate Solution to the Eikonal Equation on Cartesian Domains. *IEEE Transactions on Pattern Analysis and Machine Intelligence* **29** (9): 1563-1574. DOI: 10.1109/TPAMI.2007.1154.

He, Z.,Yoon, S., and Datta-Gupta, A. 2002. Streamline-Based Production Data Integration With Gravity and Changing Field Conditions. *SPE Journal* **7** (4): 423-436. SPE-81208-PA. DOI: 10.2118/81208-PA.

Hohl, D.,Jimenez, E., and Datta-Gupta, A. 2006. Field Experiences With History Matching an Offshore Turbiditic Reservoir Using Inverse Modeling. Paper SPE 101983 presented at SPE Annual Technical Conference and Exhibition, San Antonio, Texas, USA, 24-27 September. DOI: 10.2118/101983-MS.

Holditch, S.A. 2006. Tight Gas Sands. *SPE Journal of Petroleum Technology* **58** (6). SPE-103356-MS. DOI: 10.2118/103356-MS.

Holland, J.H. 1992. Genetic Algorithms. *Scientific American* **267** (1): 44-50.

Iman, R.L.,Davenport, J.M., and Zeigler, D.K. 1980. *Latin Hypercube Sampling (Program User's Guide). [LHC, in FORTRAN]*.

Kim, J.-U.,Datta-Gupta, A.,Brouwer, R., and Haynes, B. 2009. Calibration of High-Resolution Reservoir Models Using Transient Pressure Data. Paper SPE 124834 presented at SPE Annual Technical Conference and Exhibition, New Orleans, Louisiana, USA, 4-7 October. DOI: 10.2118/124834-MS.

King, G.E. 2010. Thirty Years of Gas Shale Fracturing: What Have We Learned? Paper SPE 133456 presented at SPE Annual Technical Conference and Exhibition, Florence, Italy, 19-22 September. DOI: 10.2118/133456-MS.

Kirkpatrick, S.,Gelatt, C.D.,Jr, and Vecchi, M.P. 1983. Optimization by Simulated Annealing. *Science* **220** (4598): 671-680.

Krige, D.G. 1951. A statistical approach to some basic mine valuation problems on the Witwatersrand. *Journal of the Chemical, Metallurgical and Mining Society* **52**: 119-139.

Kundert, D.P., and Mullen, M.J. 2009. Proper Evaluation of Shale Gas Reservoirs Leads to a More Effective Hydraulic-fracture Stimulation. Paper SPE 123586 presented at SPE Rocky Mountain Petroleum Technology Conference, Denver, Colorado, USA, 14-16 April. DOI: 10.2118/123586-MS.

Lee, W.J. 1982. *Well Testing*. SPE Textbook Series. Richardson, Texas: Society of Petroleum Engineers. ISBN 978-089520-317-0.

Lee, W.J., and Hopkins, C.W. 1994. Characterization of Tight Reservoirs. *SPE Journal of Petroleum Technology* **46** (11): 956-964. SPE-29091-PA. DOI: 10.2118/29091-PA.

Li, B., and Friedmann, F. 2005. Novel Multiple Resolutions Design of Experiment/Response Surface Methodology for Uncertainty Analysis of Reservoir Simulation Forecasts. Paper SPE 92853 presented at SPE Reservoir Simulation Symposium, The Woodlands, Texas, USA, 31 January-2 Feburary. DOI: 10.2118/92853-MS.

Li, Z.,Yin, J.,Zhu, D., and Datta-Gupta, A. 2011. Using downhole temperature measurement to assist reservoir characterization and optimization. *Journal of Petroleum Science and Engineering* **78** (2): 454-463. DOI: 10.1016/j.petrol.2011.06.012.

Li, Z., and Zhu, D. 2010. Predicting Flow Profile of Horizontal Well by Downhole Pressure and Distributed-Temperature Data for Waterdrive Reservoir. *SPE Production & Operations* **25** (3): 296-304. SPE-124873-PA. DOI: 10.2118/124873-PA.

Liu, Y., and Journel, A.G. 2009. A package for geostatistical integration of coarse and fine scale data. *Computers & Geosciences* **35** (3): 527-547. DOI: 10.1016/j.cageo.2007.12.015.

Ma, X.,Al-Harbi, M.,Datta-Gupta, A., and Efendiev, Y. 2008. An Efficient Two-stage Sampling Method for Uncertainty Quantification in History Matching Geological Models. *SPE Journal* **13** (1): 77-87. SPE-102476-PA. DOI: 10.2118/102476-PA.

Mayerhofer, M.J.,Lolon, E.,Warpinski, N.R.,Cipolla, C.L.,Walser, D.W. et al. 2010. What Is Stimulated Reservoir Volume? *SPE Production & Operations* **25** (1): 89-98. SPE-119890-PA. DOI: 10.2118/119890-PA.

Mayerhofer, M.J.,Lolon, E.P.,Youngblood, J.E., and Heinze, J.R. 2006. Integration of Microseismic-Fracture-Mapping Results With Numerical Fracture Network Production Modeling in the Barnett Shale. Paper SPE 102103 presented at SPE Annual Technical Conference and Exhibition, San Antonio, Texas, USA, 24-27 September. DOI: 10.2118/102103-MS.

McCormick, G.P., and Tapia, R.A. 1972. The Gradient Projection Method under Mild Differentiability Conditions. *SIAM Journal on Control* **10** (1): 93-98. DOI: 10.1137/0310009.

Muller, D.E. 1954. Application of Boolean Algebra to Switching Circuit Design and to Error Detection. *IRE Transactions on Electronic Computers* **3**: 6-12.

Oliver, D.S.,Reynolds, A.C.,Bi, Z., and Abacioglu, Y. 2001. Integration of production data into reservoir models. *Petroleum Geoscience* **7** (S): S65-S73. DOI: 10.1144/petgeo.7.S.S65.

Olson, J.E. 2008. Multi-fracture Propagation Modeling: Applications to Hydraulic Fracturing in Shales and Tight Gas Sands. Paper ARMA 08-327 presented at The 42nd U.S. Rock Mechanics Symposium, San Francisco, CA, USA, June 29-July 2.

Ouenes, A.,Bhagavan, S.,Bunge, P.H., and Travis, B.J. 1994. Application of Simulated Annealing and Other Global Optimization Methods to Reservoir Description: Myths and Realities. Paper SPE 28415 presented at SPE Annual Technical Conference and Exhibition, New Orleans, Louisiana, USA, 25-28 September. DOI: 10.2118/28415-MS.

Paige, C.C., and Saunders, M.A. 1982. LSQR: An Algorithm for Sparse Linear Equations and Sparse Least Squares. *ACM Transactions on Mathematical Software* **8** (1): 43-71. DOI: 10.1145/355984.355989.

Pan, Y., and Horne, R.N. 1998. Improved Methods for Multivariate Optimization of Field Development Scheduling and Well Placement Design. Paper SPE 49055 presented at SPE Annual Technical Conference and Exhibition, New Orleans, Louisiana, USA, 27-30 September. DOI: 10.2118/49055-MS.

Parker, R.L. 1994. *Geophysical Inverse Theory*. Princeton, New Jersey, USA: Princeton University Press. ISBN 0691036349.

Pfeifer, H.P. 2010. An exhaustive Analysis of Recombination and Mutation variances for Genetic Algorithms. *MUNICH*.

Plackett, R.L., and Burman, J.P. 1946. The Design of Optimum Multifactorial Experiments. *Biometrika* **33** (4): 305-325. DOI: 10.1093/biomet/33.4.305.

Qassab, H., Pavlas, M.K.R., Afaleg, N., Ali, H., Kharghoria, A. et al. 2003. Streamline-based Production Data Integration Under Realistic Field Conditions: Experience in a Giant Middle-Eastern Reservoir. Paper SPE 84079 presented at SPE Annual Technical Conference and Exhibition, Denver, Colorado, USA, 5-8 October. DOI: 10.2118/84079-MS.

Reed, I.S. 1954. A class of multiple-error-correcting codes and the decoding scheme. *Transactions of the IRE Professional Group on Information Theory* **4** (4): 38-49.

Remy, N.,Boucher, A., and Wu, J. 2008. *Applied Geostatistics with SGeMS: A User's Guide*. New York, NY, USA: Cambridge University Press. ISBN 0521514142.

Rey, A.,Ballin, P.R.,Vitalis, C.F.,Parke, J., and Datta-Gupta, A. 2009. Assisted History Matching in an Offshore Turbidite Reservoir With Active Reservoir Management. Paper SPE 124950 presented at SPE Annual Technical Conference and Exhibition, New Orleans, Louisiana, USA, 4-7 October. DOI: 10.2118/124950-MS.

Romero, C.E., and Carter, J.N. 2001. Using Genetic Algorithms for Reservoir Characterisation. *Journal of Petroleum Science and Engineering* **31** (2-4): 113-123. DOI: 10.1016/S0920-4105(01)00124-3.

Rushing, J.A.,Perego, A.D., and Blasingame, T.A. 2008. Applicability of the Arps Rate-Time Relationships for Evaluating Decline Behavior and Ultimate Gas Recovery of Coalbed Methane Wells. Paper SPE 114514 presented at CIPC/SPE Gas Technology Symposium 2008 Joint Conference, Calgary, Alberta, Canada, 16-19 June. DOI: 10.2118/114514-MS.

Ryser, H.J. 1963. *Combinatorial Mathematics*. Carus Mathematical Monographs. Washington D.C., USA: Mathematical Association of America. ISBN 978-0883850145.

Sambridge, M., and Mosegaard, K. 2002. Monte Carlo Methods in Geophysical Inverse Problems. *Reviews of Geophysics* **40** (3): 1009. DOI: 10.1029/2000rg000089.

Sawyer, S.A.,Parsch, J.,Zhang, Z., and Hartl, D.L. 2007. Prevalence of positive selection among nearly neutral amino acid replacements in Drosophila. *Proceedings of the National Academy of Sciences of the United States of America* **104** (16): 6504-6510. ISI:000245869200006. DOI: 10.1073/pnas.0701572104.

Schulze-Riegert, R.W.,Axmann, J.K.,Haase, O.,Rian, D.T., and You, Y.-L. 2002. Evolutionary Algorithms Applied to History Matching of Complex Reservoirs. *SPE Reservoir Evaluation & Engineering* **5** (2): 163-173. SPE-77301-PA. DOI: 10.2118/77301-PA.

Schulze-Riegert, R.W.,Haase, O., and Nekrassov, A. 2003. Combined Global and Local Optimization Techniques Applied to History Matching. Paper SPE 79668 presented at SPE Reservoir Simulation Symposium, Houston, Texas, USA, 3-5 February. DOI: 10.2118/79668-MS.

Sen, M.K.,Datta-Gupta, A.,Stoffa, P.L.,Lake, L.W., and Pope, G.A. 1995. Stochastic Reservoir Modeling Using Simulated Annealing and Genetic Algorithms. *SPE Formation Evaluation* **10** (1): 49-56. SPE-24754-PA. DOI: 10.2118/24754-PA.

Sethian, J.A. 1999. *Level Set Methods and Fast Marching Methods: Evolving Interfaces in Computational Geometry, Fluid Mechanics, Computer Vision, and Materials Science*. New York, NY, USA: Cambridge University Press. ISBN 0521645573.

Sethian, J.A., and Vladimirsky, A. 2000. Fast Methods for the Eikonal and Related Hamilton-Jacobi Equations on Unstructured Meshes. *Proceedings of the National Academy of Sciences of the United States of America* **97** (11): 5699-5703.

Song, B., and Ehlig-Economides, C.A. 2011. Rate-Normalized Pressure Analysis for Determination of Shale Gas Well Performance. Paper SPE 144031 presented at North American Unconventional Gas Conference and Exhibition, The Woodlands, Texas, USA, 14-16 June. DOI: 10.2118/144031-MS.

Sylvester, J.J. 1867. Thoughts on Inverse Orthogonal Matrices, Simultaneous Sign-successions, and Tessellated Pavements in Two or More Colours, with Applications to Newton's Rule, Ornamental Tile-work, and the Theory of Numbers. *Philosophical Magazine* **34** (4): 461–475.

Vasco, D.,Keers, H., and Karasaki, K. 2000. Estimation of Reservoir Properties Using Transient Pressure Data: An Asymptotic Approach. *Water Resources Research* **36** (12): 3447-3465.

Vasco, D.W., and Finsterle, S. 2004. Numerical Trajectory Calculations for the Efficient Inversion of Transient Flow and Tracer Observations. *Water Resources Research* **40** (1): W01507. DOI: 10.1029/2003WR002362.

Wall, M. 1996. *GAlib: A C++ Library of Genetic Algorithm Components*.

Wang, J., and Liu, Y. 2011. Simulation Based Well Performance Modeling in Haynesville Shale Reservoir. Paper SPE 142740 presented at SPE Production and Operations Symposium, Oklahoma City, Oklahoma, USA, 27-29 March. DOI: 10.2118/142740-MS.

Weng, X.,Kresse, O.,Cohen, C.E.,Wu, R., and Gu, H. 2011. Modeling of Hydraulic Fracture Network Propagation in a Naturally Fractured Formation. Paper SPE 140253 presented at SPE Hydraulic Fracturing Technology Conference, The Woodlands, Texas, USA, 24-26 January. DOI: 10.2118/140253-MS.

White, C.D., and Royer, S.A. 2003. Experimental Design as a Framework for Reservoir Studies. Paper SPE 79676 presented at SPE Reservoir Simulation Symposium, Houston, Texas, USA, 3-5 February. DOI: 10.2118/79676-MS.

Williams, G.J.J.,Mansfield, M.,MacDonald, D.G., and Bush, M.D. 2004. Top-down Reservoir Modelling. Paper SPE 89974 presented at SPE Annual Technical Conference and Exhibition, Houston, Texas, USA, 26-29 September. DOI: 10.2118/89974-MS.

Williams, M.A.,Keating, J.F., and Barghouty, M.F. 1998. The Stratigraphic Method: A Structured Approach to History-matching Complex Simulation Models. *SPE Reservoir Evaluation & Engineering* **1** (2): 169-176. SPE-38014-PA. DOI: 10.2118/38014-PA.

Yeten, B.,Castellini, A.,Guyaguler, B., and Chen, W.H. 2005. A Comparison Study on Experimental Design and Response Surface Methodologies. Paper SPE 93347 presented at SPE Reservoir Simulation Symposium, The Woodlands, Texas, USA, 31 January-2 Feburary. DOI: 10.2118/93347-MS.

Yeten, B.,Durlofsky, L.J., and Aziz, K. 2002. Optimization of Nonconventional Well Type, Location and Trajectory. Paper SPE 77565 presented at SPE Annual Technical Conference and Exhibition, San Antonio, Texas, USA, 29 September-2 October 2002. DOI: 10.2118/77565-MS.

Yin, J.,Park, H.,Datta-Gupta, A., and Choudhary, M.K. 2010. A Hierarchical Streamline-Assisted History Matching Approach With Global and Local Parameter Updates. Paper SPE 132642 presented at SPE Western Regional Meeting, Anaheim, California, USA, 27-29 May. DOI: 10.2118/132642-MS.

Yin, J.,Xie, J.,Datta-Gupta, A., and Hill, A.D. 2011. Improved Characterization and Performance Assessment of Shale Gas Wells by Integrating Stimulated Reservoir Volume and Production Data. Paper SPE 148969 presented at SPE Eastern Regional Meeting, Columbus, Ohio, USA, 17-19 August. DOI: 10.2118/148969-MS.

Yoshioka, K.,Zhu, D.,Hill, A.D.,Dawkrajai, P., and Lake, L.W. 2005. A Comprehensive Model of Temperature Behavior in a Horizontal Well. Paper SPE 95656 presented at SPE Annual Technical Conference and Exhibition, Dallas, Texas, USA, 9-12 October. DOI: 10.2118/95656-MS.

Yoshioka, K.,Zhu, D.,Hill, A.D.,Dawkrajai, P., and Lake, L.W. 2007. Prediction of Temperature Changes Caused by Water or Gas Entry into a Horizontal Well. *SPE Production & Operations* **22** (4): 425-433. SPE-100209-PA. DOI: 10.2118/100209-PA.

APPENDIX

USER MANUAL OF GENERAL PURPOSE GLOBAL OPTIMIZATION SOFTWARE

A.1 Installation

A.1.1 Download/Checkout Source Code and Test Cases

First of all, this software will be compiled and installed from source codes.

For industry applications, stable versions can be downloaded from MCERI member page with username and password at:

http://www.pe.tamu.edu/mceri

For developing purpose, a nightly version can be checked out by subversion with developer username and password from:

https://pe-vault.pe.tamu.edu/sft/trunk

subversion software: **TortoiseSVN** for windows explorer, **AnkhSVN** for Visual Studio IDE; **subversion** for GNU/Linux command line interface, **RabbitVCS** for Gnome Nautilus, **Subclipse** for Eclipse IDE (NOT Schlumberger ECLIPSE simulators).

Checking out by subversion from windows explorer right-click menu:

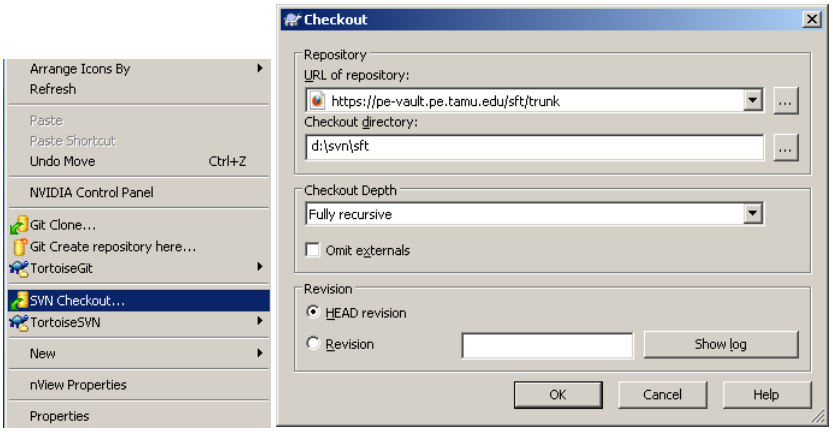

Fig. A.1 check-out from TortoiseSVN

Checking out by subversion command line interface (CLI) for instance GNU/Linux,

svn co https://pe-vault.pe.tamu.edu/sft/trunk ~/svn/sft

Here is a complete list of source code filenames (**print for your reference**):

Table A.1 list of source codes and descriptions

Sources	Descriptions
cmg.cpp **cmg.h**	simulator CMG(IMEX/GEM)
conf.h	build configuration, smart pointer, test build, external library, linear solver
counted_ptr.h	counted smart pointer, compatible with std::vector<T>, similar to boost::shared_ptr
dv_proxy.h	matlab fast marching DV/SRV calculation interface
ecl.cpp **ecl.h**	simulator ECL(ECLIPSE/E300)
eval.h	utility function for calculating expression value in template
ga.cpp **ga.h**	GA inversion
gaio.h	ASCII/Binary I/O class with unified form
gauss.cpp **guass.h**	direct linear solver with LU decomposition for kriging
inverse.h	class template for scanning .INP and overall steps of inversion
krige.cpp **krige.h**	response surface by kriging interpolation
lhdesign.cpp **lhdesign.h**	Latin Hypercube sampling, a space filling design
libdvproxy.h	header file for dvproxy.dll/dvproxy.so built from matlab
main.cpp	main entry of program
Makefile	makefile, can be customized for general purpose
owned_ptr.h	owned smart pointer, esp. for file streams, similar to boost::scoped_ptr
parameter.h	parameter class, high/low bounds, CDF
platform.cpp **platform.h**	platform check/output for binary
quadratic.cpp **quadratic.h**	response surface by quadratic polynomial regression, not recommended
rand_design.cpp **rand_design.h**	random experimental design
reservoir.h	main class template for data integration
rsf.cpp **rsf.h**	base response surface class, inherited by kriging and quadratic
stdafx.cpp **stdafx.h**	common functions
test.h	testing functions for developing purpose
well.cpp **well.h**	well class, consists of well rates, pressure, completions

A.1.2 Compiling by Visual Studio under Windows

Open sft.sln from Visual Studio 2008 or sft10.sln from Visual Studio 2010, select win32 or x64 (if x64 compilers installed), Build->Build Solution.

An executable called **sft.exe** will be generated for those folders:

sft\x64\Release	(64 bit release build, for application purpose)
sft\x64\Debug	(64 bit debug build, for debugging purpose)
sft\Release	(32 bit release build)
sft\Debug	(32 bit debug build)

Compared to location of main.cpp file and test cases:

sft\main.cpp

sft\ecl-syn-11x11x6

sft\cmg-gm-3d-shale2

A.1.3 Compiling under GNU/Linux

A makefile is already provided same directory.

```
make sft
make doc
```

A binary called **sft** will be generated when make finished.

A.2 Preparation

A.2.1 Overview of Template-based General Optimization

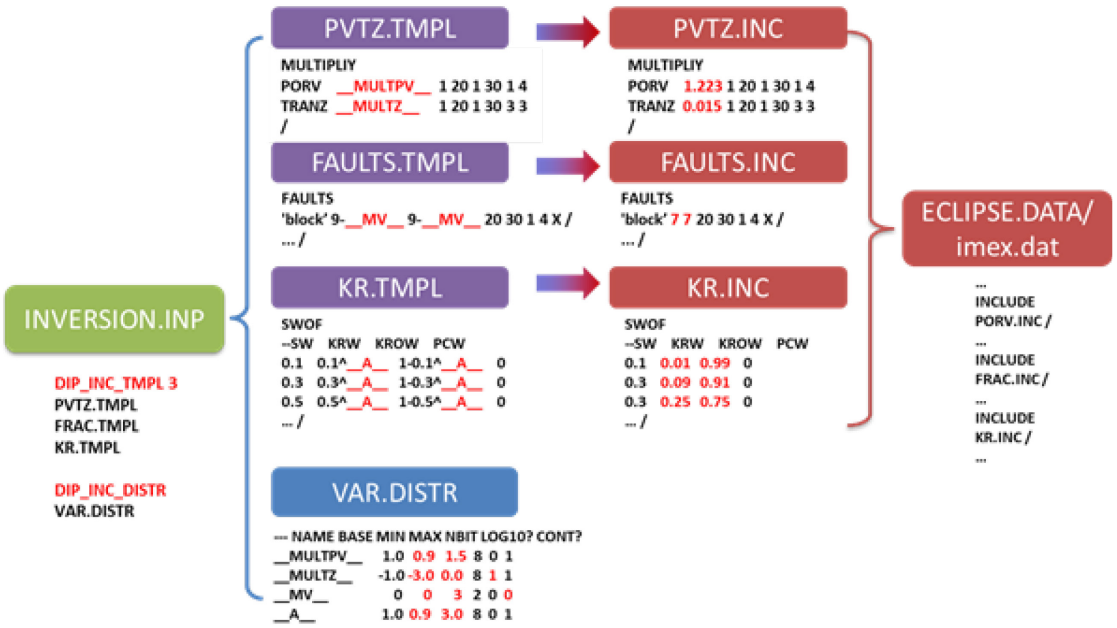

Fig. A.2 Overview of global update

A.2.2 Template (.TMPL) files and Include (.INC) Files

(1) How do templates work?

As shown in **Fig. A.2**, multiple .TMPL files contains multiple variable name in format of __VARNAME__, the number should be consistent with .DISTR file, otherwise the code will quit. Taking **KR.TMPL** in Fig. A.2 as an example.

a. Each occurrence of __A__ in a KR.TMPL will be substituted with its GA evolved value at the same location (since __A__ occurs multiple times, they will be substituted with same values).

b. Assume __A__=2.0 from GA, after substitutions, we get

SWOF
0.1 0.1^**2.0** 1-0.1^**2.0** 0
0.3 0.3^**2.0** 1-0.3^**2.0** 0
0.5 0.3^**2.0** 1-0.3^**2.0** 0
.../

Then a calculation is made for each string in which substitution occurs, which gives:

SWOF
0.1 **0.01** **0.99** 0
0.3 **0.09** **0.91** 0
0.5 **0.25** **0.75** 0
.../

This final content will be same as KR.INC for inclusion to ECLIPSE input deck or imex.dat for CMG, which doesn't change for whole inversion). Therefore, relative permeability shape updated by GA operators.

(2) Rules to make expressions in .TMPL files

a. the global code will explain every string contains __*__ as an expression, extract the template variable, substitute GA evolved values, and calculate results values. **No space is allowed within one expression**. e.g. 0.1^ __A__ will be considered as two expressions and therefore no exponential calculations will be done;

b. currently supported operators: **+, -, *, /, ^**, please use 2.71828^__A__ for exp(__A__);

c. If the expression is complex, use more ( ) to bracket your equation such as 1.0-(10^(__A__+(2.71828^__B__))) to help the program understand better. The rule of thumb is **only one operator allowed in one ( );**

d. Feel free to **check the expression evaluation result** by setting .DISTR to a fixed value (min~max);

e. For CMG grid refinement expressions: use **3* __K__** in order to result in **3*5.5**.

A.2.3 The Variable Distribution (.DISTR) File

This file contains the variable distribution, each row formatted as (examples in Fig A.2):

__VAR1__ base low high resolution log10 continuous
__VAR2__ base low high resolution log10 continuous
...

where "**base"** column of values are used for sensitivity analysis as baseline in the Tornado diagram (refer to SPE 148969). "**low**" and "**high**" column means lower and higher bounds of variables, "**resolution**" column stands for number of bits used to represent current variable in a genome binary string, e.g. 2 bits in Fig. A. will give us binary strings 00,01,10,11, which means integer numbers 0-3 for __MV__, which controls location of fault "block". "log10" column informs whether base/low/high values in current row are after log10, "**continuous**" informs this variable is continuous (1) or discrete (0, CDF mapping will be done), e.g. in Fig. A. __MULTZ__ -1.0 -3.0 0.0 8 1 1, means actually 1E-1 1E-3 1.0 for base/low/high. Only __MV__ is a discrete variable, __MULTPV__, __MULTXY__ and __A__ are continuous variables. Comments start with "--".

A.2.4 Keywords in an inversion input (.INP) file

Table A.2 An inversion input example all keywords

(mandatory keywords in red, optional in black, comments start with "--")

Keywords and formats	*Descriptions*
	1. Simulator Settings
DIP_STUDYNAME ECLRFT	Prefix of ECLIPSE/CMG input deck
DIP_SIM_CMD $e300 -ver 2010.1	Overwrite default simulator commands: $eclipse/@eclipse for ECLIPSE, mx201010.exe for CMG, can be used for compositional or parallel run
DIP_SCHED_FILE **SCHED.INC**	Optional schedule file containing COMPDAT for all wells Need specify this keyword if COMPDAT not in .DATA
DIP_USER_PRESCRIPT octave -qf < pre.m >octave.log	User script for pre-processing **before** the simulation, external software supported are: Octave /Matlab /Perl /Python etc, can be used for GCT/DCT
DIP_USER_POSTSCRIPT perl post.pl	User script for post-processing and/or generating user objective function file **after** the simulation
	2. Variable Settings
DIP_INC_TMPL 3 PVTZ.TMPL FAULTS.TMPL KR.TMPL	Include templates for variable substitutions, 3 means number of templates, should be consistent with .DISTR file
DIP_INC_DISTR VAR.DISTR	Distributions of variables included in all .TMPL files. Should contain exactly same list of vars in form of __*__
DIP_SENS_RUN	If this option turned on, Tornado sensitivity analysis will be generated to a *.SENS file, all GA/proxy settings will be skipped. Starting from base column, perturbing each variable to its lower and high bound.

Table A.2 Continued

Keywords and formats		*Descriptions*
	DIP_USER_OBJFILE post.obj	**3. Objective Settings** Objfile containing one value of overall objective, generated by DIP_USER_POSTSCRIPT or DIP_SIM_CMD. All other objective settings will be skipped.
DIP_OBJECTIVE LPT|MDT|SBHP|SRV		Build-in objective, each keyword will corresponds to following observed data. Keywords allowed includes: **LPT/OPT/WPT/GPT**: field total liq/oil/wat/gas prod. **MDT**: well MDT pressures vs. TVD **FBHP**: well flowing BHP **SBHP**: well shut-in BHP **SRV**: well drainage volume vs PTA/RTA seismic SRV
DIP_SMRY_OBS 1 SCHEDULE		Required if LPT/OPT/WPT/GPT/FBHP/SBHP included OBJECTIVE, observed data from WCONHIST or ECL Office format .FHF. SCHEDULE means obs from WCONHIST
DIP_MDT_OBS 1 obs_mdt_office.txt		Required if MDT included in OBJECTIVE, observed data in *_TRUE.RFT (reference run) or ECL Office format
DIP_DV_OBS 2 295.00 5.38386786e+07 730.00 5.88246219e+07		Required if SRV included in OBJECTIVE, observed data from direct data input, only 1st line of data: time, SRV
DIP_KEY_WELL 2 P1 P2 --S0001-5 HM, rest for prediction		Wells included in OBJECTIVE, others skipped. 2 means number of wells, followed by list of well names
DIP_KEY_TSTEP 5 1-2 3 4-5		TSTEPS included in OBJECTIVE, others skipped. 5 is number of TSTEPs, followed by TSTEP id ranges, can be used for integrating only selected data or prediction
DIP_KEY_TIME 4 0 100 300 400		Time period included in OBJECTIVE, others skipped. 4 means number of time bounds, 0-100 days, 300-400 days

Table A.2 Continued

Keywords and formats	*Descriptions*
	4. Proxy Settings
DIP_PROXY_NED 20	Number of experiments designs for initial response surface proxy. Set to large for small problems.
DIP_PROXY_TOL 0.2	Tolerance allowed for response surface proxy check
DIP_PROXY_SCAN	If this keyword exists, previous proxy will be scanned from existed .BIN file, otherwise existed .BIN/OUT/.OBJ will be removed/replaced, very useful for field case with fixed variable distribution setting, restart from previous proxy (.BIN file)
	5. GA Settings
DIP_GA_CROSSOVER 0.70 2	Default 0.50 0, uniform crossover with p=0.50. 0.70 2 means multi-point crossover with p=0.70 for each segment, 2 segments
DIP_GA_MUTATE 0.05 2	Default 0.001 0, uniform mutation with p=0.001. 0.05 2 means multi-point mutation with p=0.05 for each segment, 2 bits. p should be higher for multipoint mutation than that for uniform for same level of mutation by different schemes
DIP_GA_REPLACE 0.70	Elitism algorithm default 1.00. 0.70 means 70% of population will be replace, while top 30% good samples of generation kept to next generation, very useful for large-scale inverse problem
DIP_GA_POPSIZE 500	Population size, must be even number, long list of variable should go with larger pop size
DIP_GA_NGEN 5000	Max number of generation allowed before exit

A.2.5 (Advanced) User Pre/Post scripts and Objective Function File

An **DIP_USER_PRESCRIPT** (executed before each flow simulation) can be provided to do preparation of simulation models by external commands, for instances, coded in BATCH / Bash/ Perl/ Python/ Matlab/ Octave. This feature is used for

conversion from GCT/DCT bases and GA controlled coefficients to geological models (PERM.GRDECL) for inclusion to an simulation input deck.

The overall objective can be externally computed by an external script specified by **DIP_USER_POSTSCRIPT** (executed after each flow simulation, can also be included in **DIP_SIM_CMD** command line), which will generate a file specified by **DIP_USER_OBJFILE** containing a single value of overall objective function value.

This post-processing script for DIP_USER_OBJFILE will include steps:

a) reading observed data;
b) reading simulation outputs;
c) calculate misfits of multiple objectives;
d) calculate a weighted overall objective function;
e) write out the overall objective value to file defined in DIP_USER_OBJFILE.

A.3 Running

A.3.1 Run Perquisites

Required program/software for running global update include:

a) **zip** command line (Linux and win32), for backing up updated models;
b) **ECLIPSE**: add C:\ecl\macros or /opt/ecl/macros into system PATH. For windows, to make **$eclipse**, **$e300** and **$frontsim** callable:

Start Menu > Run ... > cmd
PATH=%PATH%;c:/ecl/macros

For Linux BASH, to make **@eclipse**, **@e300** and **@frontsim** callable:

export PATH=$PATH:/opt/ecl/macros

c) **CMG**: add those directories to PATH, for windows add these directories:
C:\Program Files (x86)\CMG\IMEX\2010.10\Win_x64\EXE
C:\Program Files (x86)\CMG\GEM\2010.10\Win_x64\EXE
C:\Program Files (x86)\CMG\BR\2010.10\Win_x64\EXE
so that **mx201010.exe**, **gm201010.exe** and **report.exe** callable.

For newer versions of CMG, the locations are:
C:\Program Files\CMG\GEM\2011.10\Win32\EXE**gm201110.exe**
C:\Program Files\CMG\IMEX\2011.10\Win32\EXE**mx201110.exe**
C:\Program Files\CMG\BR\2011.10\Win32\EXE**report.exe**

for Linux, the corresponding locations are:
/opt/cmg/imex/2008.11/Linux_x64/exe/**mx200811.exe**
/opt/cmg/gem/2008.12/Linux_x64/exe/**gm200812.exe**
/opt/cmg/br/2008.12/Linux_x64/exe/**report.exe**

A.3.2 Local Run

There several ways to call GLOBAL:

Run from Visual Studio/Eclipse IDE. If you build your executable from visual studio 2008 or 2010, build **Release of Win32 or x64**, and then change working directory and command arguments. Eclipse IDE follow similar way to setting working directory and command line arguments.

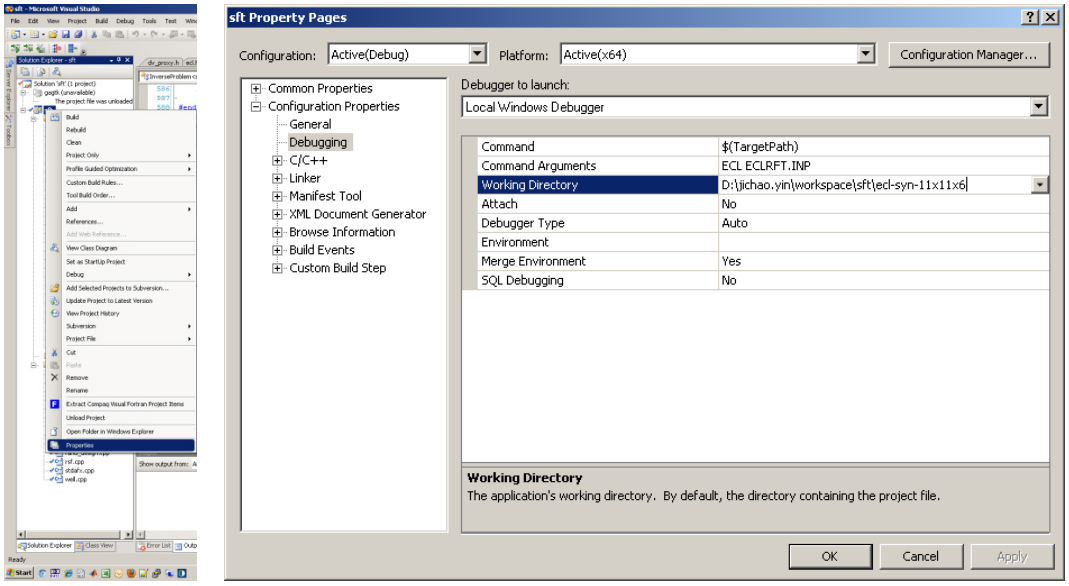

Fig. A.4 Run GLOBAL by setting command line arguments

Run from command line. For Windows users,

Start Menu > Run... > type cmd

D: (The drive your case folder is located)

cd D:\workspace\sft\ecl-syn-11x11x6

sft ECL ECLRFT.INP

For Unix/Linux, open a terminal,

cd ~/svn/sft/ecl-syn-11x11x6

../sft ECL ECLRFT.INP

Double click on the executable. You can also simply double-click on the executables and input "ECL" and "ECLRFT.INP" interactively:

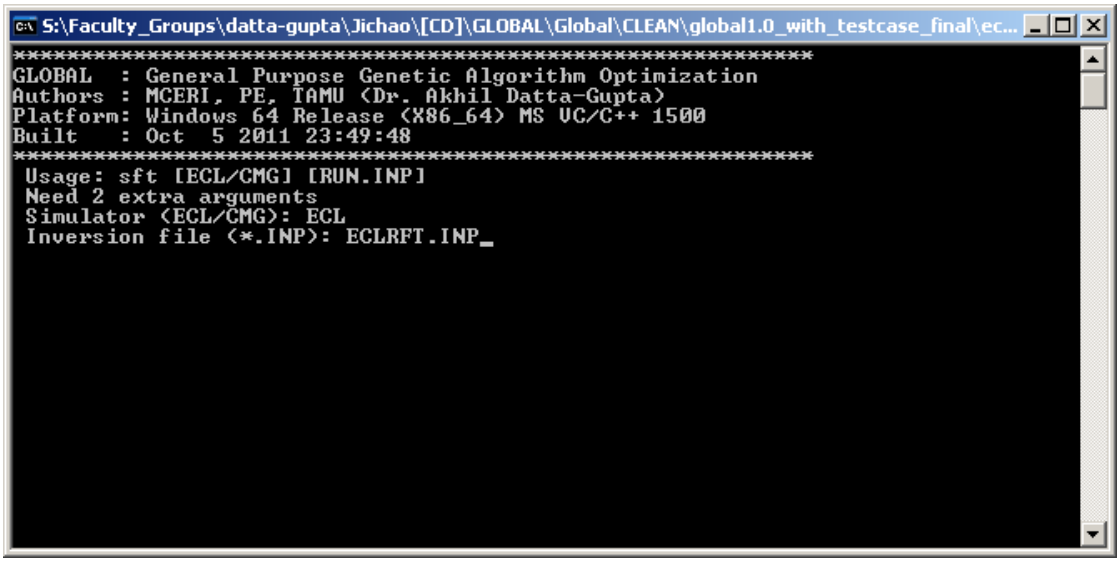

Fig. A.5 Run GLOBAL interactively

sft - main executable name

ECL - specify simulator type, ECL stands for ECLIPSE 100, ECLIPSE 300, FrontSim, S3D or CHEARS, those simulators user ECL standard format; alternatively, **CMG** stands for IMEX, GEM or STARS etc, since each family follow same input/output formats.

ECLRFT.INP - inversion input deck, specify simulator settings, variable settings, objective settings, proxy settings and GA settings. Refer to Table A.2 for keyword details.

A.3.3 Cluster Run

User may consider using HPC cluster for global model calibration, attached is a script of ecl.pbs for submitting an inversion job to Brazos HPC cluster:

```
# ecl.pbs
# job name
#PBS -N test_global
# request 1 node
#PBS -l nodes=1:ppn=8
# request 96 hours and 0 minute of walltime
#PBS -l walltime=96:00:00
# mail is sent when the job starts and when it terminates or aborts
#PBS -m bea
# to the following email address
#PBS -M firstname.lastname@pe.tamu.edu
# setup the environment
. /etc/profile.d/modules.sh
module load eclipse
# By default, PBS scripts execute in your home directory, not the
# directory from which they were submitted. The following line
# places you in the directory from which the job was submitted.
cd $HOME/svn/sft/ecl-syn-11x11x6
# run the program
../sft ECL ECLRFT.INP
exit 0
```

Then in Linux BASH

```
qsub ecl.pbs
```

More information about application for Brazos account or usage of cluster, refer: http://brazos.tamu.edu/docs.html

If your ECLIPSE/CMG simulators are installed in clusters only, you may need to overwrite DIP_SIM_CMD command line (default $eclipse for windows, @eclipse for Unix/Linux). The GLOBAL code will monitor output .**ECLEND** (ECL) or **.out** (CMG) file to tell a simulation is finished successfully or not.

A.3.4 Output Formats

There are various output files from GLOBAL update code:

XXX.OUT - this file contains results of ALL flow simulations, every row is a flow simulation, the columns are (in order):

(1) The first ***nvar*** columns are variable values (consistent with FINE.DISTR file and .TMPL files);
(2) Overall objective value;
(3) Proxy approximated objective value;
(4) Proxy objective error comparing to flow simulation;
(5) Proxy data-exact error. A proxy model constructed by kriging interpolation should reproduce data at experiment points, a polynomial regression proxy will not;
(6) ***nobj*** individual objective values. ***nobj*** is consistent with keywords defined in DIP_OBJECTIVE. For example for LPT|MDT, there will be two columns objLPT and objMDT;
(7) Simulation Run ID. For a single inversion, every flow simulation (ECLIPSE or CMG) will be marked with an unique number by the order of run.

XXX.OBJ - this file contains results of updated flow simulations when objective function reduced (or not higher than 1.10% existing min obj), same format as .OUT

XXX.BIN - same content as XXX.OUT but in binary, only for restart GA from previous run with same parameter definitions, refer to DIP_PROXY_SCAN keyword in

Table A.2.

XXX.EXP - same format as .OUT by only ***nvar*** columns of variable values after Latin Hypercube sampling design. This file is useful for design of experiments research without proxy, GA or flow simulations.

XXX.SENS - result file from DIP_SENS_RUN, each row is the sensitivity of overall objective (DIP_OBJECTIVE) with respect to a single variable, columns are:

(1) Variable name;
(2) Lower bound value of the variable;
(3) Base value;
(4) Upper bound value;
(5) Overall objective value when all other variables are set to "Base" values while perturbing current variable to its lower bound;
(6) Overall objective value when all other variables are set to "Base" values while perturbing current variable to its upper bound.

You need firstly make sure how many variables from .DISTR file!
You need secondly check what is your DIP_OBJECTIVE setting!

A.3.5 Post-processing

The user may consider monitor XXX.OBJ file for variable updating with objective value reduction, and copy the content of XXX.OBJ into spreadsheet and sort the rows by **objOverall** column from small to large in order to output models by cluster analysis.

Open .OBJ file by Microsoft Excel or LibreOffice Calc

-6.62745	-1.64706	1.274118	0.711765	1.761176	1.25098	0.486667	1.763529	**5.898977**	5.898977	0	0.00E+00	1719.28	77.3464	2
-5.60784	-5.27451	1.427059	0.629412	1.708235	1.368235	0.656863	1.883529	**5.890863**	5.890863	0	0.00E+00	2166.67	60.38739	3
-3	-1.11765	1.417647	0.547059	1.715294	1.46	0.470196	1.516471	**5.881254**	5.881254	0	0.00E+00	2683.659	47.82613	5
-3.01961	-4.72549	1.321176	0.617647	1.630588	1.449804	0.917647	1.968235	**5.577954**	5.577954	0	0.00E+00	1537.217	45.52127	9
-2.47059	-3.82353	1.34	0.841176	1.256471	2.255294	0.645882	1.191765	**5.373934**	5.373934	0	0.00E+00	655.6666	70.96706	14
-6.35294	-2.60784	1.356471	0.533333	1.228235	1.847451	0.412549	1.551765	**5.692921**	5.692921	0	0.00E+00	1187.068	74.18781	15
-2.47059	-1.47059	1.276471	0.939216	1.034118	2.26549	0.972549	1.795294	**5.601714**	5.601714	0	0.00E+00	755.9612	97.07047	16
-2.56863	-2.92157	1.06	0.664706	1.764706	1.495686	0.840784	1.767059	**5.630974**	5.630974	0	0.00E+00	2283.357	34.0744	17
-6.13726	-2.98039	1.267059	0.643137	1.443529	1.72	0.346667	1.523529	**4.878374**	4.878374	0	0.00E+00	312.2952	55.30147	23
-5.23529	-5.70588	1.316471	0.896078	1.108235	1.990196	0.596471	1.103529	**5.897245**	5.897245	0	0.00E+00	1679.292	78.91429	26
-2.66667	-3.17647	1.342353	0.805882	1.464706	2.153333	0.387843	1.767059	**5.442937**	5.442937	0	0.00E+00	1105.887	48.30195	27
-4.86275	-4.13726	1.302353	0.707843	1.535294	2.041177	0.997255	1.212941	**5.737928**	5.737928	0	0.00E+00	1232.374	78.19144	28
-5.13726	-1.47059	1.445882	0.84902	1.38	2.403137	0.3	1.763529	**5.610279**	5.610279	0	0.00E+00	987.7625	75.57421	29

Sort by **ObjOverall** column from low to high we get

-6.13726	-2.98039	1.267059	0.643137	1.443529	1.72	0.346667	1.523529	**4.878374**	4.878374	0	0.00E+00	312.2952	55.30147	23
-2.47059	-3.82353	1.34	0.841176	1.256471	2.255294	0.645882	1.191765	**5.373934**	5.373934	0	0.00E+00	655.6666	70.96706	14
-2.66667	-3.17647	1.342353	0.805882	1.464706	2.153333	0.387843	1.767059	**5.442937**	5.442937	0	0.00E+00	1105.887	48.30195	27
-3.01961	-4.72549	1.321176	0.617647	1.630588	1.449804	0.917647	1.968235	**5.577954**	5.577954	0	0.00E+00	1537.217	45.52127	9
-2.47059	-1.47059	1.276471	0.939216	1.034118	2.26549	0.972549	1.795294	**5.601714**	5.601714	0	0.00E+00	755.9612	97.07047	16
-5.13726	-1.47059	1.445882	0.84902	1.38	2.403137	0.3	1.763529	**5.610279**	5.610279	0	0.00E+00	987.7625	75.57421	29
-2.56863	-2.92157	1.06	0.664706	1.764706	1.495686	0.840784	1.767059	**5.630974**	5.630974	0	0.00E+00	2283.357	34.0744	17
-6.35294	-2.60784	1.356471	0.533333	1.228235	1.847451	0.412549	1.551765	**5.692921**	5.692921	0	0.00E+00	1187.068	74.18781	15
-4.86275	-4.13726	1.302353	0.707843	1.535294	2.041177	0.997255	1.212941	**5.737928**	5.737928	0	0.00E+00	1232.374	78.19144	28
-3	-1.11765	1.417647	0.547059	1.715294	1.46	0.470196	1.516471	**5.881254**	5.881254	0	0.00E+00	2683.659	47.82613	5
-5.60784	-5.27451	1.427059	0.629412	1.708235	1.368235	0.656863	1.883529	**5.890863**	5.890863	0	0.00E+00	2166.67	60.38739	3
-5.23529	-5.70588	1.316471	0.896078	1.108235	1.990196	0.596471	1.103529	**5.897245**	5.897245	0	0.00E+00	1679.292	78.91429	26
-6.62745	-1.64706	1.274118	0.711765	1.761176	1.25098	0.486667	1.763529	**5.898977**	5.898977	0	0.00E+00	1719.28	77.3464	2

Then users can choose models (each row is an updated model of variables) by cluster analysis or simply select models giving relatively lower ObjOverall (or some individual objXXX for certain reason) but with diverse model variables.

Each model is labelled by RUN# in last row (Refer to .OUT format), same corresponding number can be found in filename of *_####_####.zip files backed up by the **zip** utility. For example, the results from RUN 23 (first row in table above) will be name *_####_0023.zip.

A.4 Examples

A.4.1 An ECLIPSE Synthetic Case with Production and MDT Pressures

A.4.1.1 Problem Description

This synthetic case shows a three-dimensional three-phase reservoir consisting of 11×11×6 grid blocks, with one injector and four producers. For this synthetic example, we assumed that three global regions have been defined according to facies distribution

in the geologic description: layers 1-2 is region 1, layers 3-4 is region 2 and layers 5-6 is region 3. The region definition and background permeability for each layer are shown in **Fig. A.6** and **Fig. A.7**.

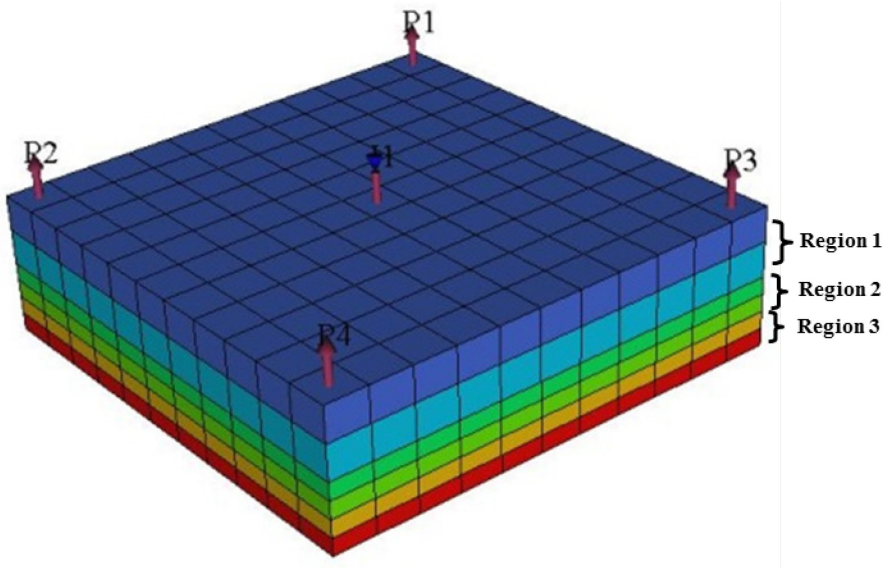

Fig. A.6 Region definition

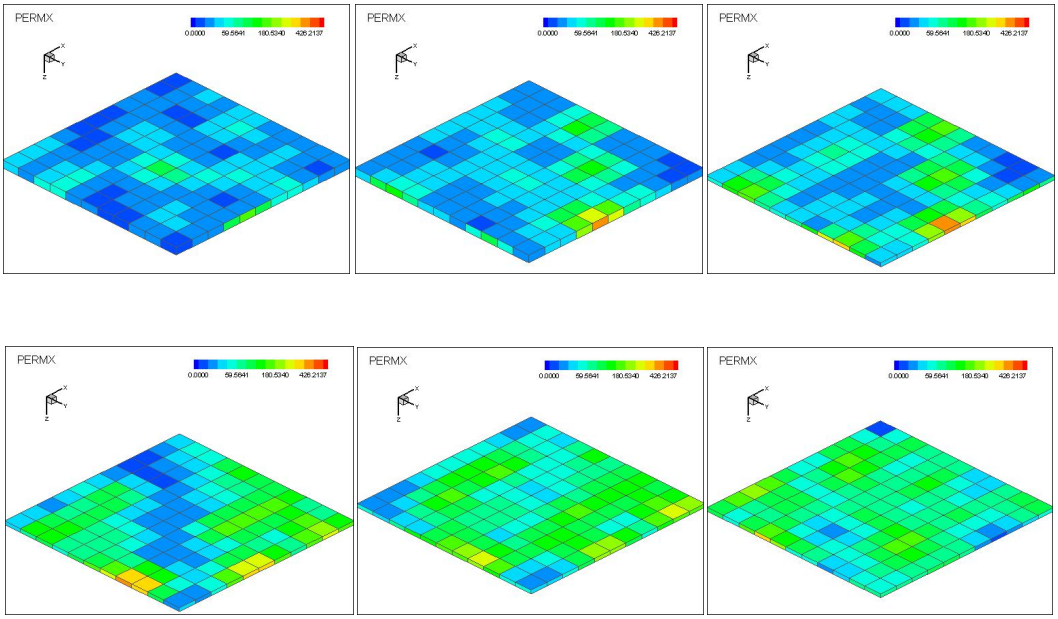

Fig. A.7 Background permeability distribution from layer 1 to layer 6

A.4.1.2 Preparation of Data Set

There are several input files needed, including:

a. ECLRFT.INP

The left side in **Fig. A.8** shows ECLRFT.INP file in the ECLIPSE synthetic case by specifying simulator settings, objective settings, variable settings, proxy settings and GA settings.

DIP_STUDYNAME ECLRFT	Simulator settings ECLIPSE
DIP_OBJECTIVE LPT|MDT	Objective settings
DIP_SMRY_OBS1 SCHEDULE	Observed production data in WCONHIST
DIP_MDT_OBS1 obs_mdt_office.txt	Observed MDT data in ECL Office format
-- use first 19 .S* file for HM, rest for prediction DIP_KEY_TSTEP 19 1-10 11 12-19	TSTEPS included for objective
DIP_INC_TMPL 1 MULTIPLY.TMPL	Variable settings Templates for variable substitution
DIP_INC_DISTR FINE.DISTR	Distribution of variables
DIP_PROXY_NED 50 DIP_PROXY_TOL 0.2	Proxy settings NO. of experiment designs Tolerance for proxy check
DIP_GA_REPLACE 0.7 DIP_GA_POPSIZE 500 DIP_GA_NGEN 5000	GA settings Elitism algorithm (Bottom 70% replaced) Population size (Even NO.) Max. NO. of generation

Fig. A.8 ECLRFT.INP prepared in ECLIPSE synthetic case

b. Observed production data prepared in WCONHIST and WCONINJH

WCONHIST is used for producers, each row consists of: well name, OPEN/SHUT, control mode, surface oil rate, surface water rate, surface gas rate, three default values, bottom-hole pressure.

WCONINJH is used for injectors, each row consists of: well name, injected phase, OPEN/SHUT, surface injected rate, bottom-hole pressure.

A report step can be **TSTEP** following by number of days operating at WCONHIST/WCONINJH, or the **DATE** until these operations finish.

```
WCONHIST
P1   OPEN RESV  440.86862   0.03600  537.37274 3* 2748.28882 /
P2   OPEN RESV  319.12308   0.01963  394.47641 3* 2754.46924 /
P3   OPEN RESV  369.23764   0.08930  569.41583 3* 2413.51709 /
P4   OPEN RESV  319.85934   0.01705  393.11703 3* 2828.47266 /
```

```
/
WCONINJH
I1 WATER OPEN  525.00000 3373.76660 /
/
TSTEP
  1.00000
/
```

c. Observed MDT data prepared in ECL Office format

The observed MDT data is input in the ECLIPSE Office column format with then normal text below replaced by customer input TVD and RFT/MDT pressure data (refer to obs_mdt_office.txt):

```
PAGE       1
ORIGIN     MDT    MEASDATE     1-03-2000
WELLNAME        P1
WTVD       WRFT
FEET       PSIA
1010       1961.4609
1030       2061.9390
1045       2072.0488
1055       2037.5930
1065       2005.8956
1075       1987.6029

PAGE       2
ORIGIN     MDT    MEASDATE     1-03-2000
WELLNAME        P2
WTVD       WRFT
FEET       PSIA
1010       2445.0100
1030       2379.5151
1045       2089.3794
1055       2093.7913
```

1065 2143.6995

1075 2149.8818

Note that: 1-03-2000, represents Mar 1 2000 not Jan 3 2000. And the user should make sure the name after WELLNAME consistent with the well names defined in COMPDAT.

d. MULTIPLY.TMPL (MULTIPLY.INC) and FINE.DISTR

Fig. A.9 shows the .TMPL file (only one template file in this example) and the GLOBAL converted .INC file. We can see that there are eight GLOBAL unknowns: TRANZ multiplier between zone 1&2, TRANZ multiplier between zone 2&3, pore volume multiplier of zone 1/2/3, and PERMX, PERMY multipliers of zone 1/2/3. In the .INC file, the template variables are extracted and substituted by GA evolved values.

.TMPL

```
MULTIPLY
 TRANZ    __MULTZ12__   1   11   1   11   2   2/
 TRANZ    __MULTZ23__   1   11   1   11   4   4/
 PORV     __MULTPV1__   1   11   1   11   1   2/
 PORV     __MULTPV2__   1   11   1   11   3   4/
 PORV     __MULTPV3__   1   11   1   11   5   6/
 TRANX    __MULTX1__    1   11   1   11   1   2/
 TRANY    __MULTX1__    1   11   1   11   1   2/
 TRANX    __MULTX2__    1   11   1   11   3   4/
 TRANY    __MULTX2__    1   11   1   11   3   4/
 TRANX    __MULTX3__    1   11   1   11   5   6/
 TRANY    __MULTX3__    1   11   1   11   5   6/
  /
```

.INC

```
MULTIPLY
 TRANZ   9.14E-05   1   11   1   11   2   2/
 TRANZ   4.86E-05   1   11   1   11   4   4/
 PORV    1.18706    1   11   1   11   1   2/
 PORV    0.754902   1   11   1   11   3   4/
 PORV    1.44706    1   11   1   11   5   6/
 TRANX   1.86784    1   11   1   11   1   2/
 TRANY   1.86784    1   11   1   11   1   2/
 TRANX   0.516863   1   11   1   11   3   4/
 TRANY   0.516863   1   11   1   11   3   4/
 TRANX   1.69294    1   11   1   11   5   6/
 TRANY   1.69294    1   11   1   11   5   6/
  /
```

Fig.A.9 MULTIPLY.TMPL and generated MULTIPLY.INC in ECL synthetic case

The .DISTR file is prepared as shown in **Fig. A.10**, which specifies the base/low/high values, resolution, whether after log10, and continuous/discrete for each variable.

--NAME?	BASE	LOW	HIGH	NBIT	LOG10?	CONT?
__MULTZ12__	-5	-7	-2	4	1	1
__MULTZ23__	-3	-6	-1	4	1	1
__MULTPV1__	1	0.9	1.5	4	0	1
__MULTPV2__	0.8	0.5	1	4	0	1
__MULTPV3__	1	0.9	1.8	4	0	1
__MULTX1__	1.5	1.2	2.5	4	0	1
__MULTX2__	0.7	0.3	1	4	0	1
__MULTX3__	1.5	1.1	2	4	0	1

Fig. A.10 FINE.DISTR file prepared in ECLIPSE synthetic case

A.4.1.3 Run Steps

- ✓ put zip command line to system PATH or working directory for backing up updated models (section **A.3.1**);
- ✓ Add ECLIPSE / CMG simulator executables or macros into the system path;
- ✓ Run ECLRFT_TRUE.DATA by ECLIPSE first to get the observed data (A.3.1);
- ✓ Run from the command line under current working directory (**Fig. A.11**) or double-click on the executable.

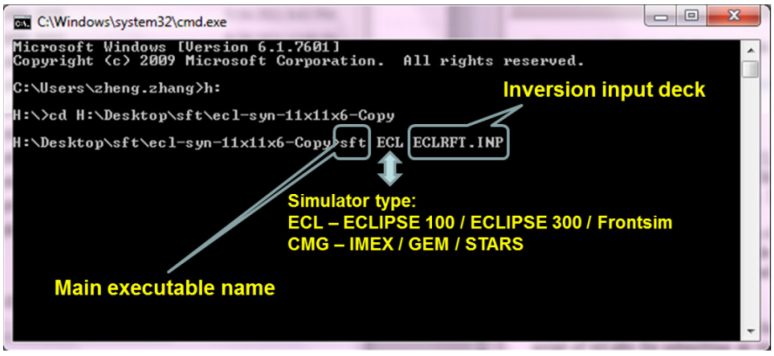

Fig. A.11 Run the ECLIPSE synthetic case from command line

A.4.1.4 Results and Post-processing

We can check all saved good models from .OBJ file (format in section A.3.4). If we open the .OBJ file by Microsoft EXCEL and sort by objectives from smallest to largest, we can choose models with smaller objectives by cluster analysis (Fig. A.11).

J34 fx 4.054814

	A	B	C	D	E	F	G	H	I	J	K	L	M	N	O	P	Q
1	NO.	VAR1	VAR2	VAR3	VAR4	VAR5	VAR6	VAR7	VAR8	Obj.	Proxy					Run times	
2	43	-4.04E+00	-4.16E+00	1.17E+00	8.18E-01	1.46E+00	1.89E+00	6.05E-01	1.66E+00	3.69E+00	3.69E+00	0.00E+00	0.00E+00	7.35E+01	2.18E+01	231	
3	64	-4.04E+00	-4.47E+00	1.17E+00	8.18E-01	1.46E+00	1.89E+00	6.05E-01	1.66E+00	3.71E+00	3.71E+00	0.00E+00	0.00E+00	7.69E+01	2.18E+01	515	
4	59	-4.08E+00	-4.31E+00	1.17E+00	8.14E-01	1.46E+00	1.88E+00	5.17E-01	1.66E+00	3.71E+00	3.71E+00	0.00E+00	0.00E+00	1.08E+02	1.55E+01	490	
5	50	-4.04E+00	-4.16E+00	1.17E+00	8.18E-01	1.46E+00	1.89E+00	6.05E-01	1.67E+00	3.73E+00	3.73E+00	0.00E+00	0.00E+00	7.83E+01	2.21E+01	337	
6	69	-4.12E+00	-4.24E+00	1.17E+00	8.18E-01	1.46E+00	1.89E+00	5.14E-01	1.66E+00	3.75E+00	3.75E+00	0.00E+00	0.00E+00	1.13E+02	1.60E+01	550	
7	54	-4.04E+00	-4.47E+00	1.17E+00	8.18E-01	1.46E+00	1.89E+00	5.17E-01	1.67E+00	3.76E+00	3.76E+00	0.00E+00	0.00E+00	1.11E+02	1.64E+01	368	
8	41	-4.04E+00	-4.31E+00	1.17E+00	8.25E-01	1.46E+00	1.89E+00	5.17E-01	1.67E+00	3.76E+00	3.76E+00	0.00E+00	0.00E+00	1.11E+02	1.65E+01	221	
9	28	-4.18E+00	-4.59E+00	1.16E+00	8.12E-01	1.50E+00	1.86E+00	7.12E-01	1.72E+00	3.76E+00	3.76E+00	0.00E+00	0.00E+00	5.33E+01	3.47E+01	66	
10	33	-4.04E+00	-4.47E+00	1.17E+00	8.22E-01	1.46E+00	1.86E+00	5.14E-01	1.66E+00	3.77E+00	3.77E+00	0.00E+00	0.00E+00	1.36E+02	1.38E+01	171	
11	56	-4.04E+00	-4.16E+00	1.17E+00	8.25E-01	1.46E+00	1.89E+00	5.17E-01	1.67E+00	3.79E+00	3.79E+00	0.00E+00	0.00E+00	1.18E+02	1.66E+01	389	
12	48	-4.04E+00	-4.24E+00	1.17E+00	8.18E-01	1.46E+00	1.87E+00	6.05E-01	1.66E+00	3.82E+00	3.82E+00	0.00E+00	0.00E+00	1.05E+02	1.96E+01	321	
13	46	-4.12E+00	-4.16E+00	1.19E+00	7.63E-01	1.46E+00	1.87E+00	5.14E-01	1.66E+00	3.82E+00	3.82E+00	0.00E+00	0.00E+00	1.49E+02	1.40E+01	262	
14	51	-4.04E+00	-4.20E+00	1.19E+00	7.63E-01	1.46E+00	1.88E+00	5.14E-01	1.66E+00	3.86E+00	3.86E+00	0.00E+00	0.00E+00	1.48E+02	1.54E+01	352	
15	57	-4.04E+00	-4.24E+00	1.17E+00	8.14E-01	1.46E+00	1.89E+00	5.17E-01	1.69E+00	3.90E+00	3.90E+00	0.00E+00	0.00E+00	1.34E+02	1.84E+01	405	
16	55	-4.04E+00	-4.31E+00	1.17E+00	8.18E-01	1.46E+00	1.89E+00	5.14E-01	1.69E+00	3.92E+00	3.92E+00	0.00E+00	0.00E+00	1.39E+02	1.84E+01	383	
17	44	-4.12E+00	-4.16E+00	1.17E+00	8.18E-01	1.46E+00	1.89E+00	5.17E-01	1.70E+00	3.94E+00	3.94E+00	0.00E+00	0.00E+00	1.42E+02	1.88E+01	241	
18	66	-4.12E+00	-4.24E+00	1.17E+00	8.18E-01	1.46E+00	1.89E+00	5.17E-01	1.70E+00	3.95E+00	3.95E+00	0.00E+00	0.00E+00	1.43E+02	1.88E+01	519	
19	38	-4.06E+00	-4.55E+00	1.20E+00	7.59E-01	1.48E+00	1.86E+00	4.29E-01	1.66E+00	3.95E+00	3.95E+00	0.00E+00	0.00E+00	1.54E+02	1.76E+01	213	
20	45	-4.04E+00	-4.39E+00	1.17E+00	8.22E-01	1.45E+00	1.97E+00	6.05E-01	1.69E+00	3.96E+00	3.96E+00	0.00E+00	0.00E+00	8.22E+01	3.35E+01	250	
21	30	-4.04E+00	-4.16E+00	1.17E+00	8.25E-01	1.46E+00	1.89E+00	5.14E-01	1.69E+00	3.96E+00	3.96E+00	0.00E+00	0.00E+00	1.49E+02	1.85E+01	129	

Fig. A.11 Results from .OBJ file

We can visualize LPT and MDT pressure by ECLIPSE Office for true model by loading the observed MDT file by Open Observed -> Column Format... -> Change " First Line of Data " to 3.

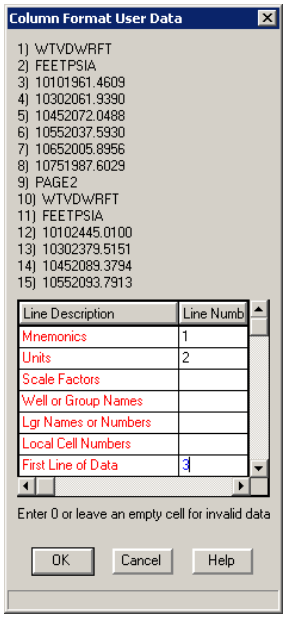

Fig. A.12 Loading ECLIPSE Office format observed MDT data

Base model and global updated models after unzipping the chosen models from the working folder can be loaded by Open -> RFT .... The visualization is shown in Fig. A.13, in which red dots refer to the true model, blue dots refer to the base model, and colored lines refer to global updated models.

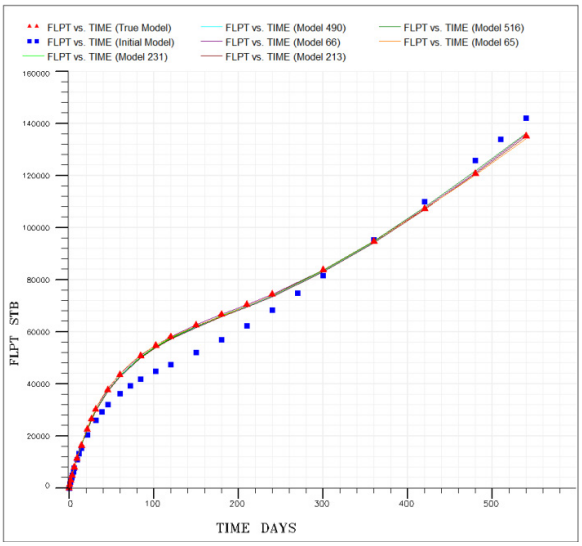

a. Liquid production from global updates

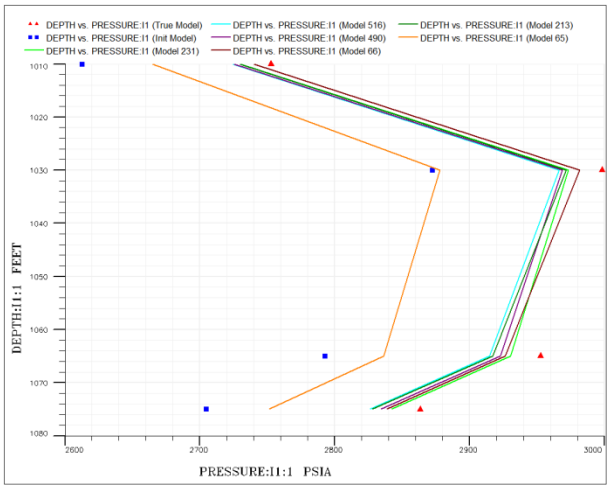

b. MDT pressure for I1

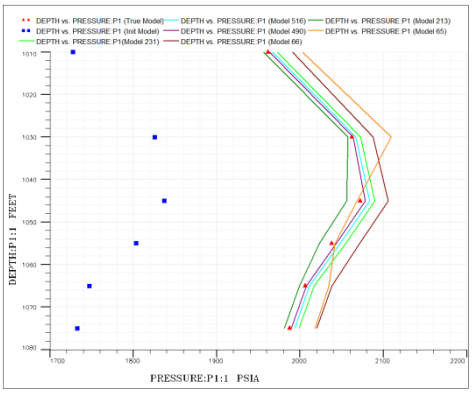

c. MDT pressure for P1

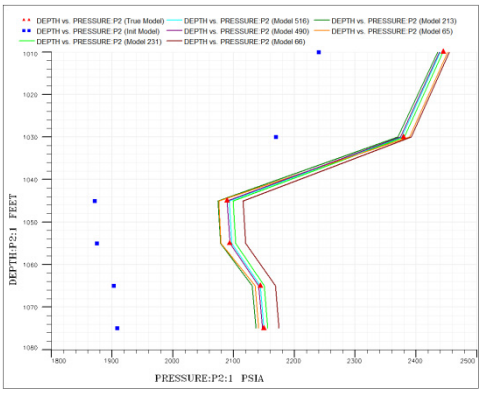

d. MDT pressure for P2

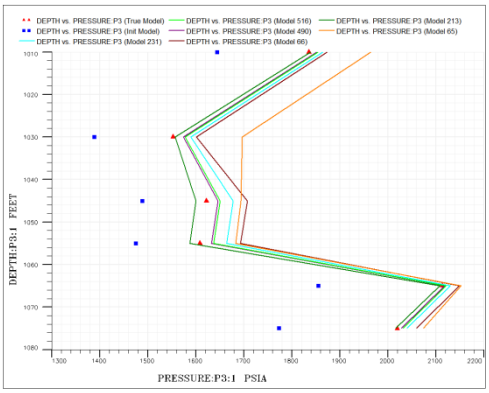

e. MDT pressure for P3

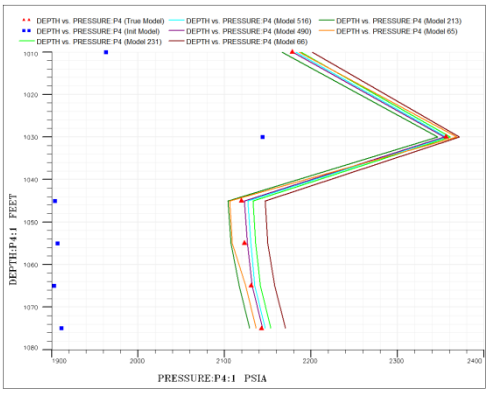

f. MDT pressure for P4

Fig. A.13 LPT and MDT pressure matches from GLOBAL updates

A.4.2 A CMG Synthetic Shale Gas Case with Flowing BHP

A.4.2.1 Problem Description

The reference model for this case is a 3D single-phase gas shale reservoir represented using single porosity compositional model designed after a Haynesville field case. The size of the grid is 264×64×5. The matrix permeability ranges from 80 nano-darcy to 150 nano-darcy. A horizontal well is completed in the center of the reservoir with 4 transverse elliptical fractures. The fracture heights fully penetrate the pay zone. Each fracture is considered surrounded by an enhanced permeability area (EPA) that

represents natural fracture and/or hydraulic fracture induced permeability enhancements as shown in Fig. A.14. The parameters to be estimated via history matching and the associated uncertainties for this example are listed in next subsection. We assume that the fracture locations are known and are as shown in Fig. A.14. The horizontal well is first produced at a constant rate of 2 MMSCF/day, until bottom-hole pressure (BHP) drops to 1000 psi when the well control switches to BHP control. In this synthetic case, the first 295 days of BHP history will be integrated to predict BHP and gas production for the following 435 days. The objective function is defined as the sum of squared differences of BHP between simulation results and the reference ('true') case for first 295 days.

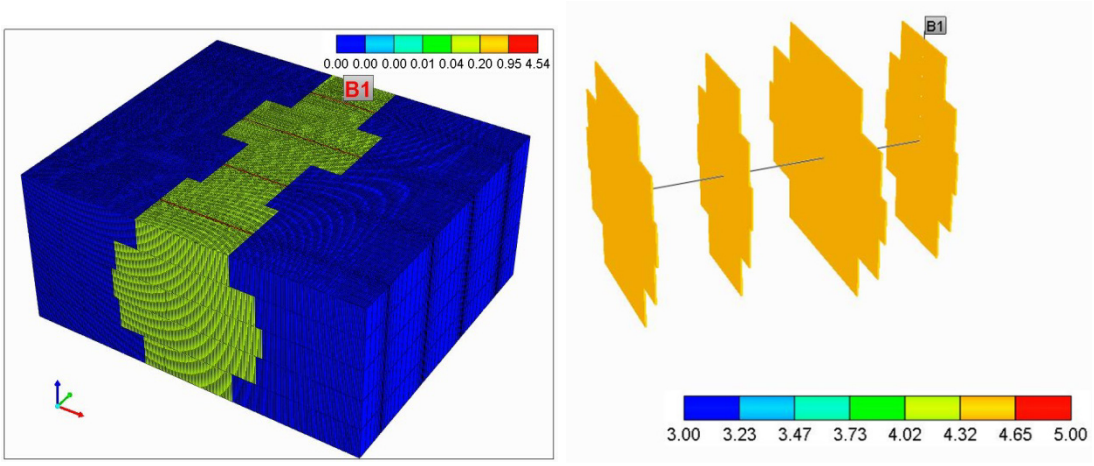

Fig. A.14 CMG synthetic shale gas reservoir setup

A.4.2.2 Preparation of Data Set

Files need to prepare are shown below:

a. frac.inp and tmpl files

DIP_SIM_CMD **gm201010.exe -doms -parasol 4**	**Simulator Settings** **(CMG, compositional model, local parallel run)**
DIP_STUDYNAME **gmsp3d2**	
DIP_INC_TMPL 5 **perm.tmpl** **rockm.tmpl** **rocke.tmpl** **rockf.tmpl** **region.tmpl**	**Variable Settings** **Templates for variable substitution**
DIP_INC_DISTR **frac_fine.distr**	**Distribution of variables**
DIP_OBJECTIVE **FBHP**	**Objective Settings** **FBHP: well flowing BHP**
DIP_SMRY_OBS 1 **gmsp3d2_true.fhf**	**Observed data from gmsp3d2_true.fhf**
DIP_KEY_TIME 2 **0 300**	**Time period in OBJECTIVE**
DIP_PROXY_NED 40 **DIP_PROXY_TOL 0.2**	**Proxy Settings** **(NO. of experiment designs for initial proxy; Tolerance for proxy check)**
DIP_GA_POPSIZE 1000	**GA Settings** **Population size (Even NO.)**

Uncertainty	.TMPL	.INC
Matrix permeability (k_M) EPA permeability (k_E) Fracture permeability (k_F)	perm.tmpl	perm.INC
Matrix compaction factor (C_M)	rockm.tmpl	rockm.INC
EPA compaction factor (C_F)	rocke.tmpl	rocke.INC
Fracture compaction factor (C_F)	rockf.tmpl	rockf.INC
Fracture 1 half long axis (X_{F1}) Fracture 2 half long axis (X_{F2}) Fracture 3 half long axis (X_{F3}) Fracture 4 half long axis (X_{F4})	region.tmpl	region.INC

--NAME	BASE	MIN	MAX	NBIT	LOG?	CONT?
__KM__	8.00E-05	7.00E-05	1.50E-04	6	0	1
__KE__	0.15	0.05	0.25	6	0	1
__KF__	3.5	1	5	6	0	1
__CM__	3.00E-04	2.00E-04	5.00E-04	6	0	1
__CE__	5.00E-04	4.00E-04	6.50E-04	6	0	1
__CF__	3.00E-04	2.00E-04	4.50E-04	6	0	1
__NF1__	40	20	60	4	0	0
__NF2__	60	40	90	4	0	0
__NF3__	60	40	90	4	0	0
__NF4__	40	20	60	4	0	0

b. Observed production data prepared in CMG .fhf format

```
** This is an field history file (fhf)
'2009-03-09'                    -->start date
'gmsp3d2_frac_0023_0001.fhf' -->This is title shown in CMG Results Graph
'2009-03-09'                    -->start date
'days'                          -->first column of data pool use days not DATE
4                               -->four column of data except first column time
'Well Pressure'     'Oil Rate SC'    'Water Rate SC' 'Gas Rate SC'
'psi''STB/day'      'STB/day'        'MSCF/day'
1
'B1'
0.017826.800        0.000   0.000    2000.000
0.035       7711.500        0.000    0.000    2000.000
0.110       7606.300        0.000    0.000    2000.000
```

Note that the --> should be removed from an actual .fhf file otherwise CMG won't load them.

c. Preparation of template files for compactions of matrix/EPA/fracture

****rockm.tmpl**, compaction of matrix, base CM = 3.89E-04, 0.00013->0.00031->0.00077

**$press por_mult hor_perm_mult ver_perm_mult

**** make sure no space within one expression

15	1	10^(__CM__*(15-10000))	10^(__CM__*(15-10000))
1000	1	10^(__CM__*(1000-10000))	10^(__CM__*(1000-10000))
2000	1	10^(__CM__*(2000-10000))	10^(__CM__*(2000-10000))
3000	1	10^(__CM__*(3000-10000))	10^(__CM__*(3000-10000))
4000	1	10^(__CM__*(4000-10000))	10^(__CM__*(4000-10000))
5000	1	10^(__CM__*(5000-10000))	10^(__CM__*(5000-10000))
6000	1	10^(__CM__*(6000-10000))	10^(__CM__*(6000-10000))
6500	1	10^(__CM__*(6500-10000))	10^(__CM__*(6500-10000))
7000	1	10^(__CM__*(7000-10000))	10^(__CM__*(7000-10000))
7500	1	10^(__CM__*(7500-10000))	10^(__CM__*(7500-10000))
8000	1	10^(__CM__*(8000-10000))	10^(__CM__*(8000-10000))
8500	1	10^(__CM__*(8500-10000))	10^(__CM__*(8500-10000))
9000	1	10^(__CM__*(9000-10000))	10^(__CM__*(9000-10000))
9500	1	10^(__CM__*(9500-10000))	10^(__CM__*(9500-10000))
10000	1	1.00000	1.00000

**__rocke.tmpl__, compaction of EPA, base CE = 5E-04, 1E-5->3E-5->1E-4

**$press por_mult hor_perm_mult ver_perm_mult

**** make sure no space within one expression

15	1	10^(__CE__*(15-10000))	10^(__CE__*(15-10000))
1000	1	10^(__CE__*(1000-10000))	10^(__CE__*(1000-10000))
2000	1	10^(__CE__*(2000-10000))	10^(__CE__*(2000-10000))
3000	1	10^(__CE__*(3000-10000))	10^(__CE__*(3000-10000))
4000	1	10^(__CE__*(4000-10000))	10^(__CE__*(4000-10000))
5000	1	10^(__CE__*(5000-10000))	10^(__CE__*(5000-10000))
6000	1	10^(__CE__*(6000-10000))	10^(__CE__*(6000-10000))
6500	1	10^(__CE__*(6500-10000))	10^(__CE__*(6500-10000))
7000	1	10^(__CE__*(7000-10000))	10^(__CE__*(7000-10000))
7500	1	10^(__CE__*(7500-10000))	10^(__CE__*(7500-10000))
8000	1	10^(__CE__*(8000-10000))	10^(__CE__*(8000-10000))
8500	1	10^(__CE__*(8500-10000))	10^(__CE__*(8500-10000))
9000	1	10^(__CE__*(9000-10000))	10^(__CE__*(9000-10000))
9500	1	10^(__CE__*(9500-10000))	10^(__CE__*(9500-10000))
10000	1	1.00000	1.00000

**rockf.tmpl, compaction of fracture, base CF = 3.00E-04, 0.001->0.002->0.004

**$press por_mult hor_perm_mult ver_perm_mult

**** make sure no space within one expression

15	1	10^(__CF__*(15-10000))	10^(__CF__*(15-10000))
1000	1	10^(__CF__*(1000-10000))	10^(__CF__*(1000-10000))
2000	1	10^(__CF__*(2000-10000))	10^(__CF__*(2000-10000))
3000	1	10^(__CF__*(3000-10000))	10^(__CF__*(3000-10000))
4000	1	10^(__CF__*(4000-10000))	10^(__CF__*(4000-10000))
5000	1	10^(__CF__*(5000-10000))	10^(__CF__*(5000-10000))
6000	1	10^(__CF__*(6000-10000))	10^(__CF__*(6000-10000))
6500	1	10^(__CF__*(6500-10000))	10^(__CF__*(6500-10000))
7000	1	10^(__CF__*(7000-10000))	10^(__CF__*(7000-10000))
7500	1	10^(__CF__*(7500-10000))	10^(__CF__*(7500-10000))
8000	1	10^(__CF__*(8000-10000))	10^(__CF__*(8000-10000))
8500	1	10^(__CF__*(8500-10000))	10^(__CF__*(8500-10000))
9000	1	10^(__CF__*(9000-10000))	10^(__CF__*(9000-10000))
9500	1	10^(__CF__*(9500-10000))	10^(__CF__*(9500-10000))
10000	1	1.00000	1.00000

d. 3D elliptical fracture definition via perm.tmpl and region.tmpl

**perm.tmpl

__KM__

*MOD

** IX1:IX2 IY1:IY2 IZ1:IZ2

**1:264 1:64 1:5 * 1e-6 **ALL PERM FROM ND to MD

** fracture 1 layer 1

132-0.6000*__NF1__ : 132+0.6000*__NF1__ 1:8 1:1 = __KE__ ** EPA

132-0.6000*__NF1__ : 132+0.6000*__NF1__ 9:9 1:1 = __KF__ ** FRAC

132-0.6000*__NF1__ : 132+0.6000*__NF1__ 10:16 1:1 = __KE__ ** EPA

** fracture 1 layer 2

132-0.9165*__NF1__ : 132+0.9165*__NF1__ 1:8 2:2 = __KE__ ** EPA

132-0.9165*__NF1__ : 132+0.9165*__NF1__ 9:9 2:2 = __KF__ ** FRAC

132-0.9165*__NF1__ : 132+0.9165*__NF1__ 10:16 2:2 = __KE__ ** EPA

```
** fracture 1 layer 3
132-1.0000*__NF1__      : 132+1.0000*__NF1__    1:8   3:3  = __KE__   ** EPA
132-1.0000*__NF1__      : 132+1.0000*__NF1__    9:9   3:3  = __KF__   ** FRAC
132-1.0000*__NF1__      : 132+1.0000*__NF1__   10:16  3:3  = __KE__   ** EPA
** fracture 1 layer 4
132-0.9165*__NF1__      : 132+0.9165*__NF1__    1:8   4:4  = __KE__   ** EPA
132-0.9165*__NF1__      : 132+0.9165*__NF1__    9:9   4:4  = __KF__   ** FRAC
132-0.9165*__NF1__      : 132+0.9165*__NF1__   10:16  4:4  = __KE__   ** EPA
** fracture 1 layer 5
132-0.6000*__NF1__      : 132+0.6000*__NF1__    1:8   5:5  = __KE__   ** EPA
132-0.6000*__NF1__      : 132+0.6000*__NF1__    9:9   5:5  = __KF__   ** FRAC
132-0.6000*__NF1__      : 132+0.6000*__NF1__   10:16  5:5  = __KE__   ** EPA

** fracture 2 layer 1
132-0.6000*__NF2__      : 132+0.6000*__NF2__   17:24  1:1  = __KE__   ** EPA
132-0.6000*__NF2__      : 132+0.6000*__NF2__   25:25  1:1  = __KF__   ** FRAC
132-0.6000*__NF2__      : 132+0.6000*__NF2__   26:32  1:1  = __KE__   ** EPA
** fracture 2 layer 2
132-0.9165*__NF2__      : 132+0.9165*__NF2__   17:24  2:2  = __KE__   ** EPA
132-0.9165*__NF2__      : 132+0.9165*__NF2__   25:25  2:2  = __KF__   ** FRAC
132-0.9165*__NF2__      : 132+0.9165*__NF2__   26:32  2:2  = __KE__   ** EPA
** fracture 2 layer 3
132-1.0000*__NF2__      : 132+1.0000*__NF2__   17:24  3:3  = __KE__   ** EPA
132-1.0000*__NF2__      : 132+1.0000*__NF2__   25:25  3:3  = __KF__   ** FRAC
132-1.0000*__NF2__      : 132+1.0000*__NF2__   26:32  3:3  = __KE__   ** EPA
** fracture 2 layer 4
132-0.9165*__NF2__      : 132+0.9165*__NF2__   17:24  4:4  = __KE__   ** EPA
132-0.9165*__NF2__      : 132+0.9165*__NF2__   25:25  4:4  = __KF__   ** FRAC
132-0.9165*__NF2__      : 132+0.9165*__NF2__   26:32  4:4  = __KE__   ** EPA
** fracture 2 layer 5
132-0.6000*__NF2__      : 132+0.6000*__NF2__   17:24  5:5  = __KE__   ** EPA
132-0.6000*__NF2__      : 132+0.6000*__NF2__   25:25  5:5  = __KF__   ** FRAC
132-0.6000*__NF2__      : 132+0.6000*__NF2__   26:32  5:5  = __KE__   ** EPA

** fracture 3 layer 1
```

```
132-0.6000*__NF3__      : 132+0.6000*__NF3__    33:40  1:1 = __KE__   ** EPA
132-0.6000*__NF3__      : 132+0.6000*__NF3__    41:41  1:1 = __KF__   ** FRAC
132-0.6000*__NF3__      : 132+0.6000*__NF3__    42:48  1:1 = __KE__   ** EPA
** fracture 3 layer 2
132-0.9165*__NF3__      : 132+0.9165*__NF3__    33:40  2:2 = __KE__   ** EPA
132-0.9165*__NF3__      : 132+0.9165*__NF3__    41:41  2:2 = __KF__   ** FRAC
132-0.9165*__NF3__      : 132+0.9165*__NF3__    42:48  2:2 = __KE__   ** EPA
** fracture 3 layer 3
132-1.0000*__NF3__      : 132+1.0000*__NF3__    33:40  3:3 = __KE__   ** EPA
132-1.0000*__NF3__      : 132+1.0000*__NF3__    41:41  3:3 = __KF__   ** FRAC
132-1.0000*__NF3__      : 132+1.0000*__NF3__    42:48  3:3 = __KE__   ** EPA
** fracture 3 layer 4
132-0.9165*__NF3__      : 132+0.9165*__NF3__    33:40  4:4 = __KE__   ** EPA
132-0.9165*__NF3__      : 132+0.9165*__NF3__    41:41  4:4 = __KF__   ** FRAC
132-0.9165*__NF3__      : 132+0.9165*__NF3__    42:48  4:4 = __KE__   ** EPA
** fracture 3 layer 5
132-0.6000*__NF3__      : 132+0.6000*__NF3__    33:40  5:5 = __KE__   ** EPA
132-0.6000*__NF3__      : 132+0.6000*__NF3__    41:41  5:5 = __KF__   ** FRAC
132-0.6000*__NF3__      : 132+0.6000*__NF3__    42:48  5:5 = __KE__   ** EPA

** fracture 4 layer 1
132-0.6000*__NF4__      : 132+0.6000*__NF4__    49:56  1:1 = __KE__   ** EPA
132-0.6000*__NF4__      : 132+0.6000*__NF4__    57:57  1:1 = __KF__   ** FRAC
132-0.6000*__NF4__      : 132+0.6000*__NF4__    58:64  1:1 = __KE__   ** EPA
** fracture 4 layer 2
132-0.9165*__NF4__      : 132+0.9165*__NF4__    49:56  2:2 = __KE__   ** EPA
132-0.9165*__NF4__      : 132+0.9165*__NF4__    57:57  2:2 = __KF__   ** FRAC
132-0.9165*__NF4__      : 132+0.9165*__NF4__    58:64  2:2 = __KE__   ** EPA
** fracture 4 layer 3
132-1.0000*__NF4__      : 132+1.0000*__NF4__    49:56  3:3 = __KE__   ** EPA
132-1.0000*__NF4__      : 132+1.0000*__NF4__    57:57  3:3 = __KF__   ** FRAC
132-1.0000*__NF4__      : 132+1.0000*__NF4__    58:64  3:3 = __KE__   ** EPA
** fracture 4 layer 4
132-0.9165*__NF4__      : 132+0.9165*__NF4__    49:56  4:4 = __KE__   ** EPA
132-0.9165*__NF4__      : 132+0.9165*__NF4__    57:57  4:4 = __KF__   ** FRAC
```

```
132-0.9165*__NF4__          : 132+0.9165*__NF4__    58:64  4:4  = __KE__   ** EPA
** fracture 4 layer 5
132-0.6000*__NF4__          : 132+0.6000*__NF4__    49:56  5:5  = __KE__   ** EPA
132-0.6000*__NF4__          : 132+0.6000*__NF4__    57:57  5:5  = __KF__   ** FRAC
132-0.6000*__NF4__          : 132+0.6000*__NF4__    58:64  5:5  = __KE__   ** EPA
```

region.tmpl has similar definition except the __K*__ now replace with region numbers, 1 means the matrix, 2 means EPA, 3 means fracture cells.

```
**region.tmpl
CTYPE       CON 1
*MOD
** IX1:IX2        IY1:IY2     IZ1:IZ2
** fracture 1 layer 1
132-0.6000*__NF1__          : 132+0.6000*__NF1__     1:8    1:1  = 2    ** EPA
132-0.6000*__NF1__          : 132+0.6000*__NF1__     9:9    1:1  = 3    ** FRAC
132-0.6000*__NF1__          : 132+0.6000*__NF1__     10:16  1:1  = 2    ** EPA
** fracture 1 layer 2
...
```

A.4.2.3 Run Inversion

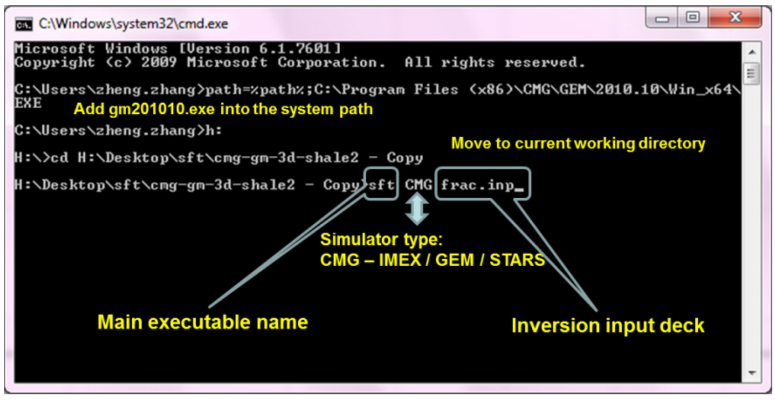

Fig. A.15 Run CMG example from command line

Or the user can copy sft.exe to working directory and double-click on the executable:

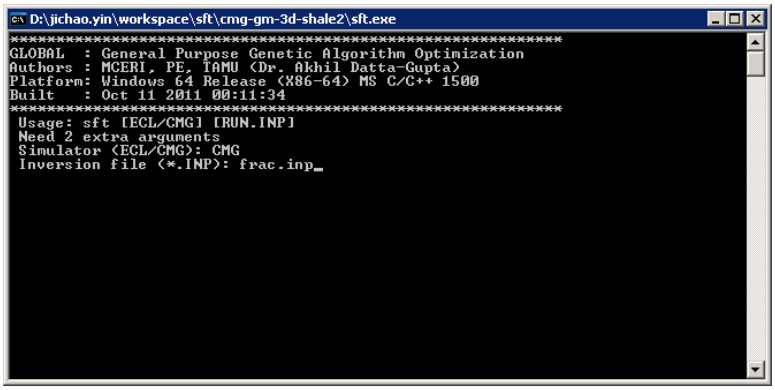

Fig. A.16 Run CMG example interactively from double-click

A.4.2.4 Results and Post-processing

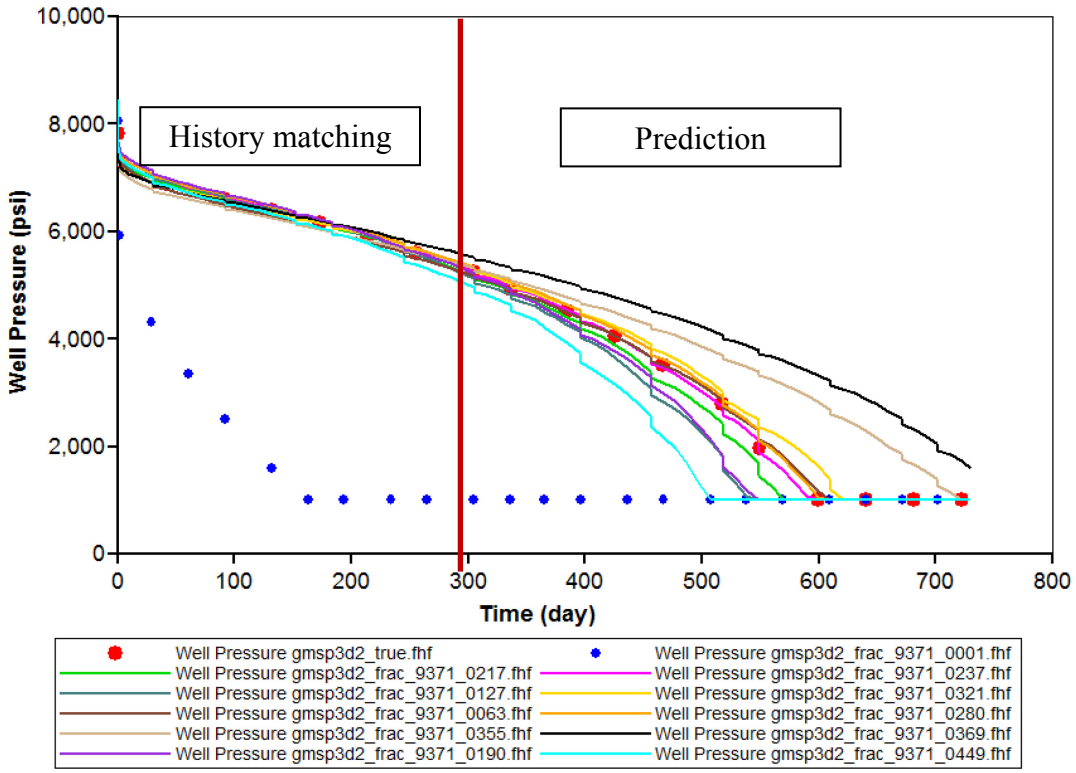

Fig. A.17 Flowing BHP history matching results

VITA

Name: Jichao Yin

Address: 3120 Buffalo Speedway, Houston Texas 77027

Email: jichao.yin@gmail.com

Education: B.S., Thermal Engineering, Tsinghua University, Beijing, China, Jul. 2005

M.S., Engineering Thermophysics, Tsinghua University, Beijing, China, Jul. 2007

Ph.D., Petroleum Engineering, Texas A&M University, College Station, TX, USA, Dec. 2011